POLITÉCNICO DE LEIRIA | ESCOLA SUPERIOR DE TECNOLOGIA E GESTÃO

POLITÉCNICO DE LEIRIA

Master Thesis:

Design of cold-formed profiles using the EMM Effective Modulus Method

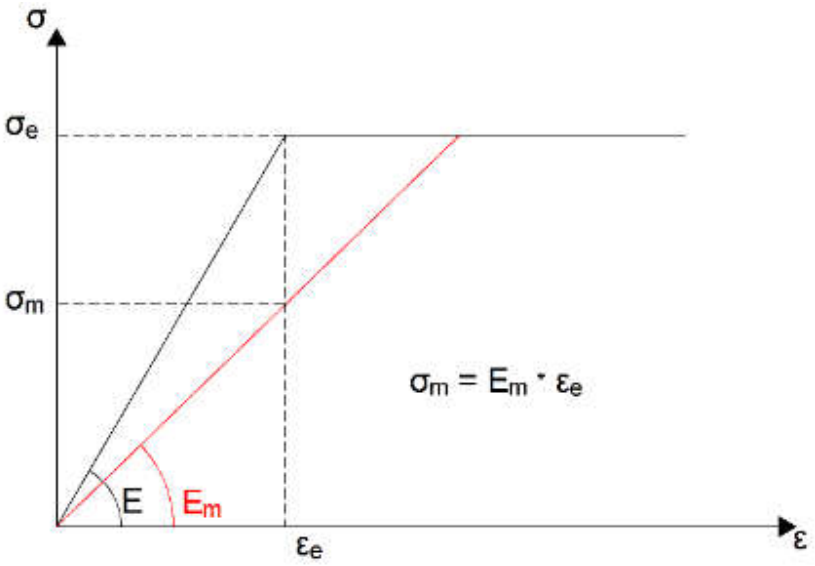

Student: **Cristiano Alexandre Garcia Monteiro. - 2210845**

Supervisor: **Luis Carlos Prola**

Co-supervisor: **Rui Miguel Barreiros Rúben**

Leiria, December 2023

POLITÉCNICO DE LEIRIA | ESCOLA SUPERIOR DE TECNOLOGIA E GESTÃO

ACKNOWLEDGEMENTS

First, I would like to thank my teacher and master's coordinator Luis Prola. His good humour and attitude motivated me to leave my comfort zone and move to Portugal at a time in my life when I wasn't sure what direction to take, and so I joined the master's programme in civil engineering at the Polytechnic Institute of Leiria. Throughout the master's, Professor Prola was always patient and willing to teach and help with the curriculum. I was also able to accompany Professor Prola on an academic trip to Finland to take part in an extracurricular academic programme and visit a company that manufactures lightweight modular construction. I've always had an interest in metal structures, but Professor Luis Prola made my interest grow even more. To the point where I decided to complete my master's degree with this work and with Professor Luis Prola as my supervisor who helped me a lot and without whom this work would not have been pushed so far.

I would also like to thank Professor Rui Rúben for his contribution and time dedicated to this work.

A special thank you goes to my friend, colleague and study partner Luis Parreira, with whom I was able to share this stage in my higher education and who has undoubtedly made it better in many ways. I congratulate him on reaching the end and successfully completing this adventure and wish him and his family every success in his professional life.

Finally, I would like to thank my parents who have done so much to guarantee me opportunities which, unfortunately, they didn't have access to. They have always been by my side, supporting me and encouraging me to pursue my higher education and my dreams in both good and bad times.

ABSTRACT

This work aims to present a proposal for verifying the safety of thin-walled profiles based on the concept of effective elasticity modulus. This method has the advantage, compared to the classical Effective Width method, of not requiring the alteration of geometric properties of the section to account for the effects of post-buckling resistance on local and distortional instability modes. Furthermore, it maintains theoretical consistency by considering the variation of post-buckling average stresses relative to deformations.

The dissertation begins with a literature review on plate instability. Then a literature review on section instability is conducted to demonstrate the consistency of applying the concept of effective modulus to post-buckling resistance, illustrating examples of effective elasticity modulus distributions in the post-buckling stage of columns and beams.

Following this, an algorithm for calculating the resistance of columns and beams based on the concept of Effective Elasticity Modulus is proposed. Initially, an innovative criterion for post-buckling resistance of plates without imperfections is introduced, using a new relationship between stresses and deformations, where the post-buckling resistance of the plate is reached when the average stress corresponds to yield deformations, by means an effective elasticity modulus. Subsequently, as a comprehensive parametric study has not yet been conducted to calibrate the equations of effective modulus for local and distortional instability modes, reduction coefficients of modulus equivalent to the well-known Direct Strength Method are employed.

The proposed calculation algorithm for the Effective Modulus Method is then tested in comparison with experimental and numerical results available in the literature. The method is applied to take into account the interaction of local, distortional, and global instability modes in columns and local and distortional modes in beams.

SIMBOLS LIST

LATIN LETTERS

a	length
b_{eff}	effective width
b_f	width of the flange's flat area
b_s	width of the stiffener flat area
b_w	width of the web flat area
CFS	Cold formed steel
GBT	General Beam Theory
GBTUL	GBT at University of Lisbon (software)
D	flexural stiffness of the plate
DL	Distortional/ local without global approach
DLG 6 it	Distortional/ local with 6 iterations
E_{eff}	effective elasticity modulus
EDLG	Simplified distortional/ Local without iterations.
ELDG	Simplified distortional/ Local without iterations.
EMM	Effective Modulus Method
EWM	Effective Width Method
FEM	Finite element method
f_{exp}	resistance obtained trough experimental testing.
f_{num}	resistance obtained trough computational simulation.
f_y	yield stress
$F_{(x, y)}$	stress function of Airy

L	length
LD	Local/ distortional without global approach
LDG 6 it	Local/ distortional with 6 iterations
M_{crL}	Local critical buckling moment
M_{crD}	Distortional critical Buckling moment
M_{crG}	Global critical Buckling moment
P	axial load
P_{crL}	Local critical buckling load
P_{crD}	Distortional critical buckling load
P_{crG}	Global critical buckling load
P_n	nominal resistance load
P_y	yield load.
t	thickness
v_{b-r}	lateral displacement of the flange-stiffener
w	the transverse (flexural) displacement

GREEK LETTERS

$\Delta\varepsilon$	strain increment
$\overline{\lambda}_p$	normalized slenderness of the plate
σ	normal stress
σ_{cr}	critical stress
σ_e	edge stress
σ_m	average stress
σ_x, σ_x , τ_{xy}	normal and tangential stresses

$\Delta\sigma$ stress increment

INDEX OF FIGURES

Figure 1 Axially compressed simply supported plate. 2
Figure 2 Support conditions: longitudinal edges: (a) rigid and (b) free. [7] 4
Figure 3 (a) Trajectories and (b) stress distributions (post-buckling behaviour). [7] 4
Figure 4 Plate stress obtained by Abaqus program [39] 6
Figure 5 Evolution of the distribution of normal stresses on the transverse edges 9
Figure 6 Effective width concept 9
Figure 7 Lipped channel (a) geometry and cross-section deformed shapes associated with column (b) local, (c) distortional and (d) global (flexural-torsional (d_1) and flexural (d_2)) 13
Figure 8 Lipped channel (a) local, (b) distortional and (c) global (flexural-torsional) 13
Figure 9 Evolution of the stress diagram in the mid-span section (column), local mode [7]..... 20
Figure 10 Evolution of the stress diagram in the mid-span section (beam), local mode. [7]..... 22
Figure 11 Characterization of warping caused by distortional instability. [7] 23
Figure 12 Evolution of the stress diagram in the mid-span section (column) in distortional mode. [7] 24
Figure 13 Evolution of the stress diagram in the mid-span section (beam) in distortional mode [7] ..... (a) Positive values of v_{b-r} and (b) Negative values of v_{b-r}. 25
Figure 14 Effective modulus of elasticity (E_{eff}) concept: (a) LM (b) DM. 27
Figure 15 Evolution of the effective modulus diagram, uniform compression, local mode. [7] 28
Figure 16 Evolution of the effective modulus diagram, pure bending, local mode. 29
Figure 17 Evolution of the effective modulus diagram, uniform compression, distortional mode with $v_{b-r} > 0$ [7]. 31
Figure 18 Evolution of the effective modulus diagram, uniform compression, distortional mode with $v_{b-r} < 0$ [7]. 31
Figure 19 Evolution of the effective modulus diagram, pure bending, distortional mode [7] 32
Figure 20 Evolution of the effective modulus diagram, pure bending, distortional mode with $v_{b-r} < 0$ [7]. 32
Figure 21 (a) post-buckling stress distributions and (b) models for stress resultants 34
Figure 22 Definition of the effective modulus of elasticity of a plate..... 35
Figure 23 Effective width and effective modules reducing factors. 36
Figure 24 The EMM flowchart: (a) Local distortional sequence (b) Distortional local sequence 41
Figure 25 The EMM flowchart for DL and LD methodologies..... 46
Figure 26 Compression test Set-up [119]..... 48
Figure 27 Deformed specimens after testing.[119]..... 48
Figure 28 Comparison EMM × experimental results of LC specimens..... 50
Figure 29 Comparison EMM × experimental results..... 51
Figure 30 Typical theoretical analysis and experimental test of specimen [120] 52
Figure 31 Comparison EMM × numerical results of LC specimens with fy 300MPa..... 53
Figure 32 Comparison EMM × numerical results of LC specimens fy 500MPa..... 54
Figure 33 Comparison EMM × numerical results of LC specimens..... 55
Figure 34 Comparison EMM × numerical results of LC specimens..... 56
Figure 35 Various buckling modes of CS profiles [121] determined in GBTUL 57
Figure 36 Comparison EMM × numerical results of CS1 specimens..... 59
Figure 37 Comparison EMM × numerical results of CS2 specimens..... 61
Figure 38 Comparison EMM × numerical results of CS3 specimens..... 63

Figure 39 Comparison EMM × numerical results of CS4 specimens 65
Figure 40 Comparison EMM × numerical results of CS5 specimens 67
Figure 41 Comparison EMM × numerical results of CS6 specimens 69
Figure 42 Comparison EMM × numerical results of CS7 specimens 71
Figure 43 Comparison EMM × numerical results of CS8 specimens 73
Figure 44 Comparison EMM × numerical results of CS9 specimens 75
Figure 45 Comparison EMM × numerical results of CS10 specimens 77
Figure 46 Depictions of Rack-sections and buckling modes. 78
Figure 47 Pictures of set-up during compression tests 78
Figure 48 Comparison EMM × experimental results of Rack specimens 80
Figure 49 Boundary conditions used to determine the critical loads P_{crL}, P_{crD} , P_{crG} of the specimens.(GBTUL [92]) 81
Figure 50 Comparison EMM × numerical results of C-profile specimens 83
Figure 51 Comparison EMM × numerical results of C-profile specimens (only LD & DL) 84
Figure 52 Geometrical proprieties of sigma sections used [124] 85
Figure 53 Comparison between of A specimen experimentally and theoretically tested [124] .. 86
Figure 54 Support conditions used in CBTUL to obtain the critical values of the Sigma specimens. 86
Figure 55 Comparison EMM × experimental results of Sigma specimens 87
Figure 56 Comparison EMM × numerical results of Sigma specimens 88
Figure 57 Bending moment diagram acting on the beam specimens tested [114] 89
Figure 58 Comparison EMM × experimental results 91
Figure 59 simple C sections “C” & web stiffened C-sections “SC” [117] 92
Figure 60 tests with and without straps [116] 93
Figure 61 Comparison EMM × experimental results 94
Figure 62 Comparison EMM × experimental results 97

INDEX OF TABLES

No table of figures entries found.

Table 1 LC column specimens' dimensions & critical loads P_{crL}, P_{crD} , P_{crG}. [119] 49
Table 2 Comparison EMM × experimental results of LC specimens 49
Table 3 Colum specimen's dimensions and critical loads [120] 50
Table 4 Comparison EMM × experimental results of specimens 51
Table 5 Comparison EMM × numerical results of LC specimens with f_y 300MPa 53
Table 6 Comparison EMM × numerical results of LC specimens f_y 500MPa 54
Table 7 Comparison EMM × numerical results of LC specimens f_y 700MPa 55
Table 8 Comparison EMM × numerical results of LC specimens f_y 900MPa 56
Table 9 CS column specimen's dimensions & critical loads P_{crL}, P_{crD} , P_{crG}. 57
Table 10 Comparison EMM × numerical results of CS1 specimens 58
Table 11 Comparison EMM × numerical results of CS2 specimens 60
Table 12 Comparison EMM × numerical results of CS3 specimens 62
Table 13 Comparison EMM × numerical results of CS4 specimens 64
Table 14 Comparison EMM × numerical results of CS5 specimens 66
Table 15 Comparison EMM × numerical results of CS6 specimens 68
Table 16 Comparison EMM × numerical results of CS7 specimens 70
Table 17 Comparison EMM × numerical results of CS8 specimens 72
Table 18 Comparison EMM × numerical results of CS9 specimens 74
Table 19 Comparison EMM × numerical results of CS10 specimens 76
Table 20 Rack column specimen's dimensions & critical loads P_{crL}, P_{crD} , P_{crG}. 79
Table 21 Comparison EMM × experimental results of Rack specimens 80
Table 22 column specimen's dimensions & critical loads P_{crL}, P_{crD} , P_{crG}. 82
Table 23 Comparison EMM × numerical results of C-profile specimens 82
Table 24 Comparison EMM × numerical results of C-profile specimens (only LD & DL) 84
Table 25 column specimen's dimensions & critical loads P_{crL}, P_{crD} , P_{crG}. 86
Table 26 Comparison EMM × experimental results of Sigma specimens 87
Table 27 Comparison EMM × numerical results of Sigma specimens 88
Table 28 Beam specimen's dimensions. 90
Table 29 Comparison EMM × experimental results 91
Table 30 Column specimen's dimensions [18 92
Table 31 Comparison EMM × experimental results 94
Table 32 Beam specimen's dimensions. 95
Table 33 Comparison EMM × experimental results 96

INDEX OF CONTENT

1. INTRODUCTION 1
1.1 STABILITY OF PLATES 2
1.1.1 Linear stability analysis 2
1.1.2 Post-buckling behaviour 3
1.1.3 Effective width concept 8
1.2 WORK ORGANISATION 11
1.3 OBJECTIVES OF THIS WORK 12
2. STABILITY OF COLD-FORMED PROFILES 13
2.1 LINEAR STABILITY ANALYSIS 13
2.2 POST BUCKLING BEHAVIOUR 18
2.2.1 Distribution of post-buckling stresses 19
2.2.2 Distribution of elasticity modulus 26
3. CONCEPT OF THE EFFECTIVE MODULE 33
3.1 DISTRIBUTION OF EFFECTIVE MODULUS 34
3.1.1 Concept of Effective Modulus for plates 34
3.1.2 Concept of Effective Modulus for a Cross-Section 35
3.2 PROPOSAL FOR THE EFFECTIVE MODULUS METHOD, COMPRESSION 37
3.3 PROPOSAL FOR THE EFFECTIVE MODULUS METHOD, BENDING 46
4. COMPARISON OF RESULTS 47
4.1 RESULTS FOR COMPRESSION 48
4.1.1 Articles from 2017 part I and II: Lc and L48f sections 48
4.1.1.1 Experimental Results 48
4.1.1.2 Numerical results 52
4.1.2 Article from 2016 CS-Profiles 57
4.1.3 Article from 2014 Rack 78
4.1.4 Article from 2012 C-profiles Loughlan 81
4.1.5 Article from 2017 Sigma -Profiles 85
4.1.5.1 Experimental Results 87
4.1.5.2 Numerical results 88
4.2 RESULTS FOR BENDING 89
4.2.1 Uniform Bending 89
4.2.1.1 Article from 2020 89
4.2.1.2 Article from 2012 92

4.2.2 Non-uniform Bending 95
5. CONCLUSIONS AND FUTURE WORKS 98
5.1 Conclusions 98
5.2 Future works 100
6. REFERENCES 101

1. INTRODUCTION

In this work, a new methodology is proposed to characterize the resistance of thin-walled steel sections and, to this end, the concept of effective modulus of elasticity is used. First applied to the case of the resistance of thin plates, and then, in chapter 2, it is proposed for thin-walled profiles.

The concept of effective modulus of elasticity is used to characterize the plate post-buckling behaviour and is based on the non-uniform distribution of post-critical stresses for local and distortional modes. More specifically, it uses the concept of mean post-buckling stresses to propose a strength criterion.

In this case, the loss of post-buckling stiffness is simulated by the loss of material properties (in this case, the elasticity mode) instead of the decrease in geometric properties, traditionally used in the method of effective widths (or areas) of the cross-section.

Starting by introducing a subject widely studied over the years: the stability of thin-walled plates. Initially, the linear analysis of plates (critical stresses and instability modes) is presented to then review the post-buckling behaviour, the basis of the proposal for the effective module method. This knowledge will serve as a basis for formulating the concept of effective modulus of elasticity.

This methodology has already been suggested by Rasmussen [1-3] and later studied by Camotim and Prola [4, 5]. To account for the loss of stiffness, Prola [7] proposed modifying the elastic modulus along the post-buckling path as the load increased in the finite element program FINLOC [6]. To achieve this, a database of effective modulus was developed using a geometrically nonlinear analysis program based on the finite strip method that employed spline functions.

Subsequently, (i) a review on plate stability is updated, and (ii) examples of post-buckling stress variations and distribution of effective modulus in cold-formed steel profiles are presented based on Prola's work [7].

1.1 STABILITY OF PLATES

1.1.1 Linear stability analysis

The differential equilibrium equation (1) of a plate simply supported on all its edges subjected to uniaxial compression represented in the Figure 1, was derived by Saint-Venant [8]

$$\nabla^4 w \equiv \frac{\partial^4 w}{\partial x^4} + 2\frac{\partial^4 w}{\partial x^2 \partial y^2} + \frac{\partial^4 w}{\partial y^4} = -\frac{\sigma t}{D}\frac{\partial^2 w}{\partial x^2} \quad (1)$$

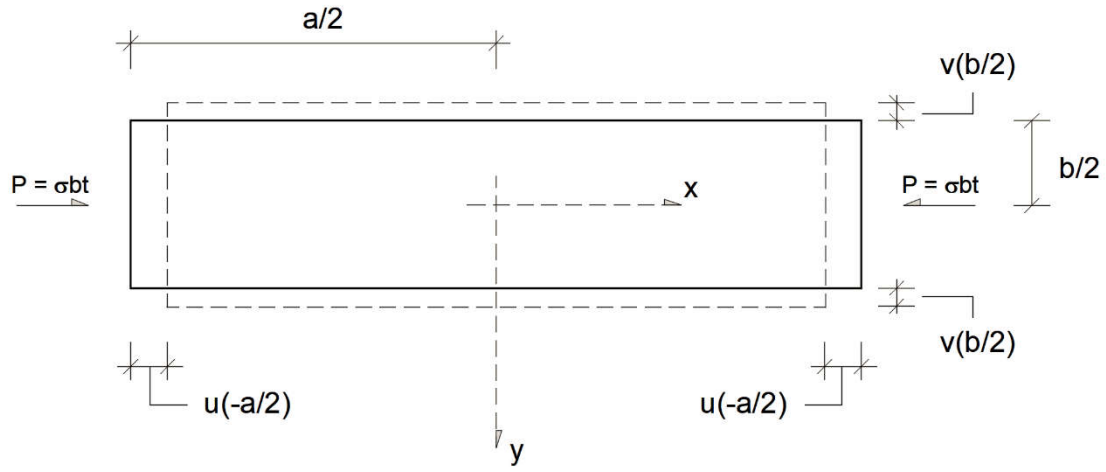

Figure 1 Axially compressed simply supported plate.

where ω(x, y) is the transverse (flexural) displacement of the plate's midplane, σ is the applied compression stress and t and D are, respectively, the thickness and flexural stiffness of the plate. The first solution to this equation was obtained by Bryan [9], in 1891, for the case of a plate simply supported on all edges and subjected to uniform compression. For others support conditions, Timoshenko [10] and Reissner [11] obtained solutions for uniformly compressed plates.

Subsequently, the linear stability of plates was studied by a considerable number of researchers. Bulson's book [12], in 1970, presents a vast set of results, relating to bifurcation stresses in plates with different support conditions and subject to different combinations of (i) compression, uni and biaxial, (ii) flexion and (iii) shear.

In present century Becque [13,14] has studied the inelastic instability behaviour of plates.

According to Prola [3], "The lack of effficient computational resources meant that the overwhelming majority of results available until the mid-1960s were calculated using analytical methods, whether exact or approximate. Among the latter, it is important to highlight the finite difference and Galerkin methods (equilibrium differential equation) or the Rayleigh-Ritz method (potential energy). From the moment the use of finite element method (FEM) became widespread, namely through the formulation of several geometrically non-linear plate elements (e.g., [15]), the number of analyses and problems addressed grew exponentially. Later, the formulation and computational implementation of a geometrically nonlinear finite range in bending displacements [16] contributed to considerably reducing the calculation effort involved in the analyses."

1.1.2 Post-buckling behaviour

The differential equations of the equilibrium of a plate without imperfections, in the post-buckling phase, were deduced by Von Kárman [17], in 1910. After, in 1939, Marguerre [1.136] introduced the effect of the presence of initial geometric imperfections and found the (coupled) system of differential equations given by equations (2), (3) e (4).

$$\frac{\partial^4(w-w_0)}{\partial x^4}+2\frac{\partial^4(w-w_0)}{\partial x^2\partial y^2}+\frac{\partial^4(w-w_0)}{\partial y^4}=\frac{t}{D}\left(\frac{\partial^2F}{\partial y^2}\frac{\partial^2w}{\partial x^2}+\frac{\partial^2F}{\partial x^2}\frac{\partial^2w}{\partial y^2}-2\frac{\partial^2F}{\partial x\partial y}\frac{\partial^2w}{\partial x\partial y}\right) \quad (2)$$

$$\frac{\partial^4F}{\partial x^4}+2\frac{\partial^4F}{\partial x^2\partial y^2}+\frac{\partial^4F}{\partial y^4}=E\left[\left(\frac{\partial^2w}{\partial x\partial y}\right)^2-\left(\frac{\partial^2w_0}{\partial x\partial y}\right)^2-\frac{\partial^2w}{\partial x^2}\frac{\partial^2w}{\partial y^2}+\frac{\partial^2w_0}{\partial x^2}\frac{\partial^2w_0}{\partial y^2}\right] \quad (3)$$

$$\sigma_x=\frac{\partial^2F}{\partial y^2}\qquad \sigma_y=\frac{\partial^2F}{\partial x^2}\qquad \tau_{xy}=-\frac{\partial^2F}{\partial x\partial y} \quad (4)$$

where (i) w(x, y) and w_0(x, y) are the total and initial transverse (bending) displacements of the plate's midplane, (ii) σ_x, σ_x and τ_{xy} are the normal, membrane and tangential

stresses, (iii) t, D and E are, respectively, the thickness, bending stiffness and modulus of elasticity of the plate and (iv) F(x, y) is the tension function of Airy [18].

Levy [20], in 1942, expressed the flexural displacements of the plate in terms of a double Fourier series and arrived at an exact solution to the Von Kárman equations, for the case of a rectangular plate subjected to uniform uniaxial compression and with all edges simply supported and rigid (in the plane of the plate - see figure 2(a)). Later, Coan [21] used the same technique to approximately solve Marguerre's equations and determine post-buckling trajectories of rectangular plates with small initial imperfections and uniformly compressed. The two situations represented in Figure 2 were considered: (i) rigid longitudinal edges (the case studied by Levy) and (ii) edges free to defform. Figures 3(a) and 3 (b) show results obtained by Levy and Coan, respectively, consisting of (i) equilibrium paths (applied stress vs. mid-span deflection) for perfect and imperfect plates and (ii) distributions of normal membrane stresses in the post-buckling behaviour.

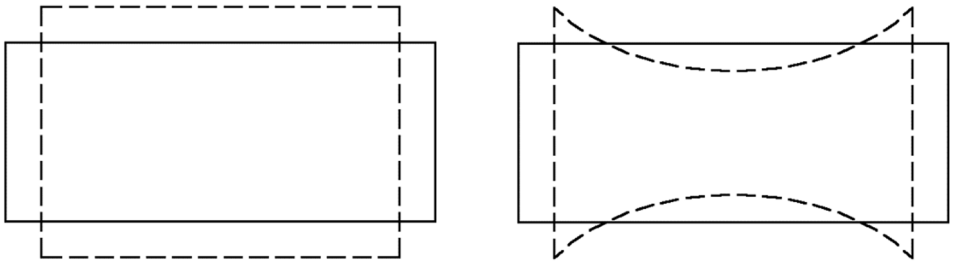

Figure 2 Support conditions: longitudinal edges: (a) rigid and (b) free. [7]

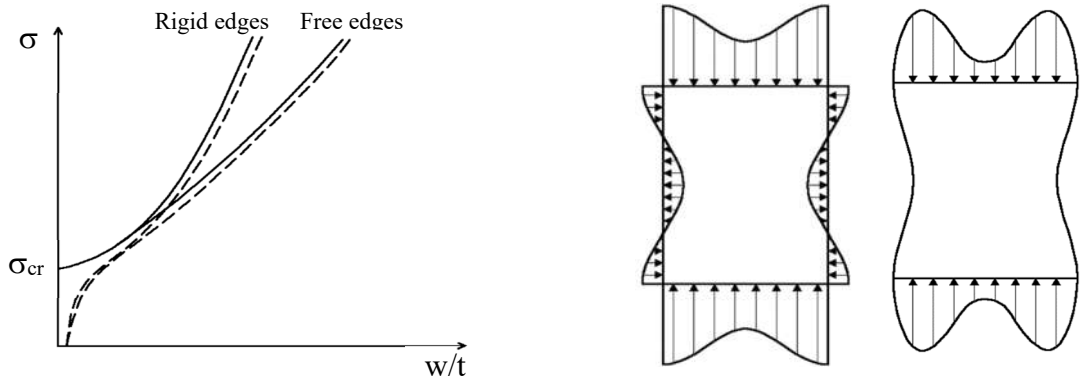

Figure 3 (a) Trajectories and (b) stress distributions (post-buckling behaviour). [7]

The stiffening of longitudinal edges introduces a significant increase in the post-buckling resistance of the plate. On the other hand, the configuration of the distribution of longitudinal normal stresses also changes, with the maximum value now located at the ends of the transverse edges. Regarding transverse normal stresses (self-equilibrated), it is important to note that tensions occurring in the central zone of the plate are the main contributors to the increased post-buckling resistance [7].

The difficulties arising from coupling the equilibrium equations, both Von Kárman and Marguerre, were largely overcome through the use of approximate methods, particularly energy methods [22]. Some of the most relevant works on this issue are described by Prola [7] and mentioned below:

(i) Yamaki [23] used the Galerkin method to study the post-buckling behaviour of plates, both perfect and imperfect, with different boundary conditions related to membrane and/or flexural displacements.

(ii) Rhodes and his collaborators [24, 25, 26, 27] studied the post-buckling behaviour of plates with various support conditions and subjected to different distributions of applied stresses.

(iii) Usami [28] employed an energy method to study the evolution of the distribution of longitudinal normal stresses along the post-buckling trajectory in simply supported rectangular plates subjected to combined bending with compression (linearly variable applied stresses), with the transverse and longitudinal edges being rigid and free, respectively (see Figure 2(b)). These results were later used to establish empirical formulas for estimating the post-buckling resistance of plates [29].

(iv) Sherbourne and Bedair [30] employed the Principle of Minimum Potential Energy to study the influence of boundary conditions related to membrane displacements and flexural rotations of longitudinal edges on the post-buckling behaviour of plates.

In more recent years, the tremendous progress in computational techniques and calculation methods has given numerical methods a prominent role in the analysis of nonlinear problems. Among these methods, the Finite Element Method (FEM) stands out for its efficiency, versatility, and generality. In the case of plate post-buckling, the first application of FEM is credited to Turner et al. [31] in 1960, and later, Brebbia and Connor

[32], Murray and Wilson [33], Yang [34], and Rerkshanandana et al. [35], for example, proposed other formulations of FEs to study these types of problems.

In the 21st century, with the development of finite elements for geometrically and physically nonlinear problems, the use of commercial finite element programs for studying the stability of compressed plates has become widespread. Figure 4 illustrates stress results obtained by Becque [38] by using Abaqus program [39].

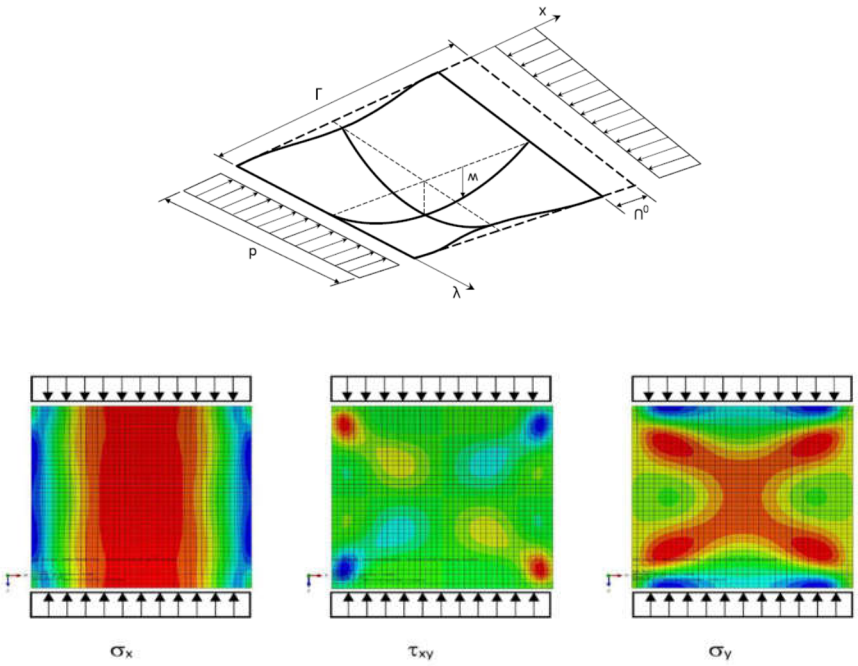

Figure 4 Plate stress obtained by Abaqus program [39]

FEM requires discretization that usually introduce a high number of degrees of freedom and lead to excessive computational effort. Therefore, the Finite Strip Method (FSM) gained popularity from the middle 1970s. By not discretising the structural element in the transverse direction, it provides a substantial savings in processing time. The work of Ueda et al. [40] is one of the first in which FSM is used to analyse the post-buckling of compressed plates. Subsequently, Graves-Smith and Sridharan [41], Gierlinski and Graves-Smith [42], Hancock [43, 44], Cheung and Li [45], and Bradford and Hancock [46] also studied the geometrically nonlinear behaviour of plates using FSM.

The computational implementation of a new finite strip for nonlinear stability analysis, formulated with "B3-Spline" functions and due to Kwon and Hancock [47], was tested

and validated by applying it to determine the post-buckling behaviour of plates with various boundary conditions and subjected to different distributions of applied stresses. Prola [7] used this formulation to develop a program based on splines finite strip.

1.1.3 Effective width concept

Figure 5 shows the evolution, with an increase in the level of applied stress, of the stress distribution along the transverse edges (considered rigid, see figure 2(a)) It can be observed that the stress (i) is uniform until the critical stress is reached and (ii) progressively the nonlinear behaviour becomes more pronounced.as the post-buckling phase of the plate progresses. In fact, normal stresses move away from the central zone and accumulate along the longitudinal edges, meaning that the plate's resistance capacity is concentrated in bands adjacent to these edges. The value of the maximum stress σ_e, which occurs at the ends of the transverse edges, can be adopted to characterize the evolution of the plate's behaviour along the post-buckling trajectory.

The concept of effective width (b_{eff})is used to characterize the plate's behaviour in the post-buckling phase, and it was proposed by Von Kárman et al. [48] in 1932. It can be defined as: "the width of a fictitious plate subject to a uniform stress distribution with a value of σ_e and statically equivalent to the stress distribution actually installed in the real plate" [49].

Thus, the determination of b_{eff}, illustrated in Figure 6, can be made through the relationship.

$$b_{ef} = \frac{\int_0^b \sigma_x(y)\ dy}{\sigma_e} = \frac{\sigma_m\ b}{\sigma_e} \tag{5}$$

where $\sigma_x(y)$ is the distribution of normal stresses installed on the transverse edge, of width b, and σ_m is its mean value. There is thus a one-to-one correspondence between the values of σ_e and b_{eff}, for $\sigma_m > \sigma_{cr}$ (post-buckling phase). Obviously, $b_{eff} = b$ for $\sigma_m \leq \sigma_{cr}$.

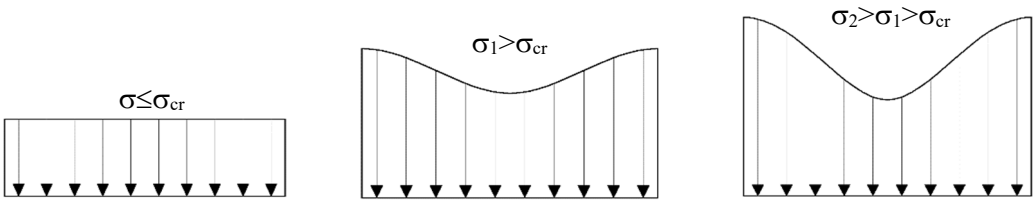

Figure 5 Evolution of the distribution of normal stresses on the transverse edges

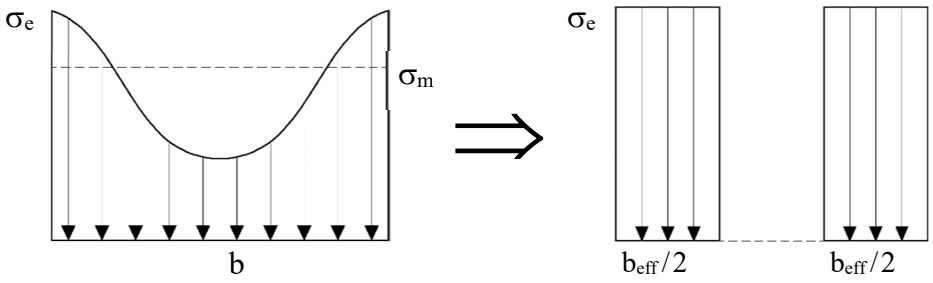

Figure 6 Effective width concept

The practical utility of the concept of effective width results from the fact that, by introducing it, Von Kárman also proposed the adoption of a semi-analytical strength criterion consisting of

(i) Equating the maximum stress installed in the real plate (σ_e) to the critical stress of a fictitious plate with width b_{eff}, which leads to the relation

$$b_{ef} = \sqrt{\frac{\sigma_{cr}}{\sigma_e}}\, b \tag{6}$$

(ii) Assuming that the collapse of the plate occurs when σ =fy, where fy is the yield stress of the steel constituting the plate. Thus,

$$\left(\frac{b_{ef}}{b}\right)_{colapse} = \sqrt{\frac{\sigma_{cr}}{f_y}} \equiv \frac{1}{\bar{\lambda}_p} \tag{7}$$

where $\overline{\lambda}_p$ is the known normalized slenderness of the plate.

Based on the analysis of a large number of experimental results, incorporating the influence of imperfections, Winter [50] proposed modifying the Von Kárman formula to equation (8) applied to cold-formed steel sections.

$$b_{ef} = \sqrt{\frac{\sigma_{cr}}{\sigma_e}}\left(1 - 0.25\sqrt{\frac{\sigma_{cr}}{\sigma_e}}\right) b \tag{8}$$

The expression corresponding to the collapse criterion is given in the equation (9).

$$\left(\frac{b_{ef}}{b}\right)_{colaps} = \sqrt{\frac{\sigma_{cr}}{f_y}} \equiv \left(1 - \frac{0.25}{\bar{\lambda}_p}\right)\frac{1}{\bar{\lambda}_p} \tag{9}$$

Later, the coefficient 0.25 was changed to 0.22 [30], and with this modification, formula (9) has been included in most steel construction codes. Despite the change in the coefficient, expression (9) is often referred to as the "Winter formula."

Recently, Becque [38] simplified the system given by expressions (2), (3), and (4) to just one equation, preserving the main mechanisms that affect the post-buckling behaviour of the plate. This yielded the following expression (10).

$$\frac{P_u}{P_y} = \frac{1}{3}\left(1 - \frac{2}{\bar{\lambda}_p}\right) \tag{10}$$

where P_u, is the ultimate load (which is reduced by a Winter-type coefficient) and P_y the yield load.

1.2 WORK ORGANISATION

The present dissertation is organized into five chapters, with the first being the Introduction and the last reserved for Conclusions and future works. Chapter 2 addresses the stability of members composed of thin-walled sections, and in Chapter 3, the proposal of the Effective Modulus Method (EMM) is described. Chapter 4 includes comparisons with experimental and numerical results.

Due to the theoretical background of the proposed method originating from an innovative criterion for the post-buckling strength of plates, the decision was made to begin the work, in Chapter One, with a historical review of critical and post-critical stability of plates, addressing the concept of effective width (based on a post-buckling strength criterion).

Following this, Chapter 2 provides a literature review on the stability of members consisting of thin-walled sections. This chapter is subdivided into (i) linear stability analysis and (ii) post-buckling behaviour. In addition to the literature review, illustrative examples of post-buckling stress distributions across the section of members for local and distortional modes are shown and analysed. This sets the stage for justifying the general concept of the effective modulus (of post-buckling), also illustrating examples of its distributions across the section.

In Chapter 3, the most significant part of the work, the Effective Modulus Method (EMM) is presented and explained. Starting from the derivation of the expression for the effective modulus deduced for an imperfection-free plate, the chosen expressions for the modulus of column and beam sections in local, distortional, and global modes are then presented. A calculation algorithm for interactions between these instability modes is also introduced.

Validation tests of the method on cold-formed steel profiles are conducted in Chapter 4, utilizing experimental data and numerical calculations (performed by the finite element method) available in the literature.

Finally, conclusions regarding the work are drawn, and suggestions for further studies are proposed.

1.3 OBJECTIVES OF THIS WORK

In a succinct manner, the main objectives intended to be achieved through the completion of this work are outlined as follows:

(i) Conduct a literature review on the stability of plates and thin-walled sections.

(ii) Justify the validity of the general concept of effective elasticity modulus based on the distribution of post-buckling stresses and strain in thin-walled sections.

(iii) Propose an expression for the effective modulus of an imperfection-free plate that relies on an innovative criterion for post-buckling strength.

(iv) Propose a calculation methodology (algorithm) for assessing the strength of structural elements (columns and beams) made of cold-formed steel, utilizing simplified formulas for effective modulus.

(v) Demonstrate the potential of the method, suggesting further studies for its future consolidation.

2. STABILITY OF COLD-FORMED PROFILES

2.1 LINEAR STABILITY ANALYSIS

A linear stability analysis provides critical loads and critical moments and their respective modes of instability (local, distortional and global). Figure 7 and Figure 8 illustrate characteristic instability modes for cold-formed profiles (in this case for C-sections), specifically for columns and beam, respectively.

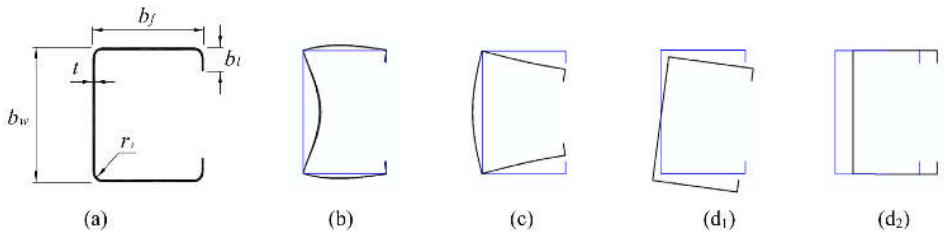

Figure 7 Lipped channel (a) geometry and cross-section deformed shapes associated with column (b) local, (c) distortional and (d) global (flexural-torsional (d_1) and flexural (d_2))

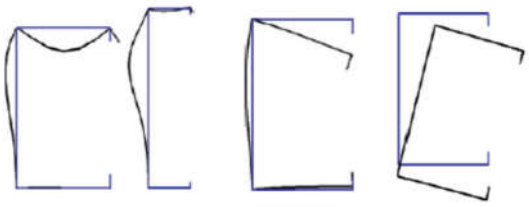

Figure 8 Lipped channel (a) local, (b) distortional and (c) global (flexural-torsional)

The linear stability analysis of a section, in comparison to that of an isolated plate, is complicated by the need to make compatible the rotations occurring at the longitudinal edges. The instability of the section can be analysed through the behaviour of any of its walls (plates), provided that the degree of rotation restraint at the longitudinal edges of that wall is precisely known. A conservative approach to the problem is to assume that this stiffness is zero, which is equivalent to saying that all longitudinal edges are hinged. Thus, the instability of each plate is independent of the others, and therefore, it is assumed that the bifurcation stress of the section is provided by its slenderness plate, assumed to have articulated (internal) longitudinal edges.

In his PhD thesis, Prola [7] develops a historical review of studies instability of thin-walled sections, which is described in the following paragraphs:

a) For local mode

(i) The first systematic and consistent analysis of section stability was carried out by Lundquist et al. [51] in 1943, using the method of moment distribution to solve the system of differential equilibrium equations for uniformly compressed sections. Their results were subsequently experimentally validated by Chilver [52].

(ii) Another approach was taken by Bleich [53] in 1952, who determined expressions for the bifurcation stress in the FEM by solving the differential equilibrium equations for each plate simultaneously with the satisfaction of static and kinematic boundary conditions related to the continuity of deformations at the longitudinal edges. Similar approaches were used by various authors, including Chilver [54] in 1953 and Bulson [55] about fifteen years later, who formulated the equilibrium equations in a matrix form whose coefficients depend nonlinearly on the load parameter (stress). The smallest value of this parameter that nullifies the determinant of the matrix provides the critical bifurcation stress of the section.

(iii) Walker [56], on the other hand, studied the stability of C-sections subjected to combined bending (linearly variable compression). He used a calculation model that considers separately the behaviours of (i) the web, treated as a uniformly compressed plate with rotation elastically restricted at the longitudinal edges, and (ii) the flanges, treated as plates subjected to variable compression, with one longitudinal edge articulated (flange- stiffener) and the other longitudinally elastic restrained (flange-web). The value of the bifurcation stress is obtained by imposing the condition of simultaneous instability on both plates.

(iv) Rhodes and Harvey [57] investigated the behaviour of U-sections subjected to eccentric compression (uniform compression in the web and linearly variable in the flanges), presenting results for various levels of eccentricity. They used an energetic method based on a specific formulation of the Principle of Stationarity of Deformations Energy (i.e., Potential Energy), which they had previously developed in the context of plate analysis [58, 59].

(v) With the advancement of automatic calculation tools and the emergence of effective computational techniques, especially the finite element method (FEM), there was a progressive substitution of analytical methods by numerical analyses from the second half

of the 1960s. This is reflected in the widespread use of the FEM to solve geometrically nonlinear problems, including linear stability analyses of structural elements. The works of Gallagher and Padlog [60], Kapur and Hantz [61], Wittrick [62], and Przemieniecki [63, 64] exemplify this trend, reinforced by the commercialization of increasingly versatile and sophisticated finite element programs (e.g., [39]). It is worth noting a work by Chin et al. [65], in which a thin plate element with 6 nodes and 30 degrees of freedom is formulated. The stiffness and geometric matrices were determined analytically, avoiding the need for numerical integration techniques, and the implemented FEM was applied to the linear stability analysis of sections with different geometric configurations and arbitrary boundary and loading conditions.

(vi) As mentioned earlier, when addressing the case of isolated plates, the formulation and computational implementation of a geometrically nonlinear finite strip by Przemieniecki [16] in 1973 decisively contributed to the current use of section stability analyses. The Finite Strip Method (FSM) was subsequently used by several researchers to study the FEM of sections with different geometries. In this context, the works of Graves Smith and Sridharan [66], Hancock [67], and Batista [68] can be mentioned.

(vii) Regarding developments in the FSM, it is important to mention, in addition to the contributions of Lau and Hancock [69] and Bradford and Azhari [70], the works of Khong [71] and Azhari and Bradford [72]. With the aim of improving the method's convergence (i.e., reducing the number of finite strips needed to obtain accurate results), these researchers proposed new functions to approximate flexural displacements in the transverse direction: 5^{th}-degree polynomials and "bubble" functions, respectively.

b) For distortional mode

(i) About distortional mode (DM) instability, Sharp addressed such a phenomenon in 1966 [73]. Only in 1978 a mode of instability with these characteristics was again mentioned in a study by Hancock [67] on the stability of I-section beams. Three years later, Desmond et al. [74, 75] referred to it as the stiffener instability mode" and attributed its occurrence to the stiffener t not being sufficiently rigid (wide) to prevent the membrane displacement of the longitudinal edge of the "reinforced" wall. Shortly after, Sridharan [76], in the context of the post-buckling analysis of C-sections, referred to it as the "local

torsion mode." However, despite this initial divergence, the term "distortional mode" is now universally accepted.

(ii) A decisive contribution to understanding the phenomenon of distortional mode instability is attributed to the work developed since the mid-1980s by a team of researchers at the University of Sydney, Australia, under the stimulus and guidance of G. Hancock. This research work, meticulously planned and executed, involved several aspects, including: (i) Identification, characterization, and analysis of the structural behaviour associated with the occurrence of distortional mode (DM) [77]. (ii) Formulation and implementation of computational tools particularly suited for conducting linear and nonlinear stability analyses of structural elements susceptible to instability in DM [78]. (iii) Planning and execution of a comprehensive set of experimental tests, conducted with great care and comprehensive instrumentation, which allowed for the construction of a significant and reliable database of results related to the instability of structural elements in DM [79, 80]. (iv) Development, validation, and calibration of approximate formulas and design rules that allow designers to easily assess the susceptibility of a structural element to DM instability [81].

(iii) Thus, in 1985, Hancock [77] published a paper, analytical and experimental, on the behaviour of columns in storage structures, presenting a detailed characterization of MD. In this work, the linear stability analysis (LSA) of the columns is performed using the Finite Strip Method (FSM), based on the finite strip formulated by Plank and Wittrick [82]. The fact that this formulation includes membrane deformations makes the detection of DM possible.

(iv) A little later, in 1987, Lau and Hancock [83, 84] developed analytical expressions to calculate bifurcation stresses in DM for sections subjected to uniform compression. For this, they considered structural models of the instability due to flexural-torsional coupling of a column with torsional rotations elastically restricted along a longitudinal edge. The authors also proposed simplified formulas. About ten years later, Hancock [85] developed and validated analogous simplified formulas, applicable to sections subjected to pure bending about the major axis of inertia. Finally, it should be noted that the same methodology was applied by Bambach et al. [86], in 1998.

(v) The results of linear stability analysis of sections that destabilize in DM, subjected to both uniform compression and pure bending, were used by Hancock et al. [87] to propose a design curve based on experimental results obtained by Kwon and Hancock [88, 89].

Presently, in most cases, computational programs are used for linear stability analysis. Among the various automatic calculation programs for linear stability analysis (critical stresses and their respective modes of instability), the following stand out, widely used by the technical and scientific community in the field of thin-walled profiles: (i) CUFSM, developed in the late 1990s by Schafer [90], based on the Finite Strip Method (FSM). (ii) THIN-WALL, developed at the University of Sydney, also based on FSM [91]. (iii) GBTUL, based on the Generalized Beam Theory (GBT) [92].

At the Polytechnic Institute of Leiria, the FSPLINES tool was developed, based on the Finite Strip Method with Splines Functions [93].

2.2 POST BUCKLING BEHAVIOUR

The nonlinearity of the equilibrium equations governing the behaviour of each plate (equations (2), (3) e (4)), makes it impossible to systematically obtain rigorous analytical solutions for thin-walled sections, with such solutions existing only for a limited number of problems. This is the case, for example, in the work of Benthem [94], who analytically studied the local post-buckling behaviour of a thin-walled column with a U-shaped section, achieving very precise results. However, it should be noted that all these results concern sections with a single geometric configuration (value of the ratio between the widths of the web and flanges).

Before the existence of sophisticated computational means, the post-buckling behaviour of sections could only be determined, in the general case, using approximate methods, which still involved a significant computational effort. Graves Smith [95, 96] deserves credit for obtaining the first estimate of the loss of stiffness caused by buckling in the local mode, in tubular columns with rectangular cross-section. He used the Rayleigh-Ritz method and assumed the simplifying hypothesis that the deformed configuration of the walls remains unchanged, which is (approximately) valid only in the initial phase of post-buckling. Later, he applied the same methodology to study the behaviour of box beams with a square section [97].

Rhodes and Harvey [98, 99, 100], in the 1970s, made a decisive contribution to understanding the phenomenon of post-buckling associated with local mode, through a series of works in which they analytically investigated the behaviour of "short bars" with U and C-shaped sections subjected to uniform and/or linearly variable compression. They used an energetic formulation, combined with the Rayleigh-Ritz method, and the obtained results consisted essentially of (i) estimates of the reduction in stiffness caused by local buckling and (ii) distributions of normal stresses in the post-buckling phase. It should be noted that these authors also compared their analyses with experimental results, published a few years earlier by Winter [50], observing an excellent correlation.

In the early 1980s, with the development of (i) geometrically nonlinear finite elements (namely, plate and shell finite elements) and (ii) specific numerical techniques to analyse problems involving large displacements, there was an exponential growth in the use of numerical methods (especially FEM and FSM) to study the phenomenon of post-

buckling, which persists to this day and will undoubtedly continue in the future. For this reason, the bibliography related to this domain is extremely extensive, and therefore, conducting a complete review is virtually impossible.

One of the first works to use the FEM was by Lee and Harris [100], who illustrated its application to the case of beams with U and hat-shaped sections. A little later, Desmond, Peköz, and Winter [74] investigated the influence of the presence and dimensions of end stiffeners on the local post-buckling of C-section bars. These authors also presented experimental results, and as mentioned earlier, detected the occurrence of the distortional mode.

In the context of local post-buckling of sections that Graves Smith and Sridharan [101] formulated the first finite strip (semi-analytical) to perform non-linear stability analysis and used the MFF to (i) determine equilibrium paths of U-sections uniformly compressed and (ii) estimate the stiffness reduction that occurs in them after bifurcation. Subsequently, Sridharan [102] also analysed sections subjected to variable compression (combination of compression and bending).

At the same time, Hancock [103] developed a formulation of finite strip similar to that of Graves Smith and Sridharan and used it to, together with several collaborators, study the local post-buckling behaviour of bars with different sections, often in the context of studies on interaction between local and global instability modes.

2.2.1 Distribution of post-buckling stresses

To illustrate the stress distribution across thin-walled sections, the results for C-sections are presented separately, concerning the behaviour of bars destabilizing in local and distortional modes. The results were obtained using the splines finite strip program developed by Prola [7].

In Figure 9, the evolution of the normal stress diagram in the mid-span section of the uniformly compressed member (column) is represented for the local mode of a profile supported at both ends. As evident, during the pre-buckling phase, the stress distribution remains uniform along the midline of the entire section.

Furthermore, the observation of this figure shows that in the post-buckling phase:

(i) The extreme values of normal stress occur in the central (smaller) and edge (larger) regions of the web. This is attributed to the web being the slenderest plate, thereby influencing and conditioning the post-buckling behaviour of the entire section.

(ii) Stresses remain relatively uniform in the flanges.

(iii) Stresses in the flanges "move away" from the central region and concentrate at the corners. This phenomenon is more pronounced at the connection corner to the web, explained by the fact that the web provides significantly higher bending stiffness to the flange.

(iv) Stresses in the web also move away from the central region and concentrate at the corners, despite the respective diagram being symmetrical now. It's worth noting that this stress transfer phenomenon is the basis of the concept of "effective width."

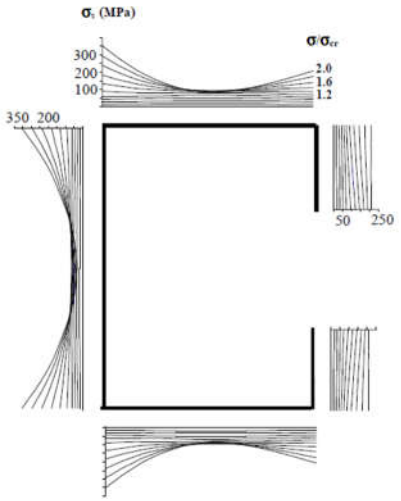

Figure 9 Evolution of the stress diagram in the mid-span section (column), local mode [7]

When the section is subjected to pure bending, instability in the local mode is influenced by the behaviour of the compressed flange, in the middle of which the highest displacement (bending) values occur. In fact, although the web is slenderer than the flange, the fact that the flange is uniformly compressed makes it more susceptible to the phenomenon of flexural instability.

In Figure 10 the evolution of the normal stress diagram in the mid-span section of the bar is represented. Obviously, during the pre-buckling phase (i.e., until $\sigma/\sigma_{cr} \approx 1.0$), the stress distribution remains uniform in the flanges and linearly variable in the web and stiffeners. Regarding the post-buckling phase, the observation of the figure 10 shows that:

(i) In the compressed flange (plate that influences and conditions the post-buckling behaviour of the entire section), the stress distribution is similar to that presented in Figure 9 (although the "asymmetry" decreases), corresponding to the uniformly compressed section.

(ii) In the tensioned flange, the stress diagram remains practically uniform along the entire equilibrium path (there is a small variation for high values of (σ/σ_{cr})).

(iii) In the web, tensile stresses remain linearly variable along the entire equilibrium path. The same does not happen with compressive stresses, where the linear trend is progressively lost due to a transfer from the central zone to the corner connecting to the compressed edge. This phenomenon can also be modelled through the concept of "effective width," now applied to partially compressed plates (walls).

(iv) In the compressed and tensioned stiffeners, the evolution of the stress diagrams exhibits characteristics similar to those of the compressed and tensioned zones of the web. It is important to note that the width of the stiffeners is about 12% of the width of the web and, Therefore, is represented on an exaggerated scale (compared to the rest of the section). However, this fact gives the impression (false) that the tensile stresses (pre- and post-buckling phases) and compressive stresses (pre-buckling phase) are practically constant. In reality, this is not the case, and these stresses are linearly variable (the variation is analogous to that occurring in the corresponding zones of the web).

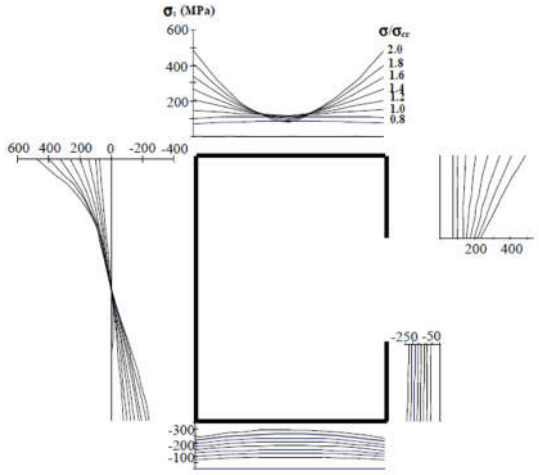

Figure 10 Evolution of the stress diagram in the mid-span section (beam), local mode. [7]

The essential characteristic of the distortional mode lies in the occurrence of displacements of the internal longitudinal edges ("corners" of the section), which means that it is essentially associated with membrane deformations of the walls adjacent to these longitudinal edges, contained in different planes. In the case of the C-section, distortion involves the flange- stiffener assemblies. The most suitable way to describe the post-buckling behaviour of a bar in this case is through the evolution of the transverse displacement of the "flange- stiffener corner," designated as "v_{b-r}," which is used to represent its nonlinear equilibrium path.

Firstly, it is convenient to mention a phenomenon that is specific to distortional instability (i.e., not relevant to local instability) and is of great importance in its characterization. This phenomenon is related to the fact that distortional mode is not symmetrical regarding the longitudinal displacements caused by the warping of the cross-sectional shapes of the bars, especially in the stiffener zones. In reality, it has been observed that, as illustrated in Figure 11:

(i) The fields of longitudinal displacements caused by the warping of the sections in the stiffeners and, to a much lesser extent, in the flange areas adjacent to the flange- stiffener corners are qualitatively different.

(ii) When distortions are negative (increasing web-flange angles - see Figure 11 (a)), a situation where it is conventionally assumed that the values of v_{b-r} are positive, the deformed configuration of the stiffeners (warping) is characterized by higher

displacements at the free ends, i.e., it is analogous to that of a beam subjected to negative bending moments.

(iii) When distortions are positive (decreasing web-flange angles - see Figure 11 (b)), a situation where it is conventionally assumed that the values of v_{b-r} are negative, precisely the opposite occurs, i.e., displacements are lower (negative) at the free ends, and the deformed configuration is analogous to that of a beam subjected to positive bending moments.

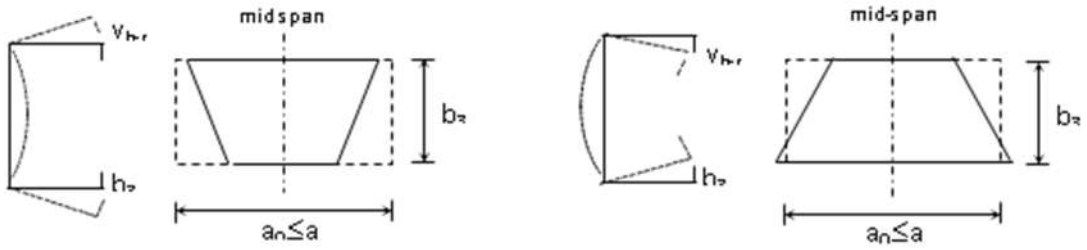

Figure 11 Characterization of warping caused by distortional instability. [7]

Figure 12 (a)-(b) show, for positive and negative values of v_{b-r}, the evolution of the diagrams of normal stresses installed in the mid-span section of the bar. Observing the two sets of four diagrams (σ/σ_{cr}=0.8-1.0-1.2-1.4) allows us to conclude that, regardless of the direction of v_{b-r}:

(i) In the pre-buckling phase, the stress distribution remains uniform along the midline of the entire section.

(ii) The trend of the stress distribution in the web is similar to what was observed for the post-buckling associated with the local mode (see Figure 11), although the non-linearity is less pronounced. Moreover, since the applied stress levels are much lower, the stress values are also significantly lower.

The influence of the direction of v_{b-r} is very noticeable in the trend of the stress distribution in the post-buckling phase (σ/σ_{cr}>1.0), especially in the stiffener and in the areas of the flanges near the flange-stiffener corners. Thus, it is observed that:

(i) When the values of v_{b-r} are positive (Figure 12 (a)), the progression of the post-buckling phase causes compressive stresses (i1) to move away from the flange-stiffener corners and (i2) to concentrate near the web-flange corners and, especially, near the free ends of the stiffener. For values of σ/σ_{cr} not much higher than 1 (e.g., $\sigma/\sigma_{cr} \geq 1.2$), the stresses in the vicinity of the flange-stiffener corners even become tensile. The (by far) highest stresses are located near the free ends of the stiffener, where the largest longitudinal displacements due to the warping of the section occur (see Figure 12 (a)). Their values can exceed more than 15 times the critical stress associated with the distortional mode.

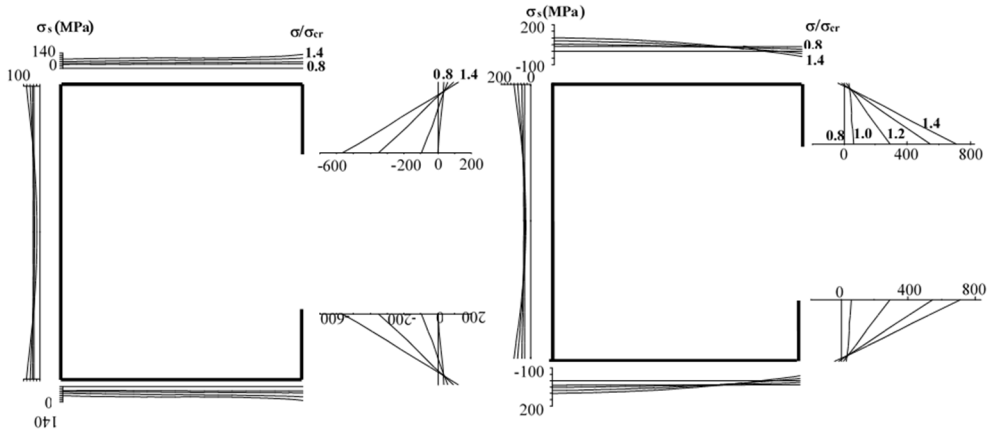

Figure 12 Evolution of the stress diagram in the mid-span section (column) in distortional mode. [7]

a) Positive values of v_{b-r} and (b) Negative values of v_{b-r}

Finally, it should be noted that the fact that the stress distribution in the section is radically different for both $v_{b-r} > 0$ and $v_{b-r} < 0$, compared to the post-buckling associated with the local mode explains the issues raised by the use of the effective width concept in assessing the ultimate strength of compressed bars whose local instability is controlled by the distortional mode. In reality, as the progression of post-buckling stresses in the flanges and stiffener is completely different, the theoretical foundations underlying the application of the concept, including the use of the Winter formula, lose all validity. In particular, it is not possible to adequately predict the high stress values located at the free ends of the stiffeners, which likely precipitate the collapse of the bar.

Finally, as done for uniform compression, Figure 13 (a)-(b) show the evolution of the stress diagram in the mid-span section (σ_s) for $v_{b-r} > 0$ and $v_{b-r} < 0$ in the case of a section subjected to a bending moment (beam). In addition to confirming that the trend of these stresses does not change in the pre-buckling phase, the observation of the diagrams allows us to conclude that:

(i) In the upper flange and stiffener(compressed), which influence the post-buckling behaviour of the entire section, the evolutions of the stress diagrams are similar to those shown in Figure 12(a)-(b) for the case of a section subjected to uniform compression.

(ii) As only tensile stresses are present in the lower flange and stiffener, the trend of the corresponding diagrams does not change along the post-buckling path.

(iii) In the web, the trends of the stress diagrams are similar to what was obtained for post-buckling associated with the local mode. Thus, tensile stresses remain linearly variable, and compressive stresses progressively lose that linearity due to the occurrence of a transfer towards the corner of the web-compressed flange.

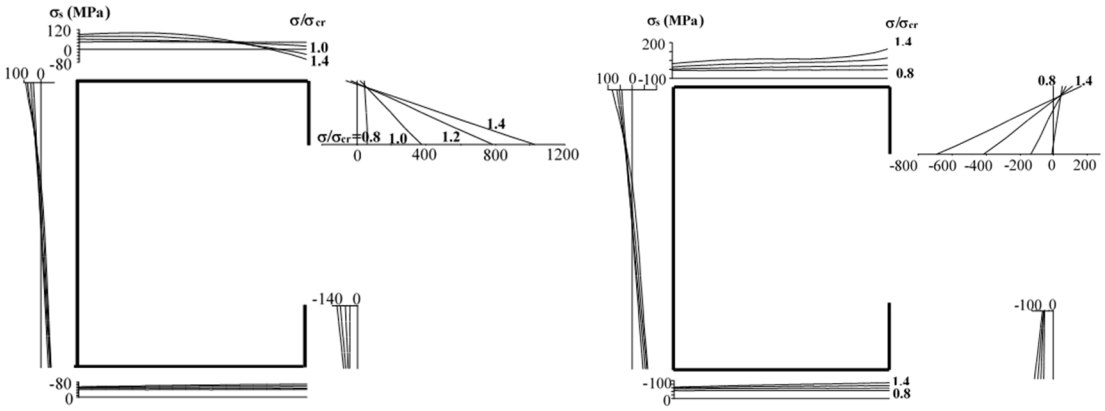

Figure 13 Evolution of the stress diagram in the mid-span section (beam) in distortional mode [7] (a) Positive values of v_{b-r} and (b) Negative values of v_{b-r}.

2.2.2 Distribution of elasticity modulus

The determination of the structural behaviour and ultimate strength of bars with open thin-walled sections subjected to combinations of forces involving compression generally requires the simultaneous consideration of local, distortional, and global instability phenomena, particularly the associated post-buckling effects. However, the complexity and computational effort involved in implementing structural analysis methods that directly account for these two aspects make their use impractical in common applications. To overcome this difficulty, methods for the indirect consideration of local post-buckling effects have been proposed by incorporating them into structural analyses of the others instability behaviour of the bars [104, 105]. This procedure is usually carried out using the concept of effective width, which simulates the effects of local post-buckling by altering the geometry of the cross-sectional shapes of the members. However, it should be noted that the concept of effective width was proposed, justified, and calibrated in the context of post-buckling associated with the local mode [50], which makes its application to bars with local instability occurring in the distortional mode questionable and without theoretical support.

It is known that the primary consequence of the presence of instability phenomena in the compressed walls of a member (the local and distortional instability) is the reduction of its axial, bending, and torsional (warping) stiffness values [2]. Thus, in the context of determining the global behaviour of the bar, it is possible to consider the influence of local instability effects (i.e., account for the interaction between local, distortional and global instability modes) through the use of a reduced stiffness of the unstable section.

The concept of "effective modulus of elasticity" (E_{eff}) is based on the principle of substituting the effects of local post-buckling (geometric nonlinearity) with a change (fictitious) of the material that constitutes the cross-sectional shape, specifically its modulus of elasticity [5]. In summary, it is as if the deformations of the cross-sectional shape were exchanged for a weakening of the material that constitutes it. To provide a better understanding of this concept, Figure 14 (a) and 13(b) illustrate its application to the case of a column (uniformly compressed bar) with a C-section that buckles, respectively, in the local mode (LM) and in the distortional mode (DM).

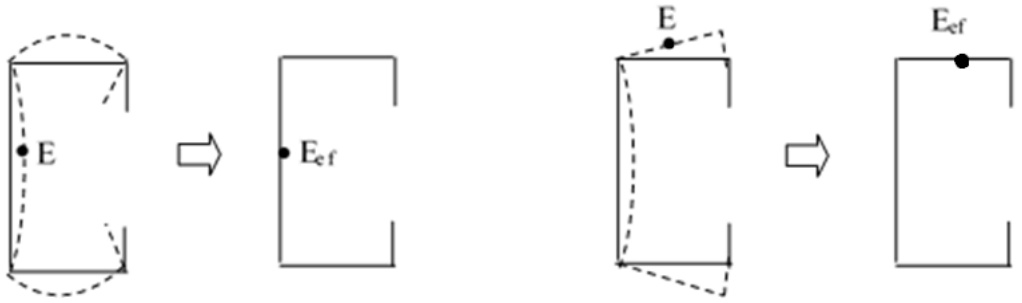

Figure 14 Effective modulus of elasticity (E_{eff}) concept: (a) LM (b) DM.

Prola [7] calculated the average values of the bar lengths of the elasticity modules (see Equation 11) through a geometrically nonlinear analysis using a spline finite strip program, obtaining effective modulus diagrams for local and distortional modes, where the effective modulus is determined by the variation of stresses over the variation of strains in each equilibrium point of the incremental-iterative process.

$$E_{eff} = \frac{\Delta\sigma}{\Delta\varepsilon} \tag{11}$$

Figure 15 depicts the evolution of the effective modulus diagram (E_{eff}/E) for a uniformly compressed bar. The values of E_{eff} are presented for six levels of applied stress (σ/σ_{cr}=0.6–0.8–1.0–1.2–1.4–2.0) and were obtained from a post-buckling analysis that includes a geometric imperfection in the shape of the local mode with an amplitude equal to 10% of the section wall thickness.

From the observation of the E_{eff}/E diagrams presented in Figure 15, the following conclusions can be drawn:

(i) As expected, as the applied stress level approaches the critical bifurcation stress (σ_{cr}=78.8 MPa), and particularly after surpassing that value, the effective modulus diagram begins a process of deviation (reduction, to be more precise) from its original configuration – uniform and with a value equal to E (E_{eff}/E=1).

(ii) Clearly, the areas of the section walls where geometrically nonlinear effects induce larger deformations (and consequently, lower stresses – see Figure 9) are precisely those

where a reduction in E_{eff} values is observed. In this particular case, this reduction occurs primarily (ii_1) in the central zone of the web (mainly), (ii_2) in the central zones of the flanges (also significantly), and (ii_3) at the free ends of the stiffeners (to a lesser extent). Note that the web, on a larger scale, and the flanges are the walls whose behaviour conditions the instability of the section. Near the web-flange and flange-stiffener corners, the decrease in axial stiffness is much less pronounced and only becomes evident in advanced stages of post-buckling.

(iii) For σ/σ_{cr} =2.0, the value of the E_{eff}/E ratio reaches approximately (iii1) 10% in the middle of the web and flanges, and (iii2) 55% at the free ends of the stiffeners.

(iv) Even for $\sigma/\ \sigma_{cr}$ =0.8, a noticeable reduction in effective modulus values is already observed in the "weaker" zones of the section. In fact, the E_{eff}/E ratio drops to about (iii1) 90% in the middle of the web and flanges and (iii2) 95% at the free ends of the stiffeners. This relatively early loss of stiffness is due to the presence of geometric imperfections.

(v) The decline in E_{eff} values is more pronounced in the vicinity of $\sigma/\ \sigma_{cr}$ =1.0. Note that for $\sigma/\ \sigma_{cr}$ >1.4, the variation of effective modulus becomes almost meaningless, especially in the web (the diagrams for $\sigma/\ \sigma_{cr}$ =1.4 and $\sigma/\ \sigma_{cr}$ =2.0 are very close to each other).

(vi) As expected, there is a significant analogy between the concepts of "effective width" and "effective modulus," as both aim to exactly represent the same phenomenon (post-buckling associated with the local mode). Thus, the lower values of E_{eff}/E are precisely located in the ineffective zones of the section.

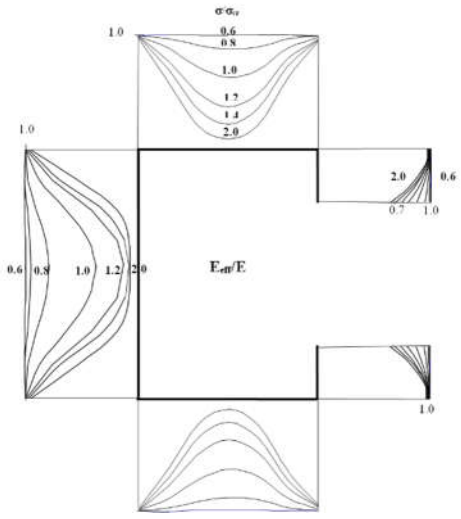

Figure 15 Evolution of the effective modulus diagram, uniform compression, local mode. [7]

When the short bar is subjected to pure bending, instability (in the local mode) is conditioned by the behaviour of the compressed flange (upper), and only the following are compressed: (i) the web (partially - upper half), (ii) the upper flange (uniform compression), and (iii) the upper stiffener (linearly variable compression). Thus, the effects of post-buckling only occur in these (zone of) walls, meaning that a reduction in the values of the effective modulus E_{eff} will only occur there. This is evident in the diagrams presented in Figure 16, which show the evolution of the E_{eff}/E diagram. In addition to what has already been mentioned, it is also observed that (for $\sigma/\sigma_{cr} > 0.6$):

(i) In the vicinity of the midpoint of the web, there is a sharp variation in the values of the effective modulus, corresponding to the transition between its tensile and compressed zones.

(ii) In the compressed zone of the web, the minimum values of E_{eff} occur about one-eighth of the width above its midpoint. As was the case for the uniformly compressed bar, in the vicinity of the web-flange corner, the values of the effective modulus practically do not change.

(iii) As expected, in the compressed flange and stiffener, the trend and evolution of the E_{eff}/E diagrams are entirely analogous to those determined for the uniformly compressed bar. Note that in this case, the instability of the section is essentially conditioned by the compressed flange (upper).

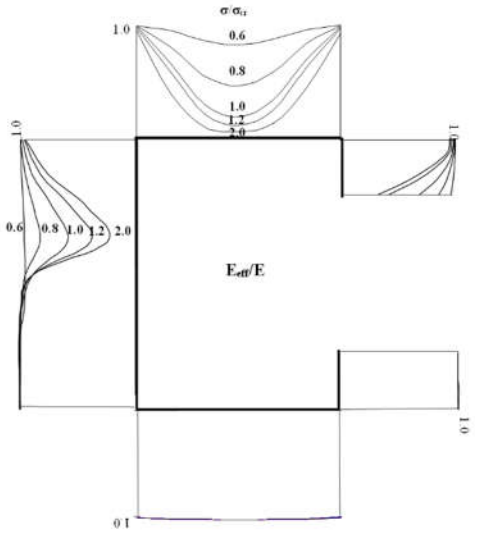

Figure 16 Evolution of the effective modulus diagram, pure bending, local mode.

The diagrams of effective modulus (E_{eff} /E) presented in Figure 17 and Figure 18 correspond to uniformly compressed bars with hinged end sections, for the distortional mode. In both cases, the initial imperfection has the shape of the critical mode of instability and an amplitude of 10% of the thickness.

The distortional post-buckling behaviour of a uniformly compressed bar (and, in particular, the evolution of the distribution of normal stresses) varies with the sign of the membrane displacements of the flange-stiffener corners (v_{b-r}), i.e., with whether the flange-stiffener sets "open" ($v_{b-r} > 0$) or "close" ($v_{b-r} < 0$). Therefore, it is expected that the values of effective modulus also depend on the sign of v_{b-r}, making it essential to determine E_{eff} /E diagrams for both situations.

The observation of the E_{eff}/E diagrams presented in Figure 17 & Figure 18 shows significant differences between the E_{eff} diagrams related to (i) post-buckling associated with the distortional mode and the local mode (see Figure 14) and (ii) distortional post-buckling with $v_{b-r} > 0$ and $v_{b-r} < 0$. Furthermore, these diagrams also allow us to conclude that:

(i) Regardless of the sign of v_{b-r}, there are significant reductions in stiffness in the central zone of the web, with E_{eff} values even becoming negative in the post-buckling phase ($\sigma/\sigma_{cr} > 1.0$). These reductions (i1) occur earlier when $v_{b-r} > 0$ (see the two diagrams for $\sigma/\sigma_{cr}=1.0$), but (i2) end up being more significant in the post-buckling phase when $v_{b-r} < 0$ (see the diagrams for $\sigma/\sigma_{cr}=1.4$). Note the small dip in E_{eff} values at the flange-web corners (the maximum values occur slightly inside).

(ii) In the flanges, effective modulus values decrease significantly as one moves from the flange-web corner to the flange-stiffener corner (except for a small disturbance near the flange-web corner). This reduction is more significant when the section "opens" (v_{b-r} values are positive), in which case E_{eff} values even become negative near the flange-stiffener corner (recall that tension stresses develop in that section area).

(iii) In the stiffeners, the E_{eff}/E diagram behaves entirely differently depending on whether v_{b-r} values are positive (section "opens") or negative (section "closes"). In the former case, E_{eff} values increase from the flange-stiffener corner to the free end, while in the latter case, the opposite occurs. In either case, the variation is almost linear and quite pronounced, particularly in the advanced post-buckling phase (i.e., for $\sigma/\sigma_{cr} \geq 1.0$).

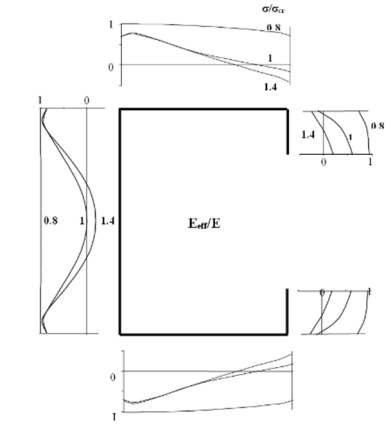

Figure 17 Evolution of the effective modulus diagram, uniform compression, distortional mode with $v_{b-r} > 0$ [7].

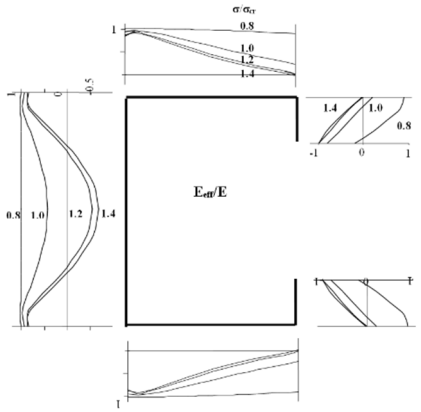

Figure 18 Evolution of the effective modulus diagram, uniform compression, distortional mode with $v_{b-r} < 0$ [7].

Next the diagrams of the effective modulus (E_{eff}/E), related to the distortional post-buckling behaviour of two bars subjected to pure bending, which exhibit, respectively, positive values of v_{b-r} (upper flange-stiffener corner, i.e., compressed) causing the section to "open" (Figure 19) and negative values of v_{b-r} causing the section to “close" (Figure 20), are presented.

Firstly, it is noteworthy that, as expected, a reduction in axial stiffness occurs only in the upper half of the section, i.e., in its compressed zone. Additionally, similar to the case of uniformly compressed bars, there are significant differences between the E_{eff}/E diagrams for positive and negative values of v_{b-r} (especially in the upper stiffener).

From the observation of the diagrams presented in Figure 19 & Figure 20, it can be concluded that:

(i) In the upper compressed flange and stiffeners, the diagrams of effective modulus are practically identical to those obtained for uniformly compressed bars, both for $v_{b-r} > 0$ and $v_{b-r} < 0$.

(ii) In the web, the most significant reductions in the value of E_{eff} occur in the central zone of the upper half (compressed). It should also be noted that the transition between the compressed ($E_{eff} < E$) and tensile ($E_{eff} = E$) zones is relatively abrupt.

(iii) In the web, the reduction in stiffness is always (slightly) greater for $v_{b-r} < 0$. Recall that, in the case of uniformly compressed bars, this reduction started earlier (lower value of σ/σ_{cr}) for positive values of v_{b-r} (see Figure 17 & Figure 18)

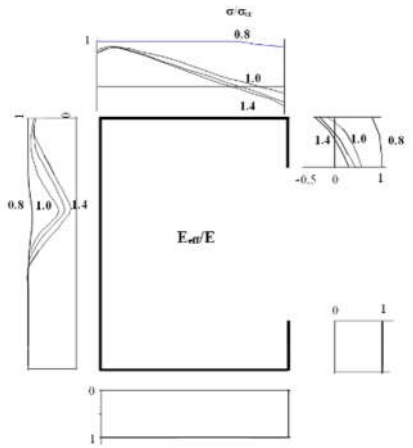

Figure 19 Evolution of the effective modulus diagram, pure bending, distortional mode [7]

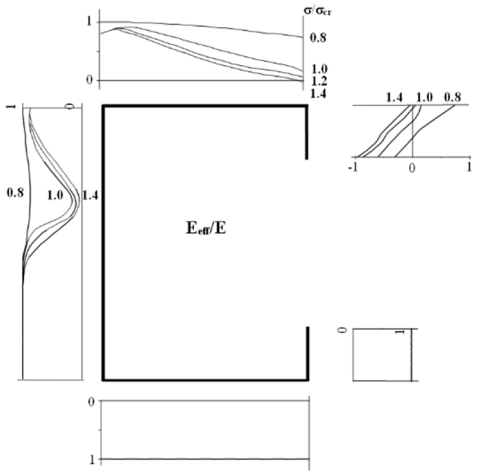

Figure 20 Evolution of the effective modulus diagram, pure bending, distortional mode with $v_{b-r} < 0$ [7].

3. CONCEPT OF THE EFFECTIVE MODULE

Effective Modulus Method (EMM) is a methodology which has already been suggested by Rasmussen [1-3] and later studied by Camotim and Prola [4, 5], it postulates that the effects of local and distortional instability modes are indirectly accounted in the global strength of uniformly compressed columns by reducing their nominal modulus of elasticity E.

Lowering the nominal modulus of elasticity, affects the value of the global critical strength of the column, which directly influences the axial resistance. A new (fictitious) decreased Modulus of Elasticity is assumed. This adjustment modifies the material's mechanical properties, introducing a new modulus of elasticity influenced by local and distortional instabilities. Regardless of the column's global instability mode (whether flexural or flexural-torsional, typical in thin-walled steel structures), the critical load is found to be linearly related to the modulus of elasticity. This relationship simplifies calculating the column's critical load, as shown in Equation (12).

$$f_{crG}(E_{eff}) = \chi_{LD} \cdot f_{crG}(E) \tag{12}$$

where $f_{crG}(E_{eff})$ represents the global critical stress of the column with an effective modulus of elasticity E_{eff}, $f_{crG}(E)$ is the critical stress of the column with nominal modulus of elasticity E and χ_{LD} is the reducing factor that considers local and distortional mode effects, given by Equation (13)

$$\chi_{LD} = \frac{E_{eff}}{E} \tag{13}$$

3.1DISTRIBUTION OF EFFECTIVE MODULUS

3.1.1 Concept of Effective Modulus for plates

Upon examining the post-buckling stress distribution in simply supported plates on all edges subjected to uniform compression—as described by Koiter's theory [107,108], and depicted in Figure 21 (a)—Von Kármán [17] proposed the Effective Width Method (EWM) as a solution to this issue, which is illustrated in Figure 21 (b). This method accounts for the effects of post-buckling strength by altering the plate's geometry. In Figure 21, σ denotes the applied stress, σ_{cr} represents the critical stress, σ_e signifies the maximum (edge) stress, σ_m indicates the average stress, b is the width, and b_{eff} is the effective width of the plate. Von Kármán established Equation (14), utilizing the equilibrium of the stress resultants as shown in Figure 21 (b), to define the effective width of a plate devoid of initial imperfections, which involves a reduction coefficient.

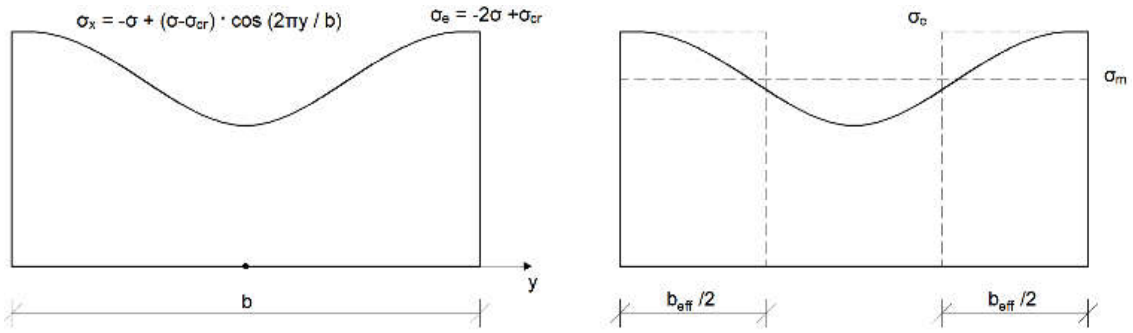

Figure 21 (a) post-buckling stress distributions and (b) models for stress resultants

$$\chi_p = \frac{b_{eff}}{b} = \frac{1}{\lambda_p} \tag{14}$$

where the slenderness λ_p is given by Equation (4):

$$\lambda_p = \sqrt{\frac{\sigma_e}{\sigma_{cr}}} \tag{15}$$

In the same Figure 21 (a), it can be found Equation (16) that relates the edge, mean and critical stresses of the plate, which can be presented in the form of Equation (17).

$$\sigma_m = \frac{\sigma_{cr}+\sigma_e}{2} \tag{16}$$

$$\frac{\sigma_m}{\sigma_e} = \frac{1}{2}\left(1 + \frac{1}{\lambda_p{}^2}\right) \tag{17}$$

In the context of post-buckling analysis, an effective modulus of elasticity, E_{eff}, is defined to correlate the limit strain ε_e with the mean stress σ_m, as depicted in Figure 22. The effective modulus of elasticity is determined as the value that yields the plate to its maximum strain capacity. By considering that $\sigma_m = E_{eff*}\varepsilon_e$ and $\sigma_e = E\varepsilon_e$, and substituting these into Equation (17), one derives the reduction factor for the modulus of elasticity, χ_m defined in Equation (18).

$$\chi_m = \frac{E_{eff}}{E} = \frac{1}{2}\left(1 + \frac{1}{\lambda_p{}^2}\right) \tag{18}$$

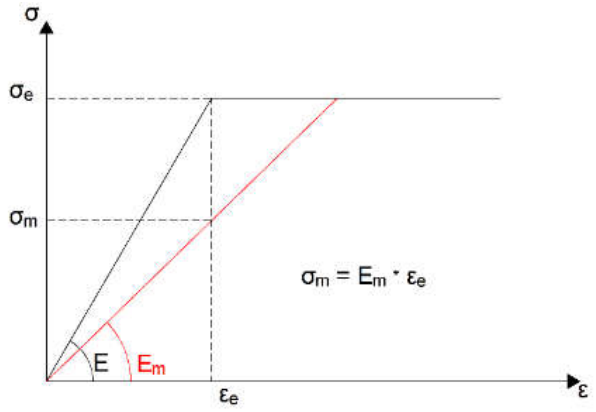

Figure 22 Definition of the effective modulus of elasticity of a plate

3.1.2 Concept of Effective Modulus for a Cross-Section

The formulas of the effective width method for the components of a cross-section (such as flanges, webs, and stiffeners) must reflect the impact of initial imperfections in the member and the level of rotational restraint provided by connected plates (web-flange, flange-stiffener interactions). This approach ensures that the collective behaviour of all component plates is considered. Drawing on empirical data, Winter [50,13] suggested an amendment to Von Kármán's effective width formula (Equation (14)) by incorporating a multiplier factor, yielding Equation (19).

$$\chi_L = \frac{b_{eff}}{b} = \left(1 - \frac{0.22}{\lambda_L}\right)/\lambda_L \text{ with } \lambda_L = \sqrt{\frac{\sigma_e}{f_{crL}}} \quad (19)$$

where f_{crL} is the critical buckling stress of each plate of the cross-section.

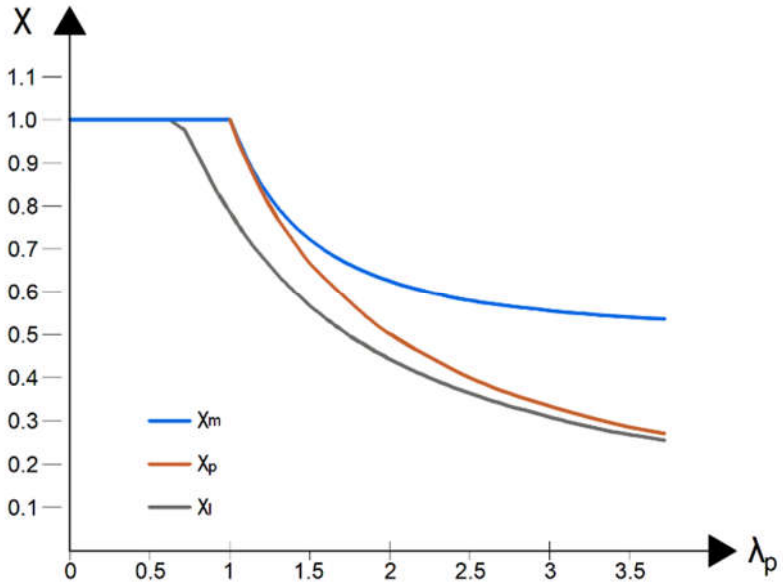

Figure 23 Effective width and effective modules reducing factors.

Figure 23 illustrates the variation of the reduction coefficients according to (i) Von Kármán, (ii) Winter and (iii) effective modulus. It is observed that the corrections suggested by Winter (equation (19)) decrease the Von Kármán reduction factor (equation (14)). The same should happen with correction factors to be applied to effective modules of the whole section.

The formula adopted by the AISI S100-16 [109] for the load reducing factor of the Direct Strength Method (DSM), initially proposed by Shaffer and Peköz [111,112], is defined in Equation (20).

$$\chi_L = \frac{b_{eff}}{b} = \left(1 - \frac{0.15}{\lambda_L^{0.8}}\right)/\lambda_L^{0.8} \text{ with } \lambda_L > 0.776 \quad (20)$$

In this context, λ_L is consistent with Equation (8), but f_{crL} pertains to the critical stress of the entire cross-section.

For distortional buckling modes, the DSM utilizes Equation (21) [39,119,120,121]:

$$\chi_D = \frac{b_{eff}}{b} = \left(1 - \frac{0.25}{{\lambda_D}^{1.2}}\right)/{\lambda_D}^{1.2} \text{ with } \lambda_D > 0.561 \quad (21)$$

where $\lambda_D = \sqrt{\sigma_e / f_{crD}}$ and f_{crD} is the critical distortional stress of the cross-section.

As observed in Figure 23, it would be necessary to adapt the coefficients of Equation (18) to apply the EMM to cross-sections. For this purpose, a campaign of comparisons with experimental and numerical data will be necessary, which the authors intend to perform in the future. For the present work, the EMM will use the same reducing coefficients as the DSM (see Equations (20) and (21)), applying it to the modulus of elasticity.

3.2 PROPOSAL FOR THE EFFECTIVE MODULUS METHOD, COMPRESSION

In the course of this work, two distinct approaches for analysing buckling modes in structural elements were examined and tested. The first approach LD adheres to a sequential methodology, starting with the local buckling critical load, progressing to distortional, and culminating with the global critical load. This hierarchical progression is premised on the notion that local instabilities typically manifest at lower stress levels, followed by distortional and then global instabilities as the load increases. By addressing the modes in this order, the analysis aims to reflect the actual physical progression of buckling in structures.

After obtaining the critical loads of the specimens with a software, like GBTUL [92] or similar, the EMM is calculated as follows:

(i) Local mode:

$$\alpha_L = \frac{f_{crL}}{f_y} \quad (22)$$

$$\lambda_L = \sqrt{\frac{1}{\alpha_D}} \quad (23)$$

$$\begin{cases} \chi_L = 1 & \lambda_L \leq 0.776 \\ \chi_L = \left(1 - 0.15{\lambda_D}^{-0.8}\right){\lambda_D}^{-0.8} & \lambda_L > 0.776 \end{cases} \quad (24)$$

(ii) Distortional mode:

$$\alpha_D = \frac{f_{crD}}{f_y} \tag{25}$$

$$\lambda_{LD} = \sqrt{\frac{\chi_L}{\alpha_D}} \tag{26}$$

$$\begin{aligned} \chi_D &= 1 && if \quad \lambda_D \leq 0.561 \\ \chi_D &= \left(1 - 0.25{\lambda_D}^{-1.2}\right){\lambda_D}^{-1.2} && if \quad \lambda_D > 0.561 \end{aligned} \tag{27}$$

Recent investigations by Martins et al. [119] have revealed that the (NDL) Approach provides an accurate prediction of experimental outcomes. According to this method, if the ratio between distortional and local critical stresses is less than 0.7, only the reduction attributed to distortional buckling is considered. Should this ratio exceed 0.8, it becomes necessary to account for the interaction between distortional and local buckling modes. In such scenarios, the critical load for the local mode is influenced by a decrease in the modulus of elasticity resulting from distortional effects—a calculation that is determined beforehand. For intermediate values of this ratio, the approach suggested by Martins et al. [119] is utilized, modified accordingly to fit the reduction of the modulus of elasticity.

After determining χ_L and χ_D the reduction factor χ_{LDG} , which considers de effects of local/distortional on global mode, is determined according to a convergence condition based on the ratio of the distortional/local critical stresses as shown in Equations 28 and 29. The convergence condition is given by equations (28) and (29).

$$DL = \frac{f_{crD}}{f_{crL}} \tag{28}$$

For $DL \leq 0.7$ use χ_D

For $DL \geq 0.8$ use χ_{DL}

For $0.7 \leq DL \leq 0.8$ use $\overline{\chi_{LD}} = \chi_L - \left[\left(\frac{\chi_L - \chi_{LD}}{0.1}\right)\left(\frac{f_{crD}}{f_{crL}} - 0.7\right)\right]$ (29)

(iii) Global mode:

$$\alpha_G = \frac{f_{crG}}{f_y} \tag{30}$$

$$\lambda_{LDG} = \sqrt{\frac{\chi_{DL}}{\alpha_G}} \tag{31}$$

$$\begin{cases} \chi_{DLG} = 0.658^{{\lambda_{DLG}}^2} & \lambda_{LDG} \leq 1.5 \\ \chi_{DLG} = \frac{0.877}{{\lambda_{DLG}}^2} & \lambda_{LDG} > 1.5 \end{cases} \tag{32}$$

The second approach DL inverts the sequence LD, starting with the distortional buckling mode, followed by the local, and finally the global mode.

After obtaining the critical loads of the specimens with a software, like GBTUL [92] or similar, the EMM is calculated as follows:

(i) Distortional mode:

$$\alpha_D = \frac{f_{crD}}{f_y} \tag{33}$$

$$\lambda_D = \sqrt{\frac{1}{\alpha_D}} \tag{34}$$

$$\begin{aligned} &\chi_D = 1 && if \quad \lambda_D \leq 0.561 \\ &\chi_D = \left(1 - 0.25{\lambda_D}^{-1.2}\right){\lambda_D}^{-1.2} && if \quad \lambda_D > 0.561 \end{aligned} \tag{35}$$

(ii) Local mode:

$$\alpha_L = \frac{f_{crL}}{f_y} \tag{36}$$

$$\lambda_{DL} = \sqrt{\frac{\chi_D}{\alpha_L}} \tag{37}$$

$$\begin{cases} \chi_{DL} = 1 & \lambda_{DL} \leq 0.776 \\ \chi_{DL} = \left(1 - 0.15{\lambda_D}^{-0.8}\right){\lambda_D}^{-0.8} & \lambda_{DL} > 0.776 \end{cases} \tag{38}$$

After determining χ_D and χ_D the reduction factor χ_{LDG} is determined according to a convergence condition based on the ratio of the distortional/local modes as shown in Equations 39 e 40.

$$DL = \frac{f_{crD}}{f_{crL}} \tag{39}$$

For $DL \leq 0.7$ use χ_D

For $DL \geq 0.8$ use χ_{DL}

For $0.7 \leq DL \leq 0.8$ use $\overline{\chi_{DL}} = \chi_D - \left[\left(\frac{\chi_D - \chi_{DL}}{0.1}\right)\left(\frac{f_{crD}}{f_{crL}} - 0.7\right)\right]$ (40)

(iii) Global mode:

$$\alpha_G = \frac{f_{crG}}{f_y} \tag{41}$$

$$\lambda_{DLG} = \sqrt{\frac{\overline{\chi_{DL}}}{\alpha_G}} \tag{42}$$

$$\begin{cases} \chi_{DLG} = 0.658^{\lambda_{DLG}^2} & \lambda_{DLG} \leq 1.5 \\ \chi_{DLG} = \frac{0.877}{\lambda_{DLG}^2} & \lambda_{DLG} > 1.5 \end{cases} \tag{43}$$

For both approaches iterative calculations should be made to refine the results and ensure accuracy. Iterations allow for the adjustment of parameters based on the outcomes of preceding steps, which is essential when the buckling modes interact and influence each other. For the purposes of this dissertation, it was determined that six iterations provided sufficient convergence for accurate and reliable results. This conclusion was reached some testing, which demonstrated that additional iterations beyond the sixth did not yield significant changes in the outcomes, indicating that the results had stabilized and could be considered convergent.

The analysis of these approaches provided valuable insights into the interdependencies of buckling modes and the importance of considering such interactions in structural design. It also highlighted the significance of iterative calculation methods in capturing the complex behaviour of structures under load, affirming the need for a rigorous computational strategy in the evaluation of buckling resistance.

Figure 24 shows the flowchart of the two EMM procedures described in the previous paragraphs.

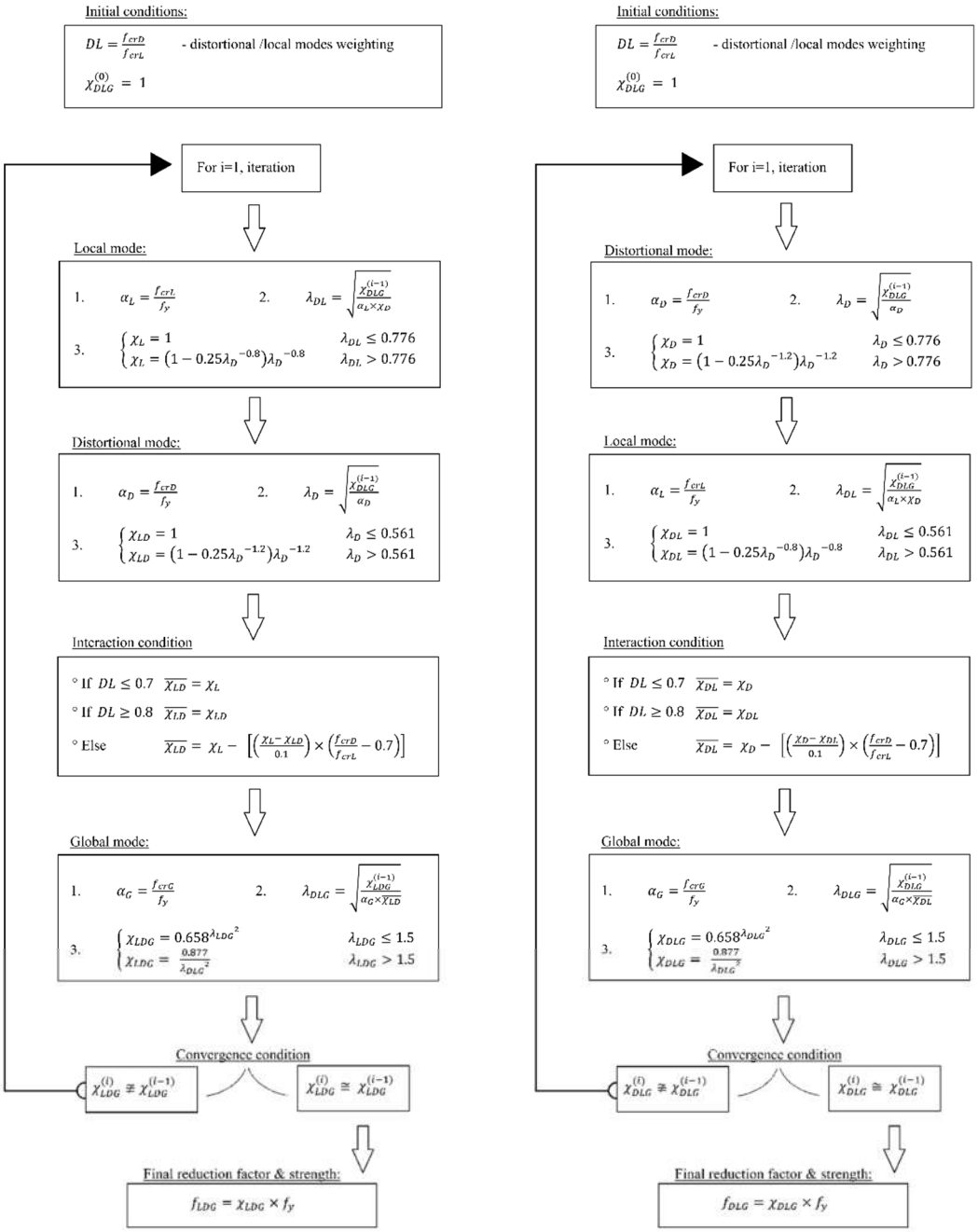

Figure 24 The EMM flowchart: (a) Local distortional sequence (b) Distortional local sequence

Aiming to address the significant number of calculations required due to the iterative nature of the Effective Modulus Method (EMM), a simplification is proposed to eliminate its iterative aspect. To achieve this, it suffices to carry out the calculations as per Equations (43) to (56) for the Local-Distortional sequence and Equations (57) to (60) for Distortional-Local sequence.

Approach LD

Global:

$$\alpha_E = \frac{f_{crG}}{f_y} \tag{44}$$

$$\lambda_E = \sqrt{\frac{1}{\alpha_E}} \tag{45}$$

$$\chi_E = \begin{cases} 0.658^{\lambda_E{}^2}, & \lambda_G \leq 1.5 \\ \frac{0.877}{\lambda_G{}^2}, & \lambda_G > 1.5 \end{cases} \tag{46}$$

Local:

$$\alpha_L = \frac{f_{crL}}{f_y} \tag{47}$$

$$\lambda_{EL} = \sqrt{\frac{\chi_E}{\alpha_L}} \tag{48}$$

$$\chi_{EL} = \begin{cases} 1, & \lambda_G \leq 0.776 \\ \left(1 - 0.15 * \lambda_G{}^{-0.8}\right) * \lambda_G{}^{-0.8}, & \lambda_G > 0.776 \end{cases} \tag{49}$$

Distortional:

$$\alpha_D = \frac{f_{crD}}{f_y} \tag{50}$$

$$\lambda_{ELD} = \sqrt{\frac{\chi_E}{\chi_{EL} * \alpha_D}} \tag{51}$$

$$\chi_{ELD} = \begin{cases} 1 & \lambda_G \leq 0.561 \\ \left(1 - 0.25 * \lambda_G{}^{-1.2}\right) * \lambda_G{}^{-1.2} & \lambda_G > 0.561 \end{cases} \tag{52}$$

Condition

$$DL = \frac{f_{crD}}{f_{crL}} \tag{53}$$

For $DL \leq 0.7$ use χ_{EL}

For $DL \geq 0.8$ use χ_{ELD}

For $0.7 \leq DL \leq 0.8$ use $\overline{\chi_{LD}} = \chi_{EL} - \left[\left(\frac{\chi_{EL} - \chi_{ELD}}{0.1}\right)\left(\frac{f_{crD}}{f_{crL}} - 0.7\right)\right]$ (54)

Global:

$$\alpha_E = \frac{f_{crG}}{f_y} \tag{55}$$

$$\lambda_{ELDG} = \sqrt{\frac{1}{\overline{\chi_{LD}}\,\alpha_G}} \tag{56}$$

$$\chi_{EDLG} = \begin{cases} 0.658^{\lambda_{ELDG}^{\,2}}, & \lambda_{ELDG} \leq 1.5 \\ \frac{0.877}{\lambda_{ELDG}^{\,2}}, & \lambda_{ELDG} > 1.5 \end{cases} \tag{57}$$

Approach DL

Global:

$$\alpha_E = \frac{f_{crG}}{f_y} \tag{58}$$

$$\lambda_E = \sqrt{\frac{1}{\alpha_E}} \tag{59}$$

$$\chi_E = \begin{cases} 0.658^{\lambda_E{}^2}, & \lambda_G \leq 1.5 \\ \frac{0.877}{\lambda_G{}^2}, & \lambda_G > 1.5 \end{cases} \tag{60}$$

Distortional:

$$\alpha_D = \frac{f_{crD}}{f_y} \tag{61}$$

$$\lambda_{ED} = \sqrt{\frac{\chi_E}{\alpha_D}} \tag{62}$$

$$\chi_{EG} = \begin{cases} 1 & \lambda_G \leq 0.561 \\ \left(1 - 0.25 * \lambda_G{}^{-1.2}\right) * \lambda_G{}^{-1.2} & \lambda_G > 0.561 \end{cases} \tag{63}$$

Local:

$$\alpha_L = \frac{f_{crL}}{f_y} \tag{64}$$

$$\lambda_{EDL} = \sqrt{\frac{\chi_E}{\chi_{ED}\ \alpha_L}} \tag{65}$$

$$\chi_{EDL} = \begin{cases} 1, & \lambda_G \leq 0.776 \\ \left(1 - 0.15 * \lambda_G{}^{-0.8}\right) * \lambda_G{}^{-0.8}, & \lambda_G > 0.776 \end{cases} \tag{66}$$

Condition:

$$DL = \frac{f_{crD}}{f_{crL}} \tag{67}$$

For $DL \leq 0.7$ use χ_{ED}

For $DL \geq 0.8$ use χ_{EDL}

For $0.7 \leq DL \leq 0.8$ use $\overline{\chi_{DL}} = \chi_{ED} - \left[\left(\frac{\chi_{ED} - \chi_{EDL}}{0.1}\right)\left(\frac{f_{crD}}{f_{crL}} - 0.7\right)\right]$ (68)

Global:

$$\alpha_E = \frac{f_{crG}}{f_y} \tag{69}$$

$$\lambda_{EDLG} = \sqrt{\frac{1}{\overline{\chi_{DL}}\,\alpha_G}} \tag{70}$$

$$\chi_{EDLG} = \begin{cases} 0.658^{\lambda_{EDLG}^2}, & \lambda_{EDLG} \leq 1.5 \\ \frac{0.877}{\lambda_{EDLG}^2}, & \lambda_{EDLG} > 1.5 \end{cases} \tag{71}$$

3.3 PROPOSAL FOR THE EFFECTIVE MODULUS METHOD, BENDING

Two approaches used within the scope of the DSM [112] are proposed in the EMM to evaluate the effects of the interaction between local and distortional modes using (i) a local slenderness affected by the distortional mode (LD) and (ii) distortional slenderness affected by the local mode (DL). The EMM calculation scheme is represented in Figure 25 for both methodologies.

Note that no formulation is proposed to evaluate the iteration between local/distortional modes with the global modes, which will be the subject of another publication, because there are not enough experimental or numerical results available in the literature. In other words, in the present work, only the influence of the interaction between the local/distortional modes on the resistance of the members are evaluated.

The EMM flow chart for beams is shown in Figure 25.

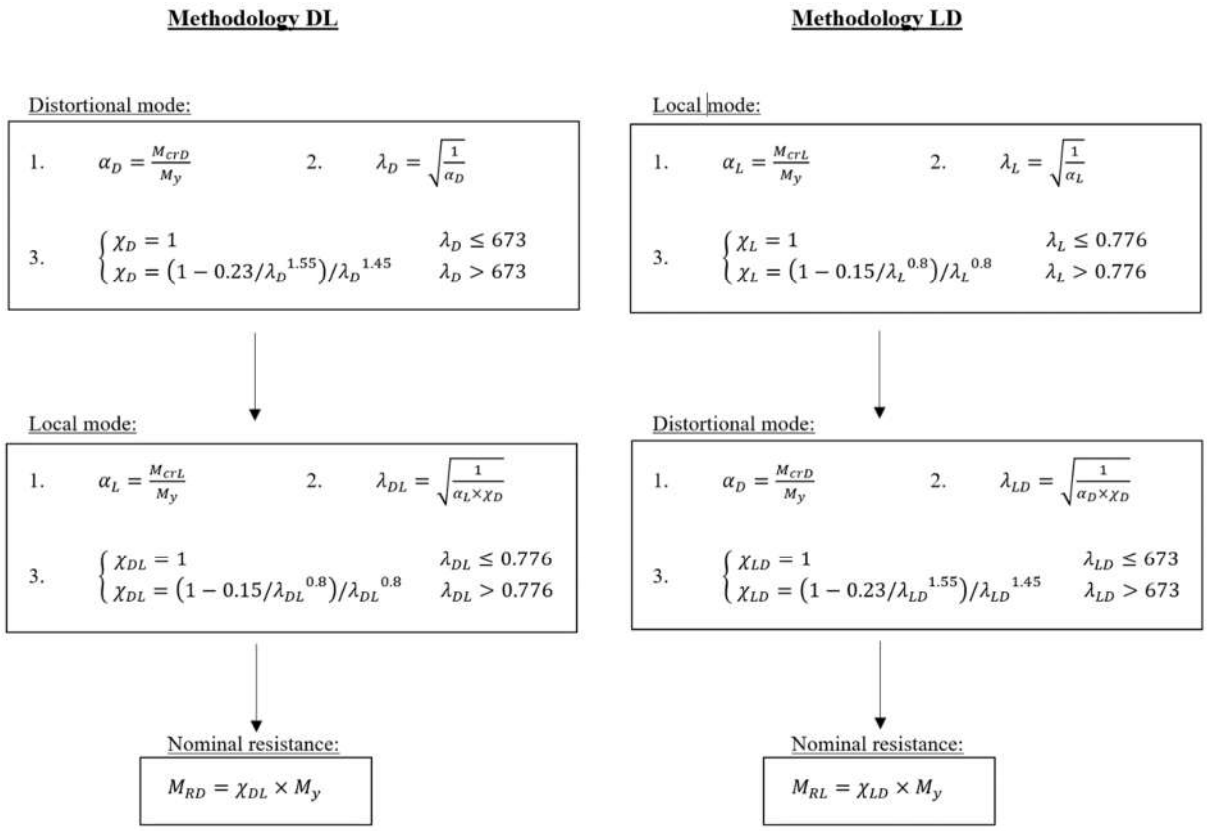

Figure 25 The EMM flowchart for DL and LD methodologies

4. COMPARISON OF RESULTS

In this thesis, a detailed investigation was conducted on the properties and final resistance of cold formed profiles, which included C-profiles, racks, Sigma profiles, and other configurations that featured stiffeners on webs or/and flanges. The analysis was based on a curated selection of literature that provided a comprehensive overview of these profiles, detailing their geometries, lengths, and material properties.

For some literature where the critical loads for local, distortional, and global buckling loads were not available, they were computed utilizing the Generalized Beam Theory (GBTUL) software [92]. GBTUL is able at assessing buckling phenomena in thin-walled structures and was instrumental in estimating the missing critical loads necessary for subsequent analysis in some references.

The core of the chapter 4 of this dissertation focused on applying the Effective Modulus Method (EMM) to the data acquired and calculated from the literature. Unlike the Effective Width Method, which modifies the width of plate elements in a cross-section, the EMM modifies the modulus of elasticity to reflect the reduced stiffness. This method is particularly suited for calculating the resistance of profiles by considering the post-buckling stiffness degradation, which is critical for an accurate buckling resistance prediction.

While most of the EMM analysis was dedicated to profiles under pure compression, attention was also given to profiles under bending loads.

The EMM calculations, encompassing both compression and bending, aimed to validate the method's effectiveness in a variety of loading and geometric conditions.

By comparing the results from the literature, with those from EMM, this study aims to evaluate the EMM's capabilities.

4.1 RESULTS FOR COMPRESSION

4.1.1 Articles from 2017 part I and II: Lc and L48f sections

4.1.1.1 Experimental Results

Camotim et al. [119] carried out experimental tests on the C-profiles described in Table 1. The critical loads P_{crL}, P_{crD} and P_{crG} were obtained using the GBTUL software and given in the article.

The specimens were compressed in a vertical set-up designed for this purpose (detailed in Figure 26 and Figure 27) and tested with fixed-ended local and distortional support conditions guaranteed by a 25 mm plate welded transversely at the ends of the specimens The plates were bolted to a flat bearing plate to which the rotations in the major and minor axes, torsion and section warping were restricted.

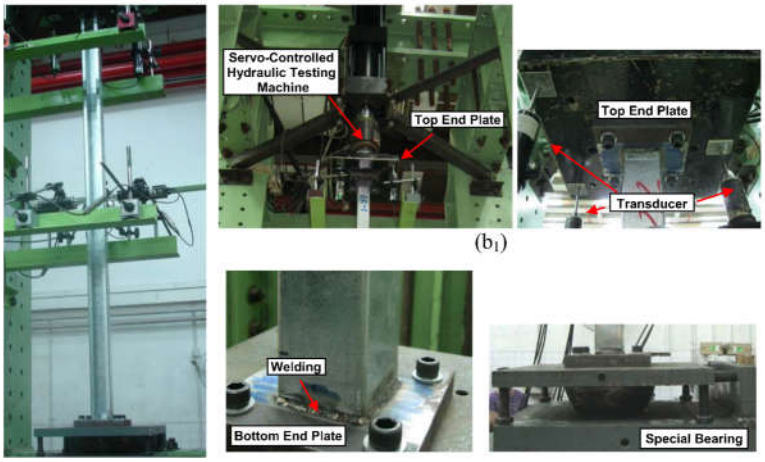

Figure 26 Compression test Set-up [119]

Figure 27 Deformed specimens after testing.[119]

Table 1 LC column specimens' dimensions & critical loads P_{crL}, P_{crD} , P_{crG}. [119]

Specimen	b_w mm	b_f mm	b_s mm	t mm	L mm	A mm^2	P_{crL} kN	P_{crD} kN	P_{crG} kN
LC1	54	56.7	12.50	0.99	1395.0	189.02	47.60	56.60	58.30
LC2-1	58	61.4	12.40	1.00	1651.0	204.48	45.20	51.70	51.60
LC2-2	58	61.4	12.50	1.00	1649.0	205.61	45.70	52.90	52.90
LC3	63	66.2	12.50	1.00	1951.0	220.22	42.00	46.40	46.00
LC4	69	71.0	12.50	0.98	2300.0	230.04	35.70	40.40	40.50
LC5	71	72.3	12.20	1.19	1896.0	286.08	63.20	59.40	69.70
LC6	71	78.3	11.90	1.20	2004.0	302.31	60.30	54.20	64.00
LC7	76	82.9	12.00	1.19	2302.0	317.01	55.30	50.20	59.00
LC8	82	87.7	11.80	1.17	2603.0	329.17	48.70	43.70	54.80
LC9	58	48.2	12.80	0.98	1401.0	176.94	47.60	63.80	65.40
LC10	63	52.6	12.70	0.99	1602.0	191.77	43.90	57.40	61.20
LC11	63	63.9	12.40	0.99	1699.0	212.50	41.20	48.20	53.70
LC12	69	57.3	12.80	0.99	1899.0	205.78	39.80	51.70	53.90
LC13	73	63.3	12.40	1.20	1851.0	270.42	67.00	69.10	78.90
LC14	78	68.4	12.50	1.17	2100.0	281.99	57.50	60.90	71.30
LC15	83	73.4	11.90	1.18	2402.0	298.59	53.70	53.00	64.10
LC16	89	78.3	12.30	1.20	2750.0	324.72	54.00	53.00	61.50

In Table 2 and Figure 28 the results from the various EMM approaches (LDG with 6 iterations, ELDG, DLG with 6 iterations and EDLG) show promising results and good level of precision with the experimental results. The approaches with iterations perform better than the simplified method, with DL with 6 iterations showing the closest results having an average of 1.21 a maximum of 1.34 and a standard deviation of 0.055.

Table 2 Comparison EMM × experimental results of LC specimens

Specimen	f_y MPa	f_{EXP} MPa	LDG 6 Iterations MPa	/ LDG	ELDG MPa	/ ELDG	DLG6 Iterations MPa	/ DLG	EDLG MPa	/ ELDG
LC1	597	253.0	221.02	1.14	198.01	1.28	226.38	1.12	221.04	1.14
LC2-1	597	237.8	183.25	1.30	164.00	1.45	188.65	1.26	182.26	1.30
LC2-2	597	222.2	186.58	1.19	166.78	1.33	191.74	1.16	185.46	1.20
LC3	597	186.5	152.36	1.22	136.88	1.36	157.66	1.18	151.78	1.23
LC4	597	177.2	127.80	1.39	114.31	1.55	131.76	1.34	127.24	1.39
LC5	594	225.1	171.20	1.31	148.74	1.51	181.33	1.24	175.28	1.28
LC6	594	204.1	149.00	1.37	129.59	1.57	158.79	1.29	153.05	1.33
LC7	594	162.4	131.09	1.24	114.07	1.42	139.49	1.16	134.50	1.21
LC8	594	149.6	115.20	1.30	98.49	1.52	122.73	1.22	118.99	1.26
LC9	597	300.4	259.02	1.16	239.67	1.25	260.68	1.15	259.56	1.16
LC10	597	273.1	224.83	1.21	199.16	1.37	226.95	1.20	224.48	1.22
LC11	597	206.7	177.57	1.16	154.05	1.34	182.08	1.14	178.13	1.16
LC12	597	232.0	186.23	1.25	163.34	1.42	188.04	1.23	184.31	1.26
LC13	594	258.8	205.06	1.26	179.57	1.44	214.44	1.21	208.73	1.24
LC14	594	224.8	176.33	1.27	151.97	1.48	183.49	1.23	178.98	1.26
LC15	594	193.5	149.12	1.30	127.93	1.51	156.70	1.23	152.50	1.27
LC16	594	166.7	133.18	1.25	115.66	1.44	140.10	1.19	135.74	1.23
			Av.	1.26		1.43		1.21		1.24
			Max	1.39		1.57		1.34		1.39
			Min	1.14		1.25		1.12		1.14
			St. dev	0.067		0.091		0.055		0.062

c

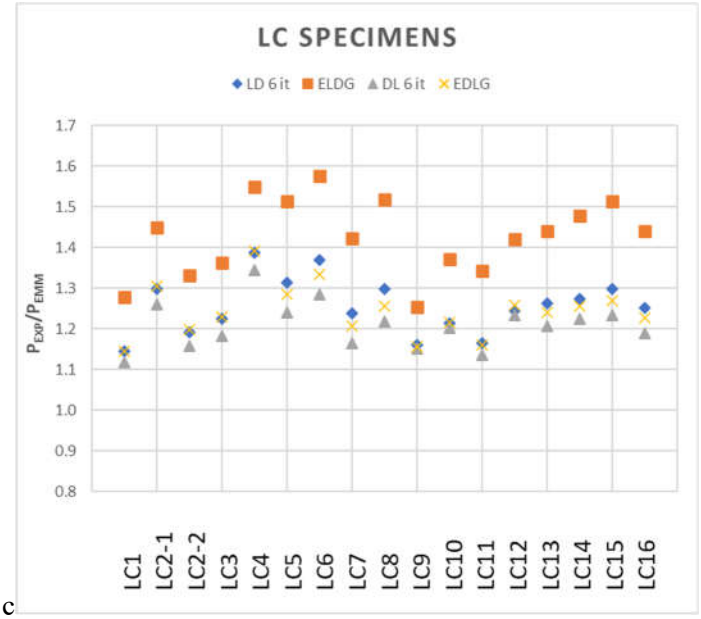

Figure 28 Comparison EMM × experimental results of LC specimens

Another set of specimens form other literature was also mentioned in [120] and is shown in Table 3. These specimens were also tested empirically and the comparison between the experimental tests and EMM method is shown in Table 4 and Figure 14. The results show slightly unsafe results. It is worth mentioning that for some experimental results in [120] the confidence in the results is not high.

Table 3 Colum specimen's dimensions and critical loads [120]

Specimen	b_w	b_f	b_s	t	L	A	P_{crL}	P_{crD}	P_{crG}
	mm	mm	mm	mm	mm	mm2	kN	kN	kN
L48F1500	96.5	48.9	12.6	1.460	1501	320.5	78.5	109.6	182.7
L48F2000	97.5	49.3	11.9	1.470	2001	323.3	80.5	103.4	118.6
A-6-1-1200	40.0	40.0	10.0	0.600	1200	84.0	15.0	22.9	21.3
A-8-1-1200	50.0	40.0	10.0	0.800	1200	120.0	28.6	37.9	41.2
A-8-2-800	40.0	40.0	10.0	0.800	800	112.0	34.9	43.5	54.5
A-8-2-1000	40.0	40.0	10.0	0.800	1000	112.0	34.9	40.9	39.8
A-8-2-1200	40.0	40.0	10.0	0.800	1200	112.0	34.9	38.3	29.5

Table 4 Comparison EMM × experimental results of specimens

Specimen	f_y	f_{EXP}	LDG 6 Iterations		ELDG		DLG6 Iterations		EDLG	
	MPa	MPa	MPa	/ LDG	MPa	/ ELDG	MPa	/ LDG	MPa	/ LDG
L48F1500	550	316.0	310.81	1.02	292.83	1.08	313.53	1.01	325.17	0.97
L48F2000	550	286.0	247.27	1.16	227.43	1.26	250.49	1.14	251.77	1.14
A-6-1-1200	628	159.0	184.19	0.86	164.66	0.97	181.53	0.88	178.31	0.89
A-8-1-1200	633	229.5	240.19	0.96	211.92	1.08	241.94	0.95	240.27	0.96
A-8-2-800	633	274.5	312.08	0.88	291.40	0.94	317.43	0.86	320.97	0.86
A-8-2-1000	633	238.1	257.79	0.92	237.95	1.00	264.21	0.90	257.93	0.92
A-8-2-1200	633	210.8	206.04	1.02	195.56	1.08	214.01	0.98	200.23	1.05
			Av.	0.97		1.06		0.96		0.97
			Max	1.16		1.26		1.14		1.14
			Min	0.86		0.94		0.86		0.86
			St. dev	0.094		0.097		0.089		0.090

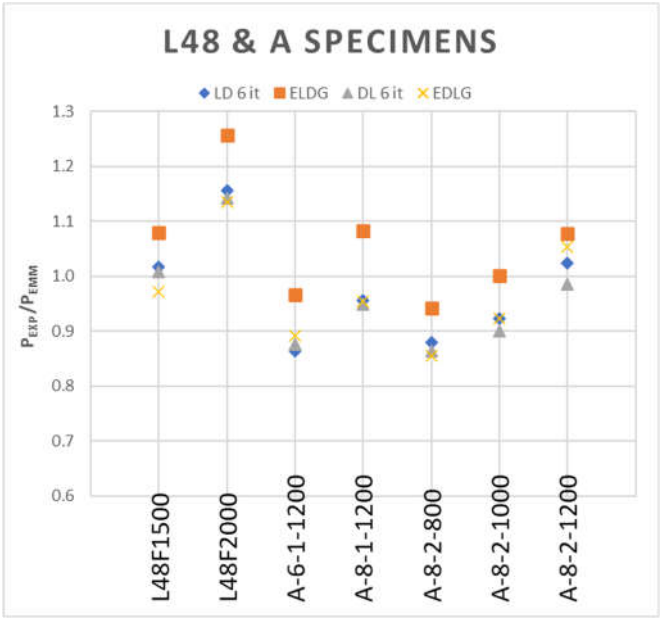

Figure 29 Comparison EMM × experimental results

4.1.1.2 Numerical results

As a part II of [119] Dinis P.B.et al. [120] did numerical simulations of the specimens shown in Table 1 varying the material resistance f_y from 300 MPa to 900 MPa for each specimen, to take into account several slenderness. The numerical tests were made by means of Abaqus shell finite element analysis (SFEA). The results of the numerical analyses and the comparison between the EMM methodology are shown in Table 5 to Table 8 and Figure 31 to Figure 34.

Figure 30 displays (i) numerical simulations and (ii) set-up of experimental work [120]

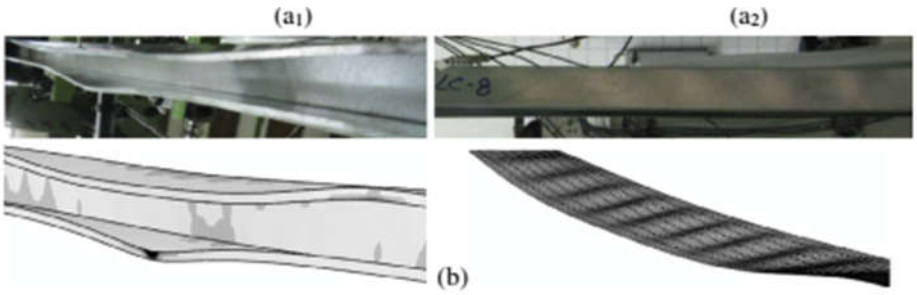

Figure 30 Typical theoretical analysis and experimental test of specimen [120]

When comparing the results of the numerical tests with varying yield stresses with the EMM depicted in Table 5 to Table 8 and Figure 31 to Figure 34, the same tendency as with the experimental results shown in Table 2 is observed showing good results with the DL with 6 iterations having the closest results. Furthermore, it can be observed that the performance of EMM is best for a range of yield stresses showing slight underperformance for yield stress below 300 MPa (Table 5) and for 900 MPa and above (Table 6). This suggests that the EMM could have the equations adjusted, taking the yield stress as a factor also into account.

Table 5 Comparison EMM × numerical results of LC specimens with f_y 300MPa

Specimen	f_y	f_{Numm}	LDG 6 Iterations		ELDG		DLG6 Iterations		EDLG	
	MPa	MPa	MPa	/ LDG	MPa	/ ELDG	MPa	/DLG	MPa	/ ELDG
LC1	300	204.0	221.02	0.92	198.01	1.03	226.38	0.90	221.04	0.92
LC2-1	300	179.0	183.25	0.98	164.00	1.09	188.65	0.95	182.26	0.98
LC2-2	300	181.0	186.58	0.97	166.78	1.09	191.74	0.94	185.46	0.98
LC3	300	157.0	152.36	1.03	136.88	1.15	157.66	1.00	151.78	1.03
LC4	300	136.0	127.80	1.06	114.31	1.19	131.76	1.03	127.24	1.07
LC5	300	169.0	171.20	0.99	148.74	1.14	181.33	0.93	175.28	0.96
LC6	300	154.0	149.00	1.03	129.59	1.19	158.79	0.97	153.05	1.01
LC7	300	140.0	131.09	1.07	114.07	1.23	139.49	1.00	134.50	1.04
LC8	300	128.0	115.20	1.11	98.49	1.30	122.73	1.04	118.99	1.08
LC9	300	227.0	259.02	0.88	239.67	0.95	260.68	0.87	259.56	0.87
LC10	300	210.0	224.83	0.93	199.16	1.05	226.95	0.93	224.48	0.94
LC11	300	178.0	177.57	1.00	154.05	1.16	182.08	0.98	178.13	1.00
LC12	300	186.0	186.23	1.00	163.34	1.14	188.04	0.99	184.31	1.01
LC13	300	196.0	205.06	0.96	179.57	1.09	214.44	0.91	208.73	0.94
LC14	300	177.0	176.33	1.00	151.97	1.16	183.49	0.96	178.98	0.99
LC15	300	153.0	149.12	1.03	127.93	1.20	156.70	0.98	152.50	1.00
LC16	300	138.0	133.18	1.04	115.66	1.19	140.10	0.99	135.74	1.02
			Av.	1.00		1.14		0.96		0.99
			Max	1.11		1.30		1.04		1.08
			Min	0.88		0.95		0.87		0.87
			St. dev	0.056		0.080		0.044		0.051

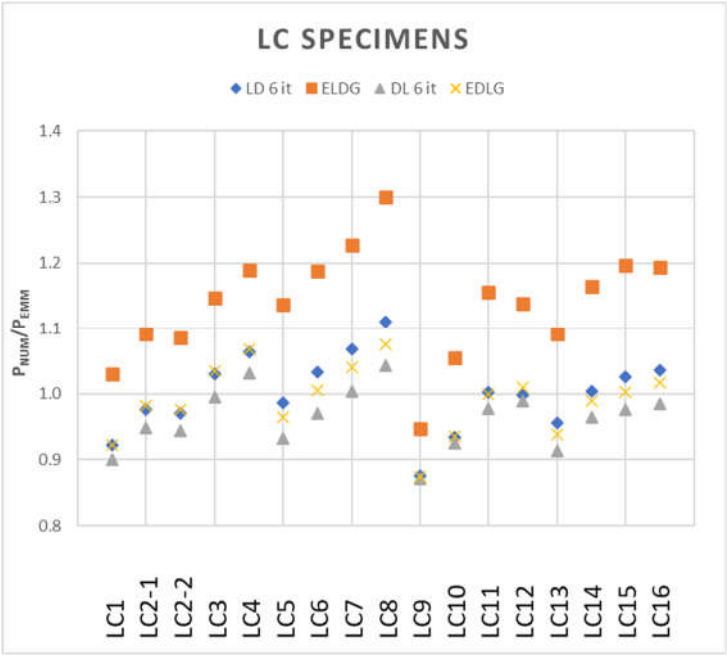

Figure 31 Comparison EMM × numerical results of LC specimens with fy 300MPa

Table 6 Comparison EMM × numerical results of LC specimens f_y 500MPa

Specimen	f_y MPa	f_{Numm} MPa	LDG 6 Iterations MPa	/ LDG	ELDG MPa	/ ELDG	DLG6 Iterations MPa	/DLG	EDLG MPa	/ ELDG
LC1	500	245.0	221.02	1.11	198.01	1.24	226.38	1.08	221.04	1.11
LC2-1	500	205.0	183.25	1.12	164.00	1.25	188.65	1.09	182.26	1.12
LC2-2	500	207.0	186.58	1.11	166.78	1.24	191.74	1.08	185.46	1.12
LC3	500	175.0	152.36	1.15	136.88	1.28	157.66	1.11	151.78	1.15
LC4	500	153.0	127.80	1.20	114.31	1.34	131.76	1.16	127.24	1.20
LC5	500	201.0	171.20	1.17	148.74	1.35	181.33	1.11	175.28	1.15
LC6	500	185.0	149.00	1.24	129.59	1.43	158.79	1.17	153.05	1.21
LC7	500	166.0	131.09	1.27	114.07	1.46	139.49	1.19	134.50	1.23
LC8	500	148.0	115.20	1.28	98.49	1.50	122.73	1.21	118.99	1.24
LC9	500	285.0	259.02	1.10	239.67	1.19	260.68	1.09	259.56	1.10
LC10	500	247.0	224.83	1.10	199.16	1.24	226.95	1.09	224.48	1.10
LC11	500	201.0	177.57	1.13	154.05	1.30	182.08	1.10	178.13	1.13
LC12	500	208.0	186.23	1.12	163.34	1.27	188.04	1.11	184.31	1.13
LC13	500	225.0	205.06	1.10	179.57	1.25	214.44	1.05	208.73	1.08
LC14	500	196.0	176.33	1.11	151.97	1.29	183.49	1.07	178.98	1.10
LC15	500	172.0	149.12	1.15	127.93	1.34	156.70	1.10	152.50	1.13
LC16	500	158.0	133.18	1.19	115.66	1.37	140.10	1.13	135.74	1.16
			Av.	1.16		1.31		1.11		1.14
			Max	1.28		1.50		1.21		1.24
			Min	1.10		1.19		1.05		1.08
			St. dev	0.059		0.083		0.042		0.049

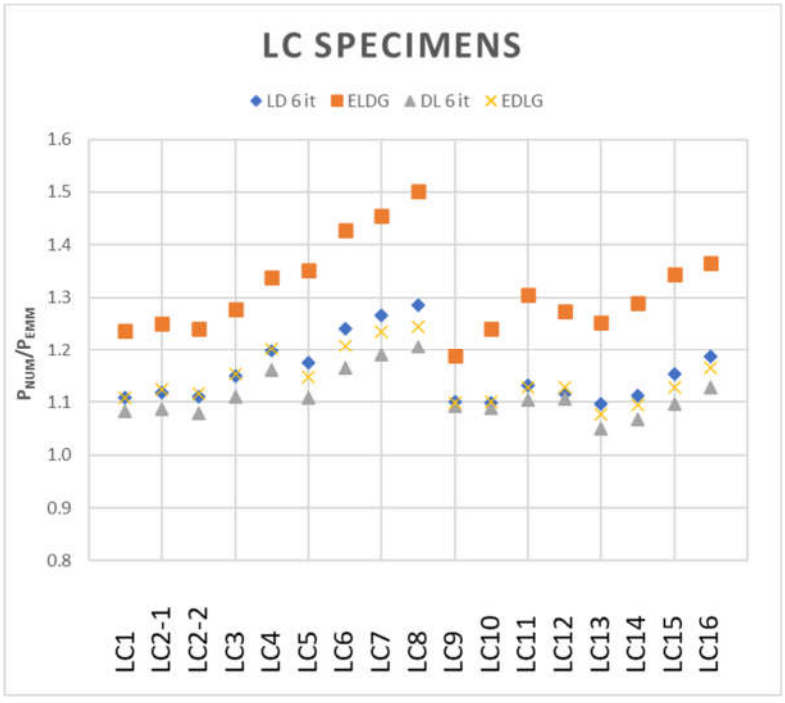

Figure 32 Comparison EMM × numerical results of LC specimens fy 500MPa

Table 7 Comparison EMM × numerical results of LC specimens f_y 700MPa

Specimen	f_y MPa	f_{Numm} MPa	LDG 6 Iterations MPa	/ LDG	ELDG MPa	/ ELDG	DLG6 Iterations MPa	/DLG	EDLG MPa	/ ELDG
LC1	700	261.0	221.02	1.18	198.01	1.32	226.38	1.15	221.04	1.18
LC2-1	700	222.0	183.25	1.21	164.00	1.35	188.65	1.18	182.26	1.22
LC2-2	700	217.0	186.58	1.16	166.78	1.30	191.74	1.13	185.46	1.17
LC3	700	186.0	152.36	1.22	136.88	1.36	157.66	1.18	151.78	1.23
LC4	700	164.0	127.80	1.28	114.31	1.43	131.76	1.24	127.24	1.29
LC5	700	217.0	171.20	1.27	148.74	1.46	181.33	1.20	175.28	1.24
LC6	700	203.0	149.00	1.36	129.59	1.57	158.79	1.28	153.05	1.33
LC7	700	181.0	131.09	1.38	114.07	1.59	139.49	1.30	134.50	1.35
LC8	700	165.0	115.20	1.43	98.49	1.68	122.73	1.34	118.99	1.39
LC9	700	301.0	259.02	1.16	239.67	1.26	260.68	1.15	259.56	1.16
LC10	700	256.0	224.83	1.14	199.16	1.29	226.95	1.13	224.48	1.14
LC11	700	215.0	177.57	1.21	154.05	1.40	182.08	1.18	178.13	1.21
LC12	700	215.0	186.23	1.15	163.34	1.32	188.04	1.14	184.31	1.17
LC13	700	238.0	205.06	1.16	179.57	1.33	214.44	1.11	208.73	1.14
LC14	700	209.0	176.33	1.19	151.97	1.38	183.49	1.14	178.98	1.17
LC15	700	183.0	149.12	1.23	127.93	1.43	156.70	1.17	152.50	1.20
LC16	700	169.0	133.18	1.27	115.66	1.46	140.10	1.21	135.74	1.25
			Av.	1.24		1.41		1.19		1.22
			Max	1.43		1.68		1.34		1.39
			Min	1.14		1.26		1.11		1.14
			St. dev	0.084		0.112		0.063		0.072

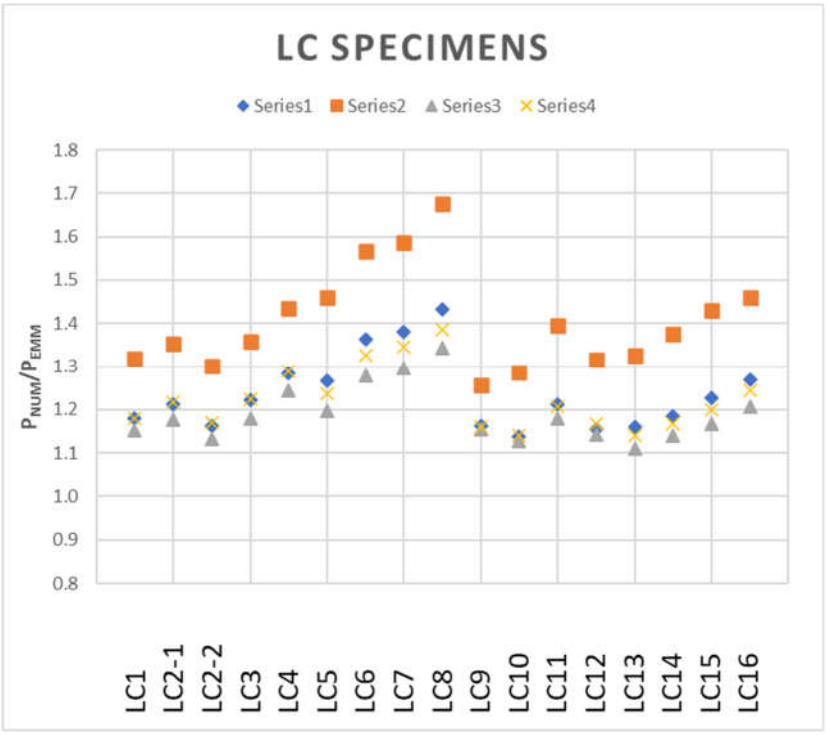

Figure 33 Comparison EMM × numerical results of LC specimens

Table 8 Comparison EMM × numerical results of LC specimens f_y 900MPa

Specimen	f_y	f_{Numm}	LDG 6 Iterations		ELDG		DLG6 Iterations		EDLG	
	MPa	MPa	MPa	/ LDG	MPa	/ ELDG	MPa	/DLG	MPa	/ ELDG
LC1	900	268.0	221.02	1.21	198.01	1.35	226.38	1.18	221.04	1.21
LC2-1	900	230.0	183.25	1.26	164.00	1.40	188.65	1.22	182.26	1.26
LC2-2	900	227.0	186.58	1.22	166.78	1.36	191.74	1.18	185.46	1.22
LC3	900	193.0	152.36	1.27	136.88	1.41	157.66	1.22	151.78	1.27
LC4	900	177.0	127.80	1.38	114.31	1.55	131.76	1.34	127.24	1.39
LC5	900	230.0	171.20	1.34	148.74	1.55	181.33	1.27	175.28	1.31
LC6	900	216.0	149.00	1.45	129.59	1.67	158.79	1.36	153.05	1.41
LC7	900	165.0	131.09	1.26	114.07	1.45	139.49	1.18	134.50	1.23
LC8	900	174.0	115.20	1.51	98.49	1.77	122.73	1.42	118.99	1.46
LC9	900	307.0	259.02	1.19	239.67	1.28	260.68	1.18	259.56	1.18
LC10	900	261.0	224.83	1.16	199.16	1.31	226.95	1.15	224.48	1.16
LC11	900	225.0	177.57	1.27	154.05	1.46	182.08	1.24	178.13	1.26
LC12	900	220.0	186.23	1.18	163.34	1.35	188.04	1.17	184.31	1.19
LC13	900	251.0	205.06	1.22	179.57	1.40	214.44	1.17	208.73	1.20
LC14	900	220.0	176.33	1.25	151.97	1.45	183.49	1.20	178.98	1.23
LC15	900	196.0	149.12	1.31	127.93	1.53	156.70	1.25	152.50	1.29
LC16	900	179.0	133.18	1.34	115.66	1.55	140.10	1.28	135.74	1.32
			Av.	1.28		1.46		1.24		1.27
			Max	1.51		1.77		1.42		1.46
			Min	1.16		1.28		1.15		1.16
			St. dev	0.094		0.124		0.074		0.082

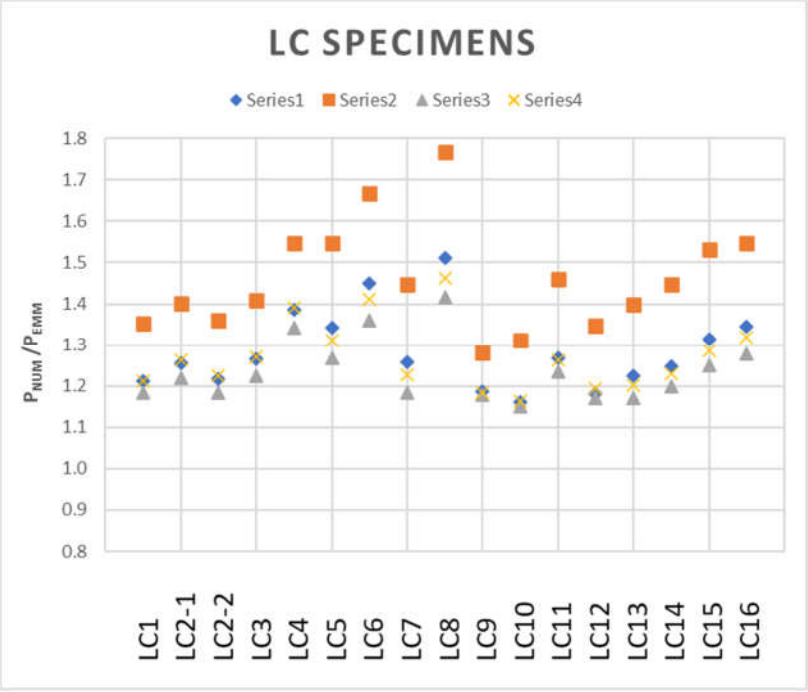

Figure 34 Comparison EMM × numerical results of LC specimens

4.1.2 Article from 2016 CS-Profiles

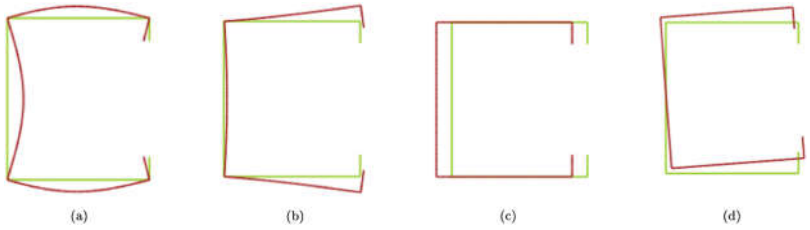

Figure 35 Various buckling modes of CS profiles [121] determined in GBTUL

In 2016 Cava D. et al. [121] conducted an investigation on the strength erosion of cold formed steel profiles due to the interaction of the 3 buckling modes depicted in Figure 35 (local (a), distortional (b), global(c) & (d)). For that purpose, using GBTUL a series of specimens named CS with proprieties shown in Table 9 were selected so that each specimen had critical buckling modes no more than 20% apart. Various yield stresses and lengths were considered to cover a wider range of slenderness totalling 459 specimen configurations. For better identification of every configuration tested, the numerical tests were named in the following manner "SPECIMEN_Length_Yield Stress" the length being in millimetre and yield stress in megapascal. For example, CS1_2300_61 means specimen CS1, length 2300 mm and yield stress 61 MPa.

Then the ultimate strengths of the specimens were analysed with Abaqus software and with fixed ended cross-sections with torsional rotation and warping constrained but movement in the major axis allowed.

The various specimen configurations results and comparison with EMM is shown in Table 10 to Table 19 and Figure 36 to Figure 45.

Table 9 CS column specimen's dimensions & critical loads P_{crL}, P_{crD} , P_{crG}.

Specimen	b_w mm	b_f mm	b_s mm	t mm	L_S mm	L_l mm	A mm²
CS1	85	75	12	1.4	2300	2700	363
CS2	80	75	12	1.2	2400	2800	305
CS3	90	74	13	1.5	2350	2750	396
CS4	110	67	12	2.0	2450	2900	536
CS5	100	60	12	2.0	2050	2400	488
CS6	62	55	11	1.1	1550	1900	213
CS7	92	54	11	1.7	2000	2350	377
CS8	75	60	10	1.0	2350	2650	215
CS9	65	47	10	1.1	1550	1850	197
CS10	80	45	11	1.6	1550	1800	307

After analysing the comparison of all the numerical 459 tests (shown in Table 10 to Table 19 and Figure 36 to Figure 45) with the EMM method, the results seem globally very good with the DL with 6 iterations approach, having the closest precision level. Only in a few instances does the ration f_u/f_{EMM} fall below the safe zone of 1.00 but not further then 0.95 which is still very close.

Also when analysing the Figure 36 to Figure 45 a tendency can be observed for every specimen, it clearly shows that for lower yield stresses the EMM precision level is very close to the numerical values but decreases as the yield stress increases, giving results "Too safe". Again, a suggestion to improve the EMM method would be to implement the yield stress factor in the equations.

Table 10 Comparison EMM × numerical results of CS1 specimens

Specimen	f_y	f_u	LDG 6 Iterations		ELDG		DLG6 Iterations		EDLG	
	MPa	MPa	MPa	/ LDG	MPa	/ ELDG	MPa	/ LDG	MPa	/ LDG
CS1_2300_61	61	56.7	54.95	1.03	54.95	1.03	54.95	1.03	54.95	1.03
CS1_2300_245	245	161.6	148.98	1.08	146.28	1.10	155.60	1.04	151.51	1.07
CS1_2300_550	550	204.8	172.19	1.19	150.15	1.36	185.15	1.11	177.81	1.15
CS1_2300_978	978	232.3	172.37	1.35	150.19	1.55	185.15	1.25	177.83	1.31
CS1_2300_1529	1529	254.7	172.37	1.48	150.19	1.70	185.15	1.38	177.83	1.43
CS1_2300_2201	2201	273.2	172.37	1.58	150.19	1.82	185.15	1.48	177.83	1.54
CS1_2350_59	59	54.7	53.17	1.03	53.17	1.03	53.17	1.03	53.17	1.03
CS1_2350_238	238	156.9	145.40	1.08	143.00	1.10	151.83	1.03	147.50	1.06
CS1_2350_534	534	201.4	168.54	1.19	148.02	1.36	181.32	1.11	173.63	1.16
CS1_2350_950	950	227.6	168.70	1.35	148.06	1.54	181.32	1.26	173.64	1.31
CS1_2350_1485	1485	248.9	168.70	1.48	148.06	1.68	181.32	1.37	173.64	1.43
CS1_2350_2138	2138	267.4	168.70	1.59	148.06	1.81	181.32	1.47	173.64	1.54
CS1_2400_58	58	53.8	52.20	1.03	52.20	1.03	52.20	1.03	52.20	1.03
CS1_2400_231	231	154.1	141.67	1.09	139.70	1.10	148.06	1.04	143.48	1.07
CS1_2400_519	519	196.2	164.90	1.19	145.94	1.34	177.49	1.11	169.45	1.16
CS1_2400_922	922	222.6	165.03	1.35	145.94	1.53	177.49	1.25	169.45	1.31
CS1_2400_1441	1441	243.4	165.03	1.47	145.94	1.67	177.49	1.37	169.45	1.44
CS1_2400_2075	2075	261.2	165.03	1.58	145.94	1.79	177.49	1.47	169.45	1.54
CS1_2450_56	56	51.8	50.43	1.03	50.43	1.03	50.43	1.03	50.43	1.03
CS1_2450_224	224	150.8	137.97	1.09	136.42	1.11	144.30	1.05	139.50	1.08
CS1_2450_503	503	193.7	161.35	1.20	143.84	1.35	173.75	1.11	165.34	1.17
CS1_2450_895	895	218.2	161.44	1.35	143.87	1.52	173.75	1.26	165.35	1.32
CS1_2450_1398	1398	237.3	161.44	1.47	143.87	1.65	173.75	1.37	165.35	1.44
CS1_2450_2013	2013	254.5	161.44	1.58	143.87	1.77	173.75	1.46	165.35	1.54
CS1_2500_54	54	49.9	48.66	1.03	48.66	1.03	48.66	1.03	48.66	1.03
CS1_2500_217	217	142.9	134.25	1.06	132.96	1.07	140.52	1.02	135.51	1.05
CS1_2500_488	488	189.5	157.73	1.20	141.71	1.34	169.98	1.11	161.20	1.18
CS1_2500_868	868	213.4	157.80	1.35	141.74	1.51	169.97	1.26	161.21	1.32
CS1_2500_1356	1356	231.3	157.80	1.47	141.74	1.63	169.97	1.36	161.21	1.43
CS1_2500_1952	1952	248.4	157.80	1.57	141.74	1.75	169.97	1.46	161.21	1.54
CS1_2550_53	53	49.1	47.70	1.03	47.70	1.03	47.70	1.03	47.70	1.03

CS1_2550_210	210	144.6	130.60	1.11	129.47	1.12	136.78	1.06	131.58	1.10
CS1_2550_473	473	183.1	154.27	1.19	139.66	1.31	166.34	1.10	157.22	1.16
CS1_2550_842	842	209.2	154.33	1.36	139.69	1.50	166.34	1.26	157.23	1.33
CS1_2550_1315	1315	227.1	154.33	1.47	139.69	1.63	166.34	1.37	157.23	1.44
CS1_2550_1894	1894	243.8	154.33	1.58	139.69	1.75	166.34	1.47	157.23	1.55
CS1_2600_51	51	46.8	45.94	1.02	45.94	1.02	45.94	1.02	45.94	1.02
CS1_2600_204	204	137.9	127.26	1.08	126.26	1.09	133.39	1.03	128.00	1.08
CS1_2600_459	459	180.2	150.90	1.19	137.63	1.31	162.80	1.11	153.34	1.18
CS1_2600_816	816	204.9	150.95	1.36	137.66	1.49	162.79	1.26	153.35	1.34
CS1_2600_1275	1275	222.0	150.95	1.47	137.66	1.61	162.79	1.36	153.35	1.45
CS1_2600_1836	1836	238.1	150.95	1.58	137.66	1.73	162.79	1.46	153.35	1.55
CS1_2650_49	49	44.5	44.17	1.01	44.17	1.01	44.17	1.01	44.17	1.01
CS1_2650_198	198	124.1	123.86	1.00	122.98	1.01	129.95	0.95	124.41	1.00
CS1_2650_445	445	175.3	147.41	1.19	135.42	1.29	159.19	1.10	149.40	1.17
CS1_2650_791	791	201.0	147.44	1.36	135.45	1.48	159.19	1.26	149.41	1.35
CS1_2650_1237	1237	216.4	147.44	1.47	135.45	1.60	159.19	1.36	149.41	1.45
CS1_2650_1781	1781	234.5	147.44	1.59	135.45	1.73	159.19	1.47	149.41	1.57
CS1_2700_48	48	43.4	43.23	1.00	43.23	1.00	43.23	1.00	43.23	1.00
CS1_2700_192	192	119.9	120.52	0.99	119.74	1.00	126.31	0.95	126.31	0.95
CS1_2700_432	432	169.1	143.77	1.18	133.22	1.27	155.75	1.09	145.69	1.16
CS1_2700_768	768	196.3	143.80	1.37	133.22	1.47	155.75	1.26	145.69	1.35
CS1_2700_1199	1199	212.2	143.80	1.48	133.22	1.59	155.75	1.36	145.69	1.46
CS1_2700_1727	1727	228.9	143.80	1.59	133.22	1.72	155.75	1.47	145.69	1.57
			Av.	1.28		1.39		1.21		1.26
			Max	1.59		1.82		1.48		1.57
			Min	0.99		1.00		0.95		0.95
			St. dev	0.206		0.276		0.172		0.197

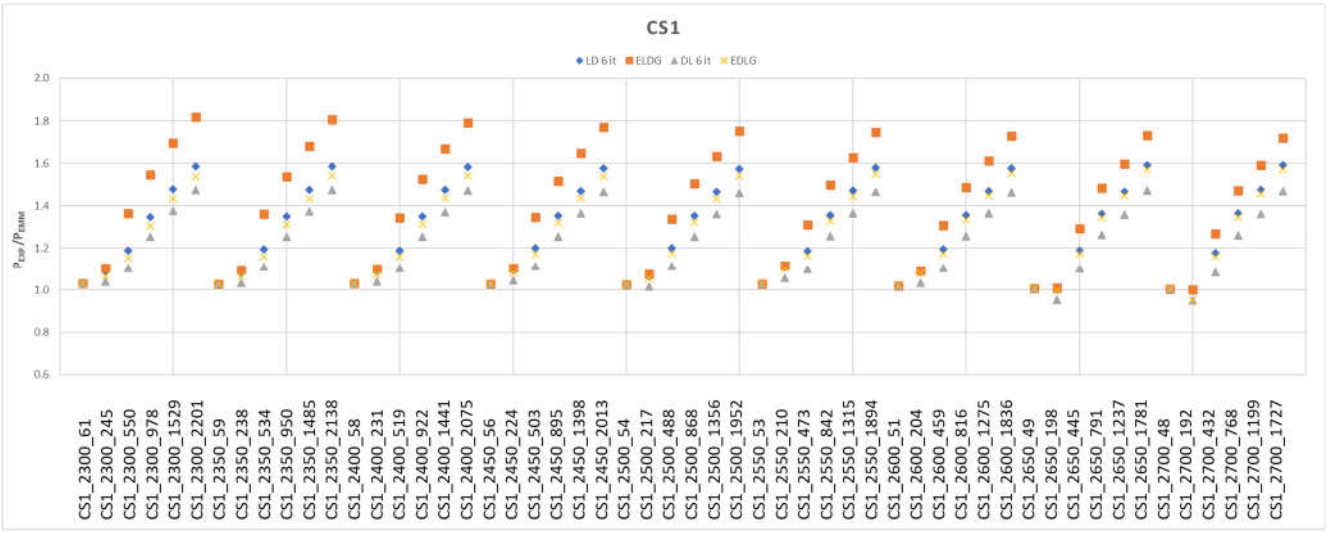

Figure 36 Comparison EMM × numerical results of CS1 specimens

Table 11 Comparison EMM × numerical results of CS2 specimens

Specimen	f_y MPa	f_u MPa	LDG 6 Iterations MPa	/ LDG	ELDG MPa	/ ELDG	DLG6 Iterations MPa	/ DLG	EDLG MPa	/ EDLG
CS2_2400_51	51	46.9	45.91	1.02	45.91	1.02	45.91	1.02	45.91	1.02
CS2_2400_203	203	131.2	124.05	1.06	121.98	1.08	128.53	1.02	125.41	1.05
CS2_2400_457	457	166.5	143.85	1.16	126.15	1.32	152.61	1.09	146.98	1.13
CS2_2400_812	812	188.4	143.96	1.31	126.15	1.49	152.61	1.23	146.98	1.28
CS2_2400_1268	1268	207.2	143.96	1.44	126.15	1.64	152.61	1.36	146.98	1.41
CS2_2400_1826	1826	223.7	143.96	1.55	126.15	1.77	152.61	1.47	146.98	1.52
CS2_2450_49	49	44.9	44.16	1.02	44.16	1.02	44.16	1.02	44.16	1.02
CS2_2450_197	197	128.2	121.02	1.06	119.19	1.08	125.39	1.02	122.06	1.05
CS2_2450_444	444	163.9	140.82	1.16	124.33	1.32	149.51	1.10	143.59	1.14
CS2_2450_789	789	185.0	140.92	1.31	124.33	1.49	149.51	1.24	143.59	1.29
CS2_2450_1233	1233	201.8	140.92	1.43	124.33	1.62	149.51	1.35	143.59	1.41
CS2_2450_1775	1775	218.0	140.92	1.55	124.33	1.75	149.51	1.46	143.59	1.52
CS2_2500_48	48	44.2	43.22	1.02	43.22	1.02	43.22	1.02	43.22	1.02
CS2_2500_192	192	126.5	118.27	1.07	116.63	1.08	122.55	1.03	119.03	1.06
CS2_2500_431	431	161.0	137.85	1.17	122.52	1.31	146.46	1.10	140.23	1.15
CS2_2500_767	767	180.6	137.94	1.31	122.55	1.47	146.46	1.23	140.24	1.29
CS2_2500_1198	1198	198.0	137.94	1.44	122.55	1.62	146.46	1.35	140.24	1.41
CS2_2500_1725	1725	213.7	137.94	1.55	122.55	1.74	146.46	1.46	140.24	1.52
CS2_2550_47	47	43.2	42.29	1.02	42.29	1.02	42.29	1.02	42.29	1.02
CS2_2550_186	186	124.0	115.26	1.08	113.84	1.09	119.43	1.04	115.71	1.07
CS2_2550_419	419	156.9	134.93	1.16	120.78	1.30	143.44	1.09	136.93	1.15
CS2_2550_744	744	177.1	135.00	1.31	120.78	1.47	143.44	1.23	136.93	1.29
CS2_2550_1163	1163	194.3	135.00	1.44	120.78	1.61	143.44	1.35	136.93	1.42
CS2_2550_1675	1675	209.8	135.00	1.55	120.78	1.74	143.44	1.46	136.93	1.53
CS2_2600_45	45	41.4	40.55	1.02	40.55	1.02	40.55	1.02	40.55	1.02
CS2_2600_181	181	121.2	112.44	1.08	111.29	1.09	116.60	1.04	112.72	1.08
CS2_2600_407	407	153.9	132.07	1.17	119.04	1.29	140.44	1.10	133.66	1.15
CS2_2600_723	723	173.6	132.13	1.31	119.04	1.46	140.44	1.24	133.66	1.30
CS2_2600_1129	1129	190.0	132.13	1.44	119.04	1.60	140.44	1.35	133.66	1.42
CS2_2600_1626	1626	205.0	132.13	1.55	119.04	1.72	140.44	1.46	133.66	1.53
CS2_2650_44	44	40.3	39.61	1.02	39.61	1.02	39.61	1.02	39.61	1.02
CS2_2650_175	175	117.9	109.34	1.08	108.48	1.09	113.48	1.04	109.43	1.08
CS2_2650_395	395	149.6	129.25	1.16	117.31	1.28	137.49	1.09	130.43	1.15
CS2_2650_702	702	170.2	129.30	1.32	117.31	1.45	137.49	1.24	130.43	1.30
CS2_2650_1096	1096	186.0	129.30	1.44	117.31	1.59	137.49	1.35	130.43	1.43
CS2_2650_1579	1579	200.9	129.30	1.55	117.31	1.71	137.49	1.46	130.43	1.54
CS2_2700_43	43	39.5	38.69	1.02	38.69	1.02	38.69	1.02	38.69	1.02
CS2_2700_170	170	114.8	106.56	1.08	105.82	1.08	110.69	1.04	106.50	1.08
CS2_2700_383	383	145.6	126.52	1.15	115.59	1.26	134.64	1.08	127.29	1.14
CS2_2700_681	681	166.9	126.56	1.32	115.62	1.44	134.63	1.24	127.30	1.31
CS2_2700_1064	1064	182.5	126.56	1.44	115.62	1.58	134.63	1.36	127.30	1.43
CS2_2700_1532	1532	197.2	126.56	1.56	115.62	1.71	134.63	1.46	127.30	1.55
CS2_2750_41	41	37.4	36.96	1.01	36.96	1.01	36.96	1.01	36.96	1.01
CS2_2750_165	165	108.1	103.79	1.04	103.14	1.05	107.91	1.00	103.58	1.04
CS2_2750_372	372	144.7	123.81	1.17	113.90	1.27	131.81	1.10	124.20	1.17
CS2_2750_661	661	163.5	123.84	1.32	113.90	1.44	131.81	1.24	124.20	1.32
CS2_2750_1033	1033	178.1	123.84	1.44	113.90	1.56	131.81	1.35	124.20	1.43
CS2_2800_40	40	36.3	36.04	1.01	36.04	1.01	36.04	1.01	36.04	1.01
CS2_2800_160	160	106.3	101.06	1.05	100.49	1.06	105.16	1.01	100.71	1.06
CS2_2800_361	361	140.3	121.17	1.16	112.20	1.25	129.07	1.09	121.20	1.16
CS2_2800_642	642	160.5	121.19	1.32	112.22	1.43	129.07	1.24	121.21	1.32
CS2_2800_1003	1003	174.9	121.19	1.44	112.22	1.56	129.07	1.36	121.21	1.44
CS2_2800_1444	1444	188.9	121.19	1.56	112.22	1.68	129.07	1.46	121.21	1.56
			Av.	1.25		1.35		1.19		1.24
			Max	1.56		1.77		1.47		1.56
			Min	1.01		1.01		1.00		1.01
			St. dev	0.192		0.258		0.165		0.186

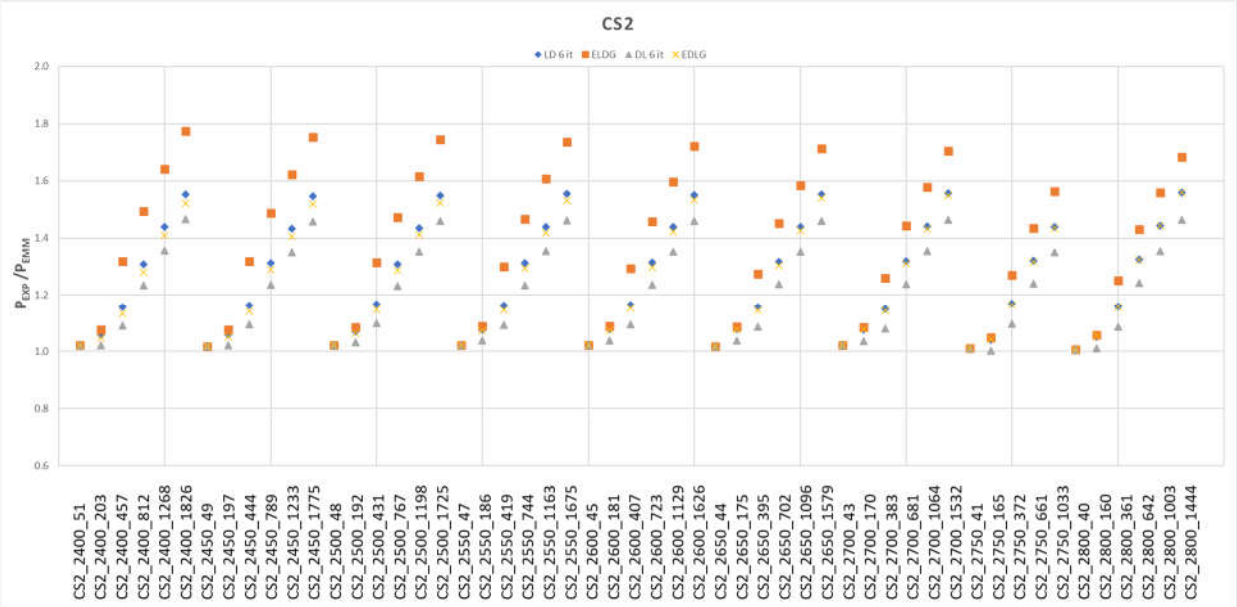

Figure 37 Comparison EMM × numerical results of CS2 specimens

Table 12 Comparison EMM × numerical results of CS3 specimens

Specimen	f_y MPa	f_u MPa	LDG 6 Iterations MPa	/ LDG	ELDG MPa	/ ELDG	DLG6 Iterations MPa	/ DLG	EDLG MPa	/ EDLG
CS3_2350_67	67	62.2	60.38	1.03	60.38	1.03	60.38	1.03	60.38	1.03
CS3_2350_269	269	180.6	164.68	1.10	161.99	1.11	170.84	1.06	166.51	1.08
CS3_2350_606	606	223.2	191.20	1.17	167.82	1.33	203.35	1.10	195.57	1.14
CS3_2350_1077	1077	250.7	191.35	1.31	167.86	1.49	203.34	1.23	195.59	1.28
CS3_2350_1684	1684	281.4	191.35	1.47	167.86	1.68	203.34	1.38	195.59	1.44
CS3_2350_2424	2424	298.0	191.35	1.56	167.86	1.78	203.34	1.47	195.59	1.52
CS3_2400_65	65	60.6	58.57	1.03	58.57	1.03	58.57	1.03	58.57	1.03
CS3_2400_261	261	178.1	160.51	1.11	158.14	1.13	166.50	1.07	161.88	1.10
CS3_2400_588	588	217.5	186.89	1.16	165.33	1.32	198.89	1.09	190.71	1.14
CS3_2400_1045	1045	245.3	187.02	1.31	165.33	1.48	198.89	1.23	190.71	1.29
CS3_2400_1632	1632	266.5	187.02	1.42	165.33	1.61	198.89	1.34	190.71	1.40
CS3_2450_63	63	58.6	56.77	1.03	56.77	1.03	56.77	1.03	56.77	1.03
CS3_2450_253	253	173.3	156.36	1.11	154.30	1.12	162.19	1.07	157.29	1.10
CS3_2450_570	570	212.9	182.69	1.17	162.83	1.31	194.52	1.09	185.92	1.15
CS3_2450_1013	1013	240.2	182.80	1.31	162.83	1.48	194.52	1.23	185.92	1.29
CS3_2450_1582	1582	260.7	182.80	1.43	162.83	1.60	194.52	1.34	185.92	1.40
CS3_2500_61	61	56.6	54.97	1.03	54.97	1.03	54.97	1.03	54.97	1.03
CS3_2500_245	245	169.1	152.12	1.11	150.46	1.12	157.89	1.07	152.73	1.11
CS3_2500_552	552	207.7	178.58	1.16	160.35	1.30	190.23	1.09	181.20	1.15
CS3_2500_982	982	235.1	178.68	1.32	160.38	1.47	190.23	1.24	181.21	1.30
CS3_2500_1534	1534	255.1	178.68	1.43	160.38	1.59	190.23	1.34	181.21	1.41
CS3_2550_59	59	54.9	53.18	1.03	53.18	1.03	53.18	1.03	53.18	1.03
CS3_2550_238	238	164.7	148.14	1.11	146.87	1.12	153.92	1.07	148.52	1.11
CS3_2550_535	535	205.1	174.56	1.17	157.90	1.30	186.02	1.10	176.58	1.16
CS3_2550_951	951	230.9	174.63	1.32	157.94	1.46	186.02	1.24	176.59	1.31
CS3_2550_1486	1486	247.8	174.63	1.42	157.94	1.57	186.02	1.33	176.59	1.40
CS3_2550_2140	2140	265.2	174.63	1.52	157.94	1.68	186.02	1.43	176.59	1.50
CS3_2600_58	58	53.9	52.20	1.03	52.20	1.03	52.20	1.03	52.20	1.03
CS3_2600_230	230	159.9	143.95	1.11	142.89	1.12	149.68	1.07	144.06	1.11
CS3_2600_519	519	200.0	170.68	1.17	155.56	1.29	181.94	1.10	172.12	1.16
CS3_2600_922	922	226.1	170.74	1.32	155.56	1.45	181.94	1.24	172.12	1.31
CS3_2600_1440	1440	242.7	170.74	1.42	155.56	1.56	181.94	1.33	172.12	1.41
CS3_2600_2074	2074	258.8	170.74	1.52	155.56	1.66	181.94	1.42	172.12	1.50
CS3_2650_56	56	51.6	50.42	1.02	50.42	1.02	50.42	1.02	50.42	1.02
CS3_2650_223	223	152.6	140.06	1.09	139.15	1.10	145.77	1.05	139.96	1.09
CS3_2650_503	503	195.5	166.85	1.17	153.19	1.28	177.94	1.10	167.74	1.17
CS3_2650_894	894	221.6	166.89	1.33	153.19	1.45	177.94	1.25	167.74	1.32
CS3_2650_1396	1396	237.9	166.89	1.43	153.19	1.55	177.94	1.34	167.74	1.42
CS3_2650_2010	2010	253.1	166.89	1.52	153.19	1.65	177.94	1.42	167.74	1.51
CS3_2700_54	54	49.6	48.65	1.02	48.65	1.02	48.65	1.02	48.65	1.02
CS3_2700_217	217	141.6	136.48	1.04	135.67	1.04	142.19	1.00	136.19	1.04
CS3_2700_487	487	191.0	163.03	1.17	150.69	1.27	173.98	1.10	163.42	1.17
CS3_2700_866	866	217.6	163.06	1.33	150.72	1.44	173.98	1.25	163.43	1.33
CS3_2700_1353	1353	232.1	163.06	1.42	150.72	1.54	173.98	1.33	163.43	1.42
CS3_2700_1949	1949	247.9	163.06	1.52	150.72	1.64	173.98	1.42	163.43	1.52
CS3_2750_52	52	47.9	46.88	1.02	46.88	1.02	46.88	1.02	46.88	1.02
CS3_2750_210	210	138.4	132.64	1.04	131.94	1.05	138.18	1.00	138.18	1.00
CS3_2750_472	472	185.8	159.30	1.17	148.15	1.25	170.20	1.09	159.31	1.17
CS3_2750_840	840	213.1	159.32	1.34	148.18	1.44	170.20	1.25	159.32	1.34
CS3_2750_1312	1312	227.6	159.32	1.43	148.18	1.54	170.20	1.34	159.32	1.43
CS3_2750_1890	1890	243.2	159.32	1.53	148.18	1.64	170.20	1.43	159.32	1.53
			Av.	1.25		1.34		1.18		1.23
			Max	1.56		1.78		1.47		1.53
			Min	1.02		1.02		1.00		1.00
			St. dev	0.173		0.234		0.146		0.170

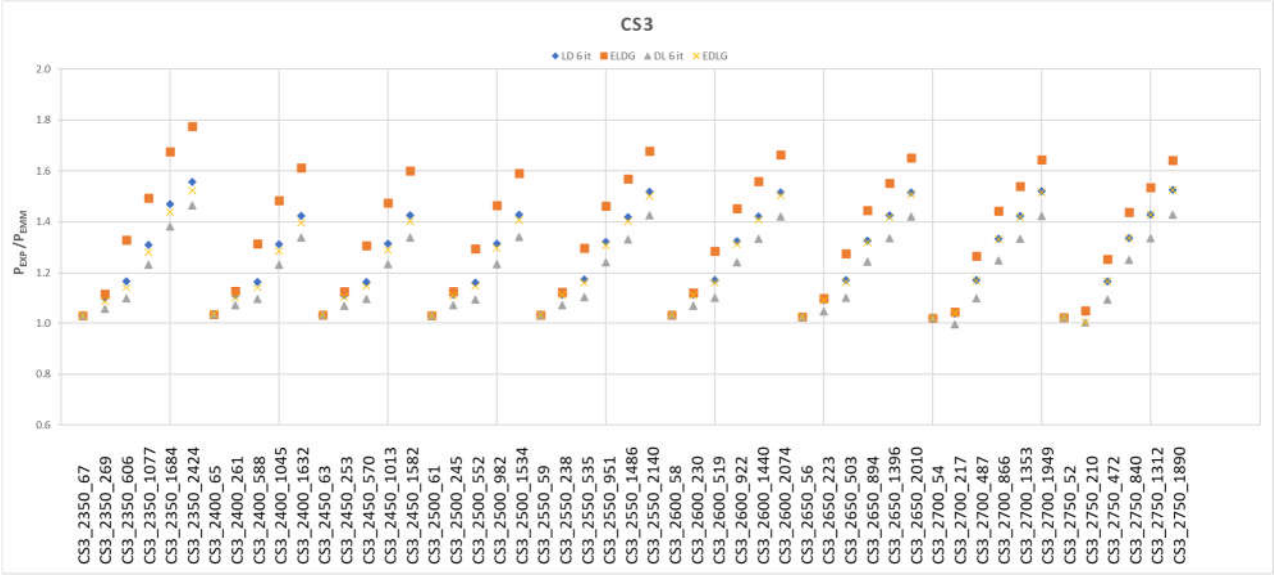

Figure 38 Comparison EMM × numerical results of CS3 specimens

Table 13 Comparison EMM × numerical results of CS4 specimens

Specimen	f_y MPa	f_u MPa	LDG 6 Iterations MPa	/ LDG	ELDG MPa	/ ELDG	DLG6 Iterations MPa	/ DLG	EDLG MPa	/ EDLG
CS4_2450_87	87	81.3	78.39	1.04	78.39	1.04	78.39	1.04	78.39	1.04
CS4_2450_350	350	246.5	214.34	1.15	210.93	1.17	221.76	1.11	216.26	1.14
CS4_2450_787	787	289.0	248.89	1.16	219.10	1.32	263.48	1.10	253.60	1.14
CS4_2450_1398	1398	320.3	249.06	1.29	219.10	1.46	263.48	1.22	253.60	1.26
CS4_2450_2185	2185	336.2	249.06	1.35	219.10	1.53	263.48	1.28	253.60	1.33
CS4_2450_3146	3146	340.6	249.06	1.37	219.10	1.55	263.48	1.29	253.60	1.34
CS4_2500_84	84	76.9	75.69	1.02	75.69	1.02	75.69	1.02	75.69	1.02
CS4_2500_338	338	214.5	208.25	1.03	205.34	1.04	215.39	1.00	209.44	1.02
CS4_2500_760	760	282.3	242.79	1.16	215.65	1.31	257.08	1.10	246.56	1.14
CS4_2500_1351	1351	312.6	242.93	1.29	215.65	1.45	257.08	1.22	246.56	1.27
CS4_2500_2111	2111	328.9	242.93	1.35	215.65	1.53	257.08	1.28	246.56	1.33
CS4_2500_3040	3040	333.6	242.93	1.37	215.65	1.55	257.08	1.30	246.56	1.35
CS4_2550_82	82	75.6	73.82	1.02	73.82	1.02	73.82	1.02	73.82	1.02
CS4_2550_326	326	210.1	202.24	1.04	199.79	1.05	209.10	1.00	202.75	1.04
CS4_2550_734	734	276.0	236.95	1.16	212.26	1.30	250.96	1.10	239.80	1.15
CS4_2550_1306	1306	305.7	237.07	1.29	212.31	1.44	250.96	1.22	239.82	1.27
CS4_2550_2040	2040	321.6	237.07	1.36	212.31	1.51	250.96	1.28	239.82	1.34
CS4_2550_2938	2938	327.0	237.07	1.38	212.31	1.54	250.96	1.30	239.82	1.36
CS4_2600_79	79	73.7	71.14	1.04	71.14	1.04	71.14	1.04	71.14	1.04
CS4_2600_316	316	209.5	196.72	1.06	194.69	1.08	203.48	1.03	196.76	1.06
CS4_2600_710	710	269.8	231.25	1.17	208.83	1.29	245.02	1.10	233.28	1.16
CS4_2600_1262	1262	298.8	231.35	1.29	208.87	1.43	245.01	1.22	233.30	1.28
CS4_2600_1972	1972	308.5	231.35	1.33	208.87	1.48	245.01	1.26	233.30	1.32
CS4_2650_76	76	70.2	68.48	1.03	68.48	1.03	68.48	1.03	68.48	1.03
CS4_2650_305	305	200.6	190.82	1.05	189.35	1.06	197.61	1.02	190.58	1.05
CS4_2650_687	687	263.7	225.69	1.17	205.37	1.28	239.26	1.10	227.01	1.16
CS4_2650_1221	1221	291.8	225.77	1.29	205.37	1.42	239.26	1.22	227.01	1.29
CS4_2650_1908	1908	311.1	225.77	1.38	205.37	1.51	239.26	1.30	227.01	1.37
CS4_2650_2747	2747	318.7	225.77	1.41	205.37	1.55	239.26	1.33	227.01	1.40
CS4_2700_74	74	68.5	66.63	1.03	66.63	1.03	66.63	1.03	66.63	1.03
CS4_2700_295	295	195.9	185.29	1.06	184.08	1.06	192.09	1.02	184.79	1.06
CS4_2700_665	665	257.6	220.30	1.17	201.91	1.28	233.67	1.10	220.90	1.17
CS4_2700_1182	1182	284.8	220.36	1.29	201.91	1.41	233.67	1.22	220.90	1.29
CS4_2700_1846	1846	295.1	220.36	1.34	201.91	1.46	233.67	1.26	220.90	1.34
CS4_2700_2659	2659	303.1	220.36	1.38	201.91	1.50	233.67	1.30	220.90	1.37
CS4_2750_72	72	66.4	64.80	1.02	64.80	1.02	64.80	1.02	64.80	1.02
CS4_2750_286	286	190.8	180.15	1.06	179.10	1.07	186.98	1.02	179.42	1.06
CS4_2750_644	644	251.7	215.15	1.17	198.56	1.27	228.33	1.10	215.07	1.17
CS4_2750_1144	1144	277.7	215.20	1.29	198.56	1.40	228.33	1.22	215.07	1.29
CS4_2750_1788	1788	288.9	215.20	1.34	198.56	1.45	228.33	1.27	215.07	1.34
CS4_2750_2574	2574	297.4	215.20	1.38	198.56	1.50	228.33	1.30	215.07	1.38
CS4_2800_69	69	64.0	62.17	1.03	62.17	1.03	62.17	1.03	62.17	1.03
CS4_2800_277	277	188.4	175.09	1.08	174.19	1.08	181.93	1.04	174.15	1.08
CS4_2800_623	623	245.2	210.12	1.17	195.22	1.26	223.17	1.10	209.42	1.17
CS4_2800_1108	1108	271.2	210.15	1.29	195.26	1.39	223.17	1.22	209.44	1.29
CS4_2800_1731	1731	283.1	210.15	1.35	195.26	1.45	223.17	1.27	209.44	1.35
CS4_2800_2493	2493	291.7	210.15	1.39	195.26	1.49	223.17	1.31	209.44	1.39
CS4_2850_67	67	61.5	60.36	1.02	60.36	1.02	60.36	1.02	60.36	1.02
CS4_2850_268	268	180.4	170.13	1.06	169.36	1.07	176.48	1.02	176.48	1.02
CS4_2850_604	604	239.2	205.33	1.16	192.01	1.25	218.25	1.10	204.06	1.17
CS4_2850_1074	1074	265.5	205.35	1.29	192.05	1.38	218.25	1.22	204.07	1.30
CS4_2850_1678	1678	277.3	205.35	1.35	192.05	1.44	218.25	1.27	204.07	1.36
CS4_2850_2416	2416	286.2	205.35	1.39	192.05	1.49	218.25	1.31	204.07	1.40
CS4_2900_65	65	60.4	58.55	1.03	58.55	1.03	58.55	1.03	58.55	1.03
CS4_2900_260	260	179.9	165.52	1.09	164.86	1.09	171.16	1.05	171.16	1.05
CS4_2900_586	586	233.7	200.67	1.16	188.87	1.24	213.46	1.09	198.85	1.18
CS4_2900_1041	1041	260.0	200.68	1.30	188.87	1.38	213.46	1.22	198.85	1.31
CS4_2900_1627	1627	272.0	200.68	1.36	188.87	1.44	213.46	1.27	198.85	1.37

CS4_2900_2343	2343	282.9	200.68	1.41	188.87	1.50	213.46	1.33	198.85	1.42
			Av.	1.21		1.30		1.16		1.21
			Max	1.41		1.55		1.33		1.42
			Min	1.02		1.02		1.00		1.02
			St. dev	0.137		0.193		0.113		0.137

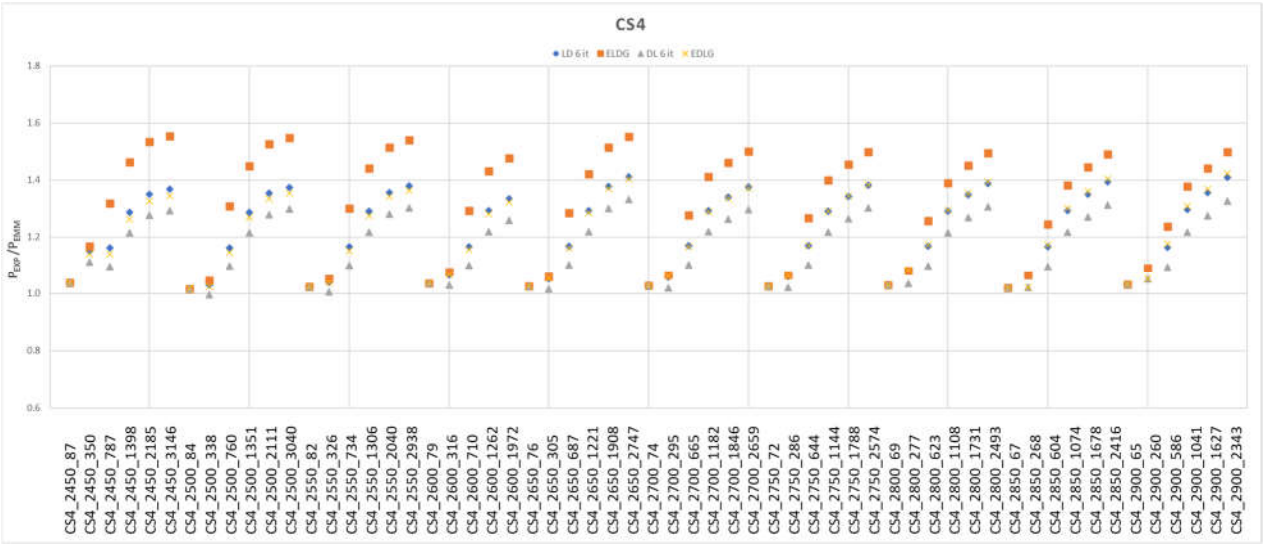

Figure 39 Comparison EMM × numerical results of CS4 specimens

Table 14 Comparison EMM × numerical results of CS5 specimens

Specimen	f_y	f_u	LDG 6 Iterations		ELDG		DLG6 Iterations		EDLG	
	MPa	MPa	MPa	/ LDG	MPa	/ ELDG	MPa	/ DLG	MPa	/ EDLG
CS5_2050_105	105	98.7	94.55	1.04	94.55	1.04	94.55	1.04	94.55	1.04
CS5_2050_419	419	299.2	257.91	1.16	254.18	1.18	266.42	1.12	259.45	1.15
CS5_2050_943	943	346.6	300.50	1.15	266.12	1.30	317.46	1.09	305.03	1.14
CS5_2050_1677	1677	379.7	300.68	1.26	266.19	1.43	317.46	1.20	305.05	1.24
CS5_2050_2620	2620	397.5	300.68	1.32	266.19	1.49	317.46	1.25	305.05	1.30
CS5_2050_3772	3772	399.8	300.68	1.33	266.19	1.50	317.46	1.26	305.05	1.31
CS5_2100_101	101	91.8	90.93	1.01	90.93	1.01	90.93	1.01	90.93	1.01
CS5_2100_402	402	253.6	249.11	1.02	246.02	1.03	257.32	0.99	249.76	1.02
CS5_2100_905	905	335.4	291.63	1.15	260.83	1.29	308.30	1.09	294.99	1.14
CS5_2100_1609	1609	369.2	291.78	1.27	260.89	1.42	308.29	1.20	295.01	1.25
CS5_2100_2515	2515	385.4	291.78	1.32	260.89	1.48	308.29	1.25	295.01	1.31
CS5_2100_3621	3621	388.0	291.78	1.33	260.89	1.49	308.29	1.26	295.01	1.32
CS5_2150_97	97	88.5	87.33	1.01	87.33	1.01	87.33	1.01	87.33	1.01
CS5_2150_386	386	246.4	240.67	1.02	238.15	1.03	248.63	0.99	240.54	1.02
CS5_2150_869	869	326.1	283.13	1.15	255.65	1.28	299.50	1.09	285.34	1.14
CS5_2150_1546	1546	359.5	283.24	1.27	255.71	1.41	299.49	1.20	285.36	1.26
CS5_2150_2415	2415	375.6	283.24	1.33	255.71	1.47	299.49	1.25	285.36	1.32
CS5_2150_3478	3478	378.6	283.24	1.34	255.71	1.48	299.49	1.26	285.36	1.33
CS5_2200_93	93	84.7	83.75	1.01	83.75	1.01	83.75	1.01	83.75	1.01
CS5_2200_371	371	238.8	232.40	1.03	230.64	1.04	240.41	0.99	231.85	1.03
CS5_2200_836	836	317.1	275.09	1.15	250.72	1.26	291.15	1.09	276.22	1.15
CS5_2200_1485	1485	349.8	275.18	1.27	250.72	1.40	291.15	1.20	276.22	1.27
CS5_2200_2321	2321	366.2	275.18	1.33	250.72	1.46	291.15	1.26	276.22	1.33
CS5_2200_3342	3342	369.9	275.18	1.34	250.72	1.48	291.15	1.27	276.22	1.34
CS5_2250_89	89	80.0	80.18	1.00	80.18	1.00	80.18	1.00	80.18	1.00
CS5_2250_357	357	228.5	224.56	1.02	223.19	1.02	232.59	0.98	223.62	1.02
CS5_2250_803	803	307.1	267.39	1.15	245.80	1.25	283.12	1.08	267.40	1.15
CS5_2250_1428	1428	341.0	267.46	1.27	245.85	1.39	283.11	1.20	267.42	1.28
CS5_2250_2232	2232	356.7	267.46	1.33	245.85	1.45	283.11	1.26	267.42	1.33
CS5_2250_3214	3214	361.0	267.46	1.35	245.85	1.47	283.11	1.28	267.42	1.35
CS5_2300_86	86	78.7	77.45	1.02	77.45	1.02	77.45	1.02	77.45	1.02
CS5_2300_344	344	225.4	217.16	1.04	216.00	1.04	225.22	1.00	215.88	1.04
CS5_2300_773	773	300.0	260.01	1.15	241.00	1.24	275.44	1.09	259.01	1.16
CS5_2300_1374	1374	332.2	260.06	1.28	241.05	1.38	275.44	1.21	259.03	1.28
CS5_2300_2147	2147	348.7	260.06	1.34	241.05	1.45	275.44	1.27	259.03	1.35
CS5_2300_3092	3092	348.7	260.06	1.34	241.05	1.45	275.44	1.27	259.03	1.35
CS5_2350_83	83	75.4	74.73	1.01	74.73	1.01	74.73	1.01	74.73	1.01
CS5_2350_331	331	217.3	209.89	1.04	208.94	1.04	217.74	1.00	217.74	1.00
CS5_2350_774	774	291.5	252.89	1.15	236.35	1.23	268.07	1.09	250.98	1.16
CS5_2350_1323	1323	324.2	252.90	1.28	236.35	1.37	268.07	1.21	250.98	1.29
CS5_2350_2068	2068	337.1	252.90	1.33	236.35	1.43	268.07	1.26	250.98	1.34
CS5_2350_2977	2977	342.1	252.90	1.35	236.35	1.45	268.07	1.28	250.98	1.36
CS5_2400_80	80	73.3	72.02	1.02	72.02	1.02	72.02	1.02	72.02	1.02
CS5_2400_319	319	214.2	203.01	1.06	202.21	1.06	209.82	1.02	209.82	1.02
CS5_2400_717	717	283.7	245.94	1.15	231.53	1.23	261.00	1.09	243.27	1.17
CS5_2400_1275	1275	316.2	245.96	1.29	231.57	1.37	260.99	1.21	243.29	1.30
CS5_2400_1992	1992	325.7	245.96	1.32	231.57	1.41	260.99	1.25	243.29	1.34
CS5_2400_2869	2869	333.1	245.96	1.35	231.57	1.44	260.99	1.28	243.29	1.37
			Av.	1.19		1.27		1.14		1.19
			Max	1.35		1.50		1.28		1.37
			Min	1.00		1.00		0.98		1.00
			St. dev	0.132		0.184		0.109		0.133

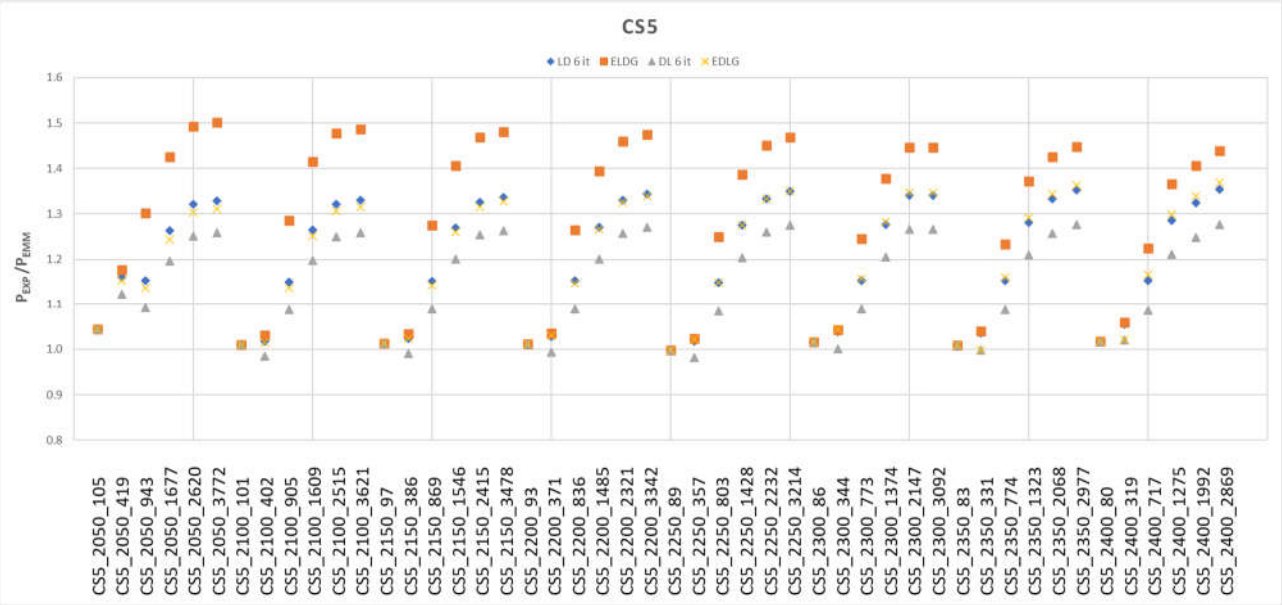

Figure 40 Comparison EMM × numerical results of CS5 specimens

Table 15 Comparison EMM × numerical results of CS6 specimens

Specimen	f_y	f_u	LDG 6 Iterations		ELDG		DLG6 Iterations		EDLG	
	MPa	MPa	MPa	/ LDG	MPa	/ ELDG	MPa	/ DLG	MPa	/ EDLG
CS6_1550_76	76	70.8	68.44	1.03	68.44	1.03	68.44	1.03	68.44	1.03
CS6_1550_304	304	202.3	186.47	1.08	183.58	1.10	192.27	1.05	187.70	1.08
CS6_1550_684	684	250.4	216.76	1.16	191.14	1.31	228.14	1.10	219.90	1.14
CS6_1550_1215	1215	276.4	216.89	1.27	191.14	1.45	228.14	1.21	219.90	1.26
CS6_1550_1899	1899	308.8	216.89	1.42	191.14	1.62	228.14	1.35	219.90	1.40
CS6_1550_2734	2734	325.9	216.89	1.50	191.14	1.71	228.14	1.43	219.90	1.48
CS6_1600_73	73	67.8	65.73	1.03	65.73	1.03	65.73	1.03	65.73	1.03
CS6_1600_291	291	195.1	179.83	1.08	177.46	1.10	185.40	1.05	180.36	1.08
CS6_1600_655	655	241.1	210.12	1.15	187.25	1.29	221.28	1.09	212.37	1.14
CS6_1600_1165	1165	271.5	210.22	1.29	187.25	1.45	221.28	1.23	212.37	1.28
CS6_1600_1820	1820	310.3	210.22	1.48	187.25	1.66	221.28	1.40	212.37	1.46
CS6_1600_2620	2620	312.2	210.22	1.49	187.25	1.67	221.28	1.41	212.37	1.47
CS6_1650_70	70	64.7	63.01	1.03	63.01	1.03	63.01	1.03	63.01	1.03
CS6_1650_279	279	178.1	173.46	1.03	171.52	1.04	178.81	1.00	173.33	1.03
CS6_1650_627	627	232.8	203.56	1.14	183.37	1.27	214.47	1.09	204.89	1.14
CS6_1650_1115	1115	259.8	203.64	1.28	183.37	1.42	214.47	1.21	204.89	1.27
CS6_1650_2508	2508	301.1	203.64	1.48	183.37	1.64	214.47	1.40	204.89	1.47
CS6_1700_67	67	61.6	60.31	1.02	60.31	1.02	60.31	1.02	60.31	1.02
CS6_1700_266	266	170.3	166.75	1.02	165.31	1.03	171.95	0.99	166.08	1.03
CS6_1700_600	600	227.1	197.17	1.15	179.50	1.27	207.81	1.09	197.57	1.15
CS6_1700_1066	1066	252.1	197.23	1.28	179.50	1.40	207.81	1.21	197.57	1.28
CS6_1700_1666	1666	273.7	197.23	1.39	179.50	1.52	207.81	1.32	197.57	1.39
CS6_1700_2398	2398	290.5	197.23	1.47	179.50	1.62	207.81	1.40	197.57	1.47
CS6_1750_64	64	58.9	57.61	1.02	57.61	1.02	57.61	1.02	57.61	1.02
CS6_1750_255	255	164.8	160.35	1.03	159.37	1.03	165.69	0.99	159.48	1.03
CS6_1750_573	573	219.4	190.63	1.15	175.11	1.25	201.19	1.09	190.34	1.15
CS6_1750_1019	1019	244.8	190.68	1.28	175.15	1.40	201.18	1.22	190.35	1.29
CS6_1750_1592	1592	265.0	190.68	1.39	175.15	1.51	201.18	1.32	190.35	1.39
CS6_1800_61	61	56.3	54.93	1.02	54.93	1.02	54.93	1.02	54.93	1.02
CS6_1800_244	244	161.0	154.00	1.05	153.18	1.05	159.48	1.01	152.99	1.05
CS6_1800_548	548	211.9	184.20	1.15	170.63	1.24	194.73	1.09	183.32	1.16
CS6_1800_974	974	237.0	184.24	1.29	170.66	1.39	194.72	1.22	183.34	1.29
CS6_1800_1522	1522	255.8	184.24	1.39	170.66	1.50	194.72	1.31	183.34	1.40
CS6_1800_2192	2192	271.8	184.24	1.48	170.66	1.59	194.72	1.40	183.34	1.48
CS6_1850_58	58	53.6	52.26	1.03	52.26	1.03	52.26	1.03	52.26	1.03
CS6_1850_233	233	155.1	147.76	1.05	147.09	1.05	153.29	1.01	153.29	1.01
CS6_1850_524	524	205.5	177.99	1.15	166.26	1.24	188.49	1.09	176.56	1.16
CS6_1850_932	932	230.8	178.01	1.30	166.29	1.39	188.49	1.22	176.57	1.31
CS6_1850_1456	1456	248.6	178.01	1.40	166.29	1.49	188.49	1.32	176.57	1.41
CS6_1850_2096	2096	264.9	178.01	1.49	166.29	1.59	188.49	1.41	176.57	1.50
CS6_1900_56	56	51.7	50.41	1.03	50.41	1.03	50.41	1.03	50.41	1.03
CS6_1900_223	223	151.7	141.97	1.07	141.42	1.07	146.68	1.03	146.68	1.03
CS6_1900_501	501	195.0	172.07	1.13	162.07	1.20	182.53	1.07	170.11	1.15
CS6_1900_891	891	223.9	172.08	1.30	162.10	1.38	182.53	1.23	170.12	1.32
CS6_1900_1393	1393	241.8	172.08	1.41	162.10	1.49	182.53	1.32	170.12	1.42
CS6_1900_2005	2005	257.4	172.08	1.50	162.10	1.59	182.53	1.41	170.12	1.51
			Av.	1.23		1.31		1.17		1.22
			Max	1.50		1.71		1.43		1.51
			Min	1.02		1.02		0.99		1.01
			St. dev	0.172		0.228		0.149		0.173

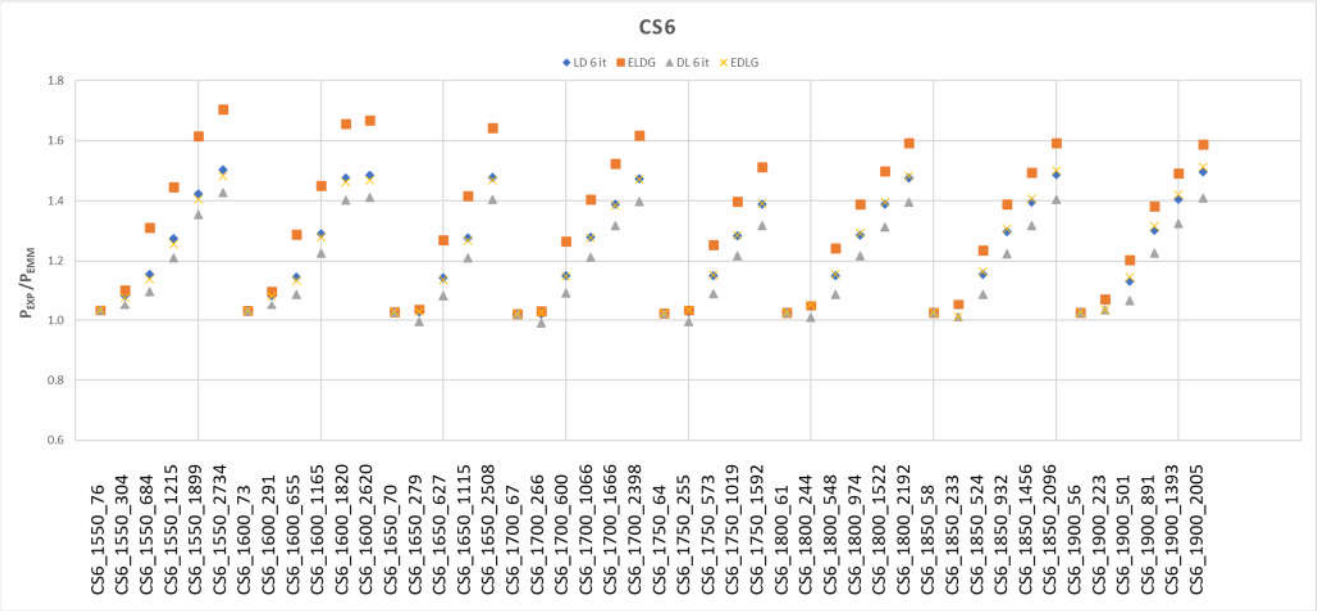

Figure 41 Comparison EMM × numerical results of CS6 specimens

Table 16 Comparison EMM × numerical results of CS7 specimens

Specimen	f_y	f_u	LDG 6 Iterations		ELDG		DLG6 Iterations		EDLG	
	MPa	MPa	MPa	/ LDG	MPa	/ ELDG	MPa	/ DLG	MPa	/ EDLG
CS7_2000_93	93	87.1	83.78	1.04	83.78	1.04	83.78	1.04	83.78	1.04
CS7_2000_373	373	266.0	230.41	1.15	227.34	1.17	236.43	1.13	230.58	1.15
CS7_2000_839	839	310.1	269.13	1.15	239.68	1.29	281.08	1.10	270.62	1.15
CS7_2000_1492	1492	333.8	269.25	1.24	239.74	1.39	281.07	1.19	270.64	1.23
CS7_2000_2331	2331	347.2	269.25	1.29	239.74	1.45	281.07	1.24	270.64	1.28
CS7_2000_3356	3356	349.7	269.25	1.30	239.74	1.46	281.07	1.24	270.64	1.29
CS7_2050_89	89	83.3	80.19	1.04	80.19	1.04	80.19	1.04	80.19	1.04
CS7_2050_357	357	254.3	222.13	1.14	219.64	1.16	227.93	1.12	221.50	1.15
CS7_2050_804	804	301.1	260.85	1.15	234.80	1.28	272.58	1.10	261.30	1.15
CS7_2050_1429	1429	324.2	260.94	1.24	234.80	1.38	272.58	1.19	261.30	1.24
CS7_2050_2233	2233	337.9	260.94	1.29	234.80	1.44	272.58	1.24	261.30	1.29
CS7_2050_3215	3215	340.7	260.94	1.31	234.80	1.45	272.58	1.25	261.30	1.30
CS7_2100_86	86	80.1	77.42	1.03	77.42	1.03	77.42	1.03	77.42	1.03
CS7_2100_342	342	244.9	214.27	1.14	212.27	1.15	219.88	1.11	212.96	1.15
CS7_2100_771	771	292.8	253.04	1.16	230.03	1.27	264.53	1.11	252.46	1.16
CS7_2100_1370	1370	315.4	253.10	1.25	230.03	1.37	264.53	1.19	252.46	1.25
CS7_2100_2140	2140	328.8	253.10	1.30	230.03	1.43	264.53	1.24	252.46	1.30
CS7_2100_3082	3082	332.2	253.10	1.31	230.03	1.44	264.53	1.26	252.46	1.32
CS7_2150_82	82	76.6	73.87	1.04	73.87	1.04	73.87	1.04	73.87	1.04
CS7_2150_329	329	236.2	207.08	1.14	205.47	1.15	212.56	1.11	205.19	1.15
CS7_2150_739	739	284.2	245.57	1.16	225.30	1.26	256.84	1.11	244.00	1.16
CS7_2150_1314	1314	306.9	245.61	1.25	225.35	1.36	256.83	1.19	244.01	1.26
CS7_2200_79	79	73.5	71.14	1.03	71.14	1.03	71.14	1.03	71.14	1.03
CS7_2200_315	315	227.1	199.47	1.14	198.47	1.14	205.04	1.11	197.30	1.15
CS7_2200_710	710	276.0	238.45	1.16	220.78	1.25	249.49	1.11	235.96	1.17
CS7_2200_1262	1262	298.8	238.48	1.25	220.78	1.35	249.49	1.20	235.96	1.27
CS7_2200_1972	1972	306.3	238.48	1.28	220.78	1.39	249.49	1.23	235.96	1.30
CS7_2200_2839	2839	312.3	238.48	1.31	220.78	1.41	249.49	1.25	235.96	1.32
CS7_2250_76	76	70.6	68.43	1.03	68.43	1.03	68.43	1.03	68.43	1.03
CS7_2250_303	303	219.1	192.55	1.14	191.73	1.14	198.24	1.11	190.17	1.15
CS7_2250_682	682	267.9	231.55	1.16	216.14	1.24	242.42	1.11	228.24	1.17
CS7_2250_1212	1212	291.0	231.57	1.26	216.14	1.35	242.42	1.20	228.24	1.27
CS7_2250_1894	1894	298.6	231.57	1.29	216.14	1.38	242.42	1.23	228.24	1.31
CS7_2250_2728	2728	304.6	231.57	1.32	216.14	1.41	242.42	1.26	228.24	1.33
CS7_2300_73	73	67.6	65.74	1.03	65.74	1.03	65.74	1.03	65.74	1.03
CS7_2300_291	291	211.0	185.75	1.14	185.08	1.14	191.57	1.10	183.23	1.15
CS7_2300_656	656	260.3	224.94	1.16	211.52	1.23	235.70	1.10	220.93	1.18
CS7_2300_1166	1166	284.2	224.95	1.26	211.52	1.34	235.70	1.21	220.93	1.29
CS7_2350_70	70	64.8	63.06	1.03	63.06	1.03	63.06	1.03	63.06	1.03
CS7_2350_280	280	203.3	179.37	1.13	178.83	1.14	184.38	1.10	184.38	1.10
CS7_2350_631	631	252.7	218.60	1.16	206.95	1.22	229.27	1.10	213.91	1.18
CS7_2350_1753	1753	284.1	218.61	1.30	206.99	1.37	229.27	1.24	213.93	1.33
CS7_2350_2524	2524	290.8	218.61	1.33	206.99	1.40	229.27	1.27	213.93	1.36
			Av.	1.19		1.26		1.15		1.19
			Max	1.33		1.46		1.27		1.36
			Min	1.03		1.03		1.03		1.03
			St. dev	0.097		0.145		0.078		0.101

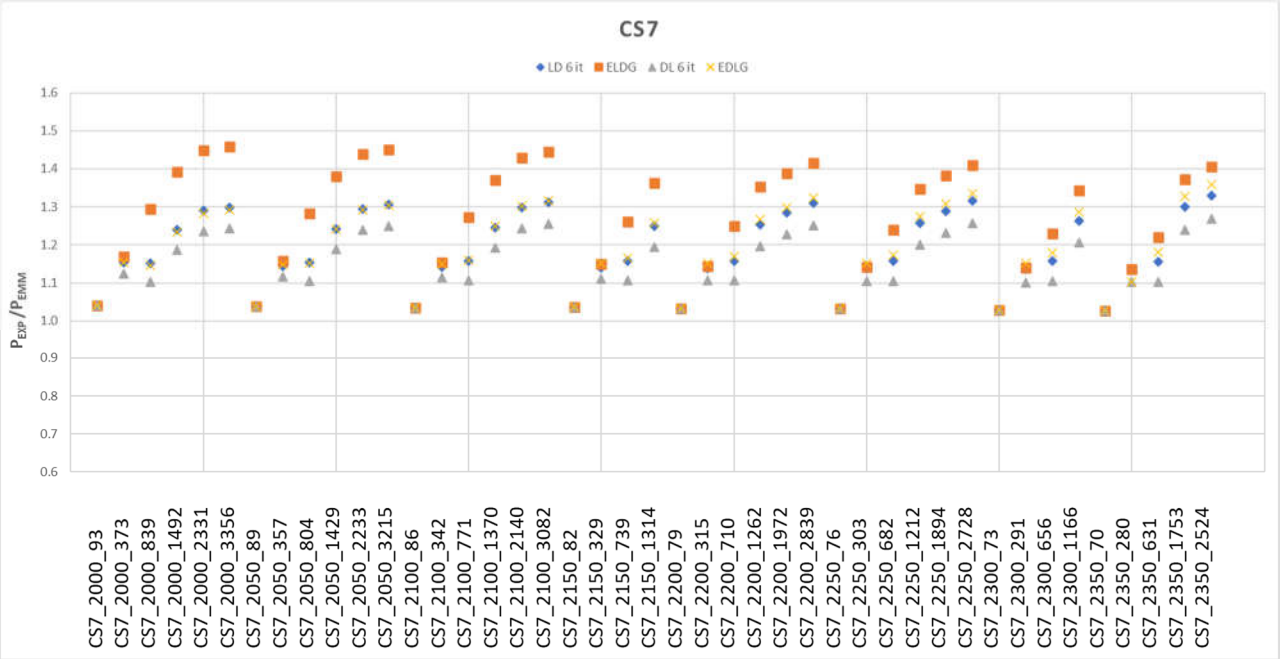

Figure 42 Comparison EMM × numerical results of CS7 specimens

Table 17 Comparison EMM × numerical results of CS8 specimens

Specimen	f_y	f_u	LDG 6 Iterations		ELDG		DLG6 Iterations		EDLG	
	MPa	MPa	MPa	/ LDG	MPa	/ ELDG	MPa	/ DLG	MPa	/ EDLG
CS8_2350_47	47	43.1	42.36	1.02	42.36	1.02	42.36	1.02	42.36	1.02
CS8_2350_189	189	125.8	116.37	1.08	114.68	1.10	119.26	1.05	116.64	1.08
CS8_2350_426	426	152.4	135.64	1.12	120.02	1.27	141.29	1.08	136.53	1.12
CS8_2350_1183	1183	187.4	135.71	1.38	120.02	1.56	141.29	1.33	136.53	1.37
CS8_2400_46	46	42.1	41.41	1.02	41.41	1.02	41.41	1.02	41.41	1.02
CS8_2400_183	183	122.1	113.15	1.08	111.68	1.09	115.99	1.05	113.13	1.08
CS8_2400_412	412	149.4	132.27	1.13	117.97	1.27	137.90	1.08	132.80	1.13
CS8_2450_44	44	40.0	39.65	1.01	39.65	1.01	39.65	1.01	39.65	1.01
CS8_2450_177	177	118.3	109.94	1.08	108.68	1.09	112.72	1.05	109.64	1.08
CS8_2450_398	398	146.2	128.94	1.13	115.92	1.26	134.53	1.09	129.10	1.13
CS8_2500_43	43	39.2	38.70	1.01	38.70	1.01	38.70	1.01	38.70	1.01
CS8_2500_171	171	114.2	106.78	1.07	105.72	1.08	109.51	1.04	106.22	1.08
CS8_2500_384	384	143.0	125.77	1.14	113.93	1.26	131.30	1.09	125.55	1.14
CS8_2500_684	684	160.0	125.80	1.27	113.95	1.40	131.30	1.22	125.56	1.27
CS8_2500_1068	1068	178.2	125.80	1.42	113.95	1.56	131.30	1.36	125.56	1.42
CS8_2500_1538	1538	190.4	125.80	1.51	113.95	1.67	131.30	1.45	125.56	1.52
CS8_2550_41	41	37.3	36.95	1.01	36.95	1.01	36.95	1.01	36.95	1.01
CS8_2550_165	165	110.5	103.64	1.07	102.75	1.08	106.31	1.04	102.84	1.07
CS8_2550_372	372	139.9	122.66	1.14	111.97	1.25	128.14	1.09	122.10	1.15
CS8_2550_1487	1487	187.2	122.69	1.53	111.97	1.67	128.14	1.46	122.10	1.53
CS8_2600_40	40	36.3	36.02	1.01	36.02	1.01	36.02	1.01	36.02	1.01
CS8_2600_160	160	107.4	100.82	1.07	100.09	1.07	103.47	1.04	99.83	1.08
CS8_2600_360	360	134.4	119.72	1.12	110.08	1.22	125.13	1.07	118.80	1.13
CS8_2600_999	999	167.5	119.74	1.40	110.08	1.52	125.13	1.34	118.80	1.41
CS8_2600_1438	1438	183.1	119.74	1.53	110.08	1.66	125.13	1.46	118.80	1.54
CS8_2650_39	39	35.2	35.09	1.00	35.09	1.00	35.09	1.00	35.09	1.00
CS8_2650_155	155	104.4	97.96	1.07	97.44	1.07	100.66	1.04	96.87	1.08
CS8_2650_348	348	133.9	116.87	1.15	108.22	1.24	122.20	1.10	115.60	1.16
CS8_2650_618	618	150.1	116.88	1.28	108.22	1.39	122.20	1.23	115.60	1.30
CS8_2650_966	966	166.5	116.88	1.42	108.22	1.54	122.20	1.36	115.60	1.44
			Av.	1.18		1.25		1.14		1.18
			Max	1.53		1.67		1.46		1.54
			Min	1.00		1.00		1.00		1.00
			St. dev	0.171		0.225		0.152		0.173

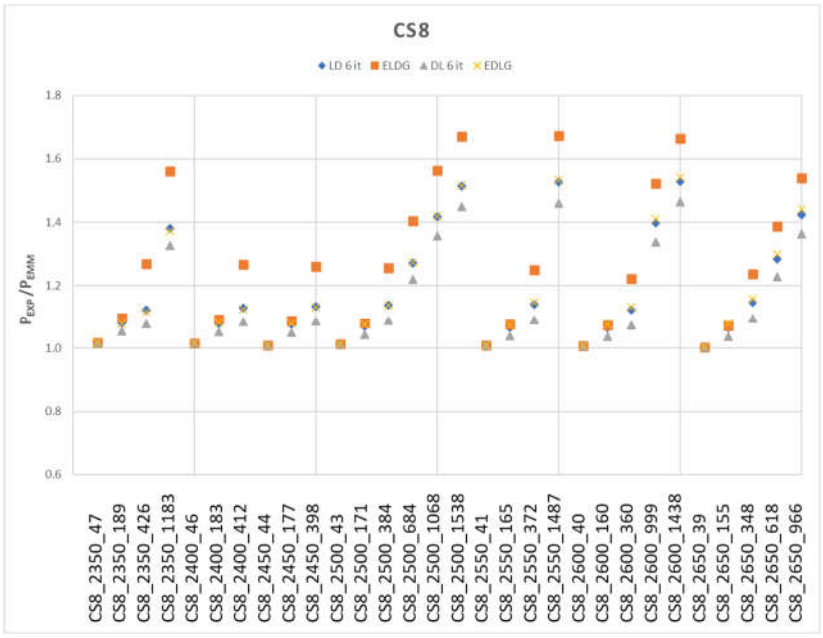

Figure 43 Comparison EMM × numerical results of CS8 specimens

Table 18 Comparison EMM × numerical results of CS9 specimens

Specimen	f_y	f_u	LDG 6 Iterations		ELDG		DLG6 Iterations		EDLG	
	MPa	MPa	MPa	/ LDG	MPa	/ ELDG	MPa	/ DLG	MPa	/ EDLG
CS9_1550_83	83	77.4	74.75	1.04	74.75	1.04	74.75	1.04	74.75	1.04
CS9_1550_332	332	228.9	203.28	1.13	200.02	1.14	207.70	1.10	203.89	1.12
CS9_1550_746	746	271.1	236.08	1.15	207.48	1.31	244.48	1.11	237.28	1.14
CS9_1550_1327	1327	293.2	236.19	1.24	207.53	1.41	244.48	1.20	237.30	1.24
CS9_1550_2073	2073	313.3	236.19	1.33	207.53	1.51	244.48	1.28	237.30	1.32
CS9_1550_2986	2986	327.8	236.19	1.39	207.53	1.58	244.48	1.34	237.30	1.38
CS9_1600_79	79	73.5	71.14	1.03	71.14	1.03	71.14	1.03	71.14	1.03
CS9_1600_315	315	217.4	194.64	1.12	192.02	1.13	198.91	1.09	194.46	1.12
CS9_1600_710	710	261.3	227.43	1.15	202.30	1.29	235.81	1.11	227.78	1.15
CS9_1600_1972	1972	300.4	227.51	1.32	202.30	1.48	235.81	1.27	227.78	1.32
CS9_1600_2839	2839	314.1	227.51	1.38	202.30	1.55	235.81	1.33	227.78	1.38
CS9_1650_75	75	69.6	67.55	1.03	67.55	1.03	67.55	1.03	67.55	1.03
CS9_1650_300	300	206.5	186.64	1.11	184.54	1.12	190.80	1.08	185.78	1.11
CS9_1650_675	675	251.5	219.17	1.15	197.19	1.28	227.49	1.11	218.63	1.15
CS9_1650_1876	1876	290.6	219.23	1.33	197.23	1.47	227.49	1.28	218.64	1.33
CS9_1650_2701	2701	304.9	219.23	1.39	197.23	1.55	227.49	1.34	218.64	1.39
CS9_1700_71	71	65.9	63.98	1.03	63.98	1.03	63.98	1.03	63.98	1.03
CS9_1700_286	286	199.8	179.05	1.12	177.40	1.13	183.10	1.09	177.58	1.13
CS9_1700_642	642	241.7	211.32	1.14	192.31	1.26	219.51	1.10	209.87	1.15
CS9_1700_1142	1142	265.7	211.36	1.26	192.35	1.38	219.51	1.21	209.89	1.27
CS9_1700_1785	1785	281.6	211.36	1.33	192.35	1.46	219.51	1.28	209.89	1.34
CS9_1700_2570	2570	295.9	211.36	1.40	192.35	1.54	219.51	1.35	209.89	1.41
CS9_1750_68	68	63.1	61.24	1.03	61.24	1.03	61.24	1.03	61.24	1.03
CS9_1750_272	272	188.6	171.58	1.10	170.33	1.11	175.53	1.07	169.57	1.11
CS9_1750_612	612	232.7	203.88	1.14	187.63	1.24	211.93	1.10	201.57	1.15
CS9_1750_1087	1087	257.1	203.91	1.26	187.63	1.37	211.93	1.21	201.57	1.28
CS9_1750_1699	1699	281.3	203.91	1.38	187.63	1.50	211.93	1.33	201.57	1.40
CS9_1750_2446	2446	294.1	203.91	1.44	187.63	1.57	211.93	1.39	201.57	1.46
CS9_1800_65	65	60.1	58.52	1.03	58.52	1.03	58.52	1.03	58.52	1.03
CS9_1800_259	259	182.0	164.38	1.11	163.58	1.11	168.38	1.08	162.04	1.12
CS9_1800_583	583	224.0	196.80	1.14	182.99	1.22	204.69	1.09	193.64	1.16
CS9_1800_1036	1036	248.6	196.82	1.26	182.99	1.36	204.69	1.21	193.64	1.28
CS9_1800_1618	1618	271.9	196.82	1.38	182.99	1.49	204.69	1.33	193.64	1.40
CS9_1800_2330	2330	284.5	196.82	1.45	182.99	1.55	204.69	1.39	193.64	1.47
CS9_1850_62	62	57.3	55.81	1.03	55.81	1.03	55.81	1.03	55.81	1.03
CS9_1850_247	247	173.5	157.51	1.10	156.95	1.11	161.66	1.07	155.00	1.12
CS9_1850_555	555	215.5	190.07	1.13	178.43	1.21	197.81	1.09	186.09	1.16
CS9_1850_987	987	245.6	190.09	1.29	178.47	1.38	197.81	1.24	186.10	1.32
CS9_1850_1543	1543	263.4	190.09	1.39	178.47	1.48	197.81	1.33	186.10	1.42
CS9_1850_2221	2221	276.2	190.09	1.45	178.47	1.55	197.81	1.40	186.10	1.48
			Av.	1.22		1.30		1.18		1.22
			Max	1.45		1.58		1.40		1.48
			Min	1.03		1.03		1.03		1.03
			St. dev	0.140		0.193		0.124		0.144

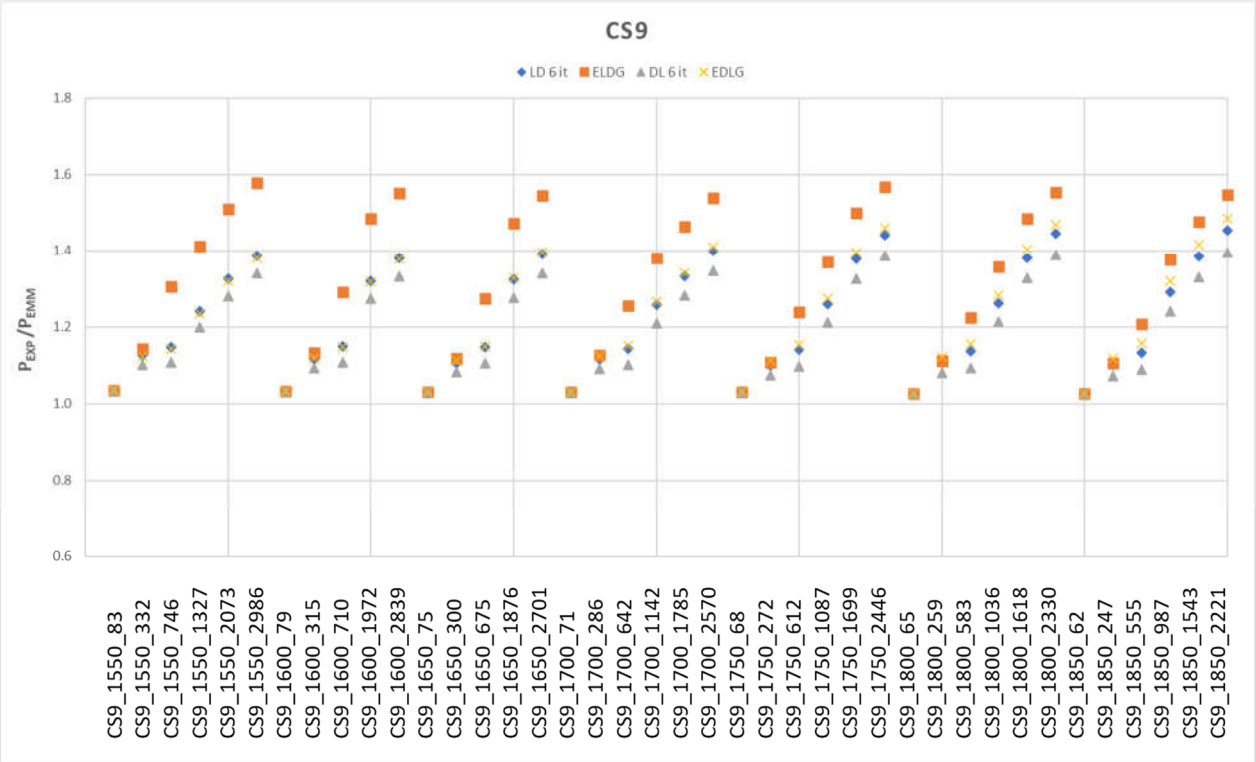

Figure 44 Comparison EMM × numerical results of CS9 specimens

Table 19 Comparison EMM × numerical results of CS10 specimens

Specimen	f_y	f_u	LDG 6 Iterations		ELDG		DLG6 Iterations		EDLG	
	MPa	MPa	MPa	/ LDG	MPa	/ ELDG	MPa	/ DLG	MPa	/ EDLG
CS10_1550_120	120	113.0	108.04	1.05	108.04	1.05	108.04	1.05	108.04	1.05
CS10_1550_478	478	345.6	294.35	1.17	290.09	1.19	299.95	1.15	294.15	1.17
CS10_1550_1077	1077	397.9	343.15	1.16	303.73	1.31	353.91	1.12	343.17	1.16
CS10_1550_1914	1914	406.0	343.28	1.18	303.73	1.34	353.91	1.15	343.17	1.18
CS10_1550_2990	2990	414.5	343.28	1.21	303.73	1.36	353.91	1.17	343.17	1.21
CS10_1600_113	113	106.1	101.79	1.04	101.79	1.04	101.79	1.04	101.79	1.04
CS10_1600_453	453	327.3	281.26	1.16	277.96	1.18	286.58	1.14	279.76	1.17
CS10_1600_1019	1019	383.2	329.79	1.16	296.01	1.29	340.26	1.13	328.12	1.17
CS10_1600_1811	1811	391.7	329.88	1.19	296.01	1.32	340.26	1.15	328.12	1.19
CS10_1600_2830	2830	401.1	329.88	1.22	296.01	1.36	340.26	1.18	328.12	1.22
CS10_1600_4075	4075	401.5	329.88	1.22	296.01	1.36	340.26	1.18	328.12	1.22
CS10_1650_107	107	100.5	96.40	1.04	96.40	1.04	96.40	1.04	96.40	1.04
CS10_1650_429	429	311.9	268.72	1.16	266.23	1.17	273.82	1.14	266.13	1.17
CS10_1650_965	965	368.6	317.31	1.16	288.49	1.28	327.50	1.13	314.03	1.17
CS10_1650_1716	1716	378.7	317.36	1.19	288.55	1.31	327.50	1.16	314.05	1.21
CS10_1650_2682	2682	388.1	317.36	1.22	288.55	1.35	327.50	1.19	314.05	1.24
CS10_1650_3862	3862	388.9	317.36	1.23	288.55	1.35	327.50	1.19	314.05	1.24
CS10_1700_102	102	95.6	91.85	1.04	91.85	1.04	91.85	1.04	91.85	1.04
CS10_1700_407	407	296.5	256.93	1.15	255.08	1.16	261.88	1.13	253.45	1.17
CS10_1700_916	916	354.0	305.49	1.16	281.17	1.26	315.42	1.12	300.78	1.18
CS10_1700_1628	1628	365.4	305.53	1.20	281.17	1.30	315.42	1.16	300.78	1.21
CS10_1700_2544	2544	374.3	305.53	1.23	281.17	1.33	315.42	1.19	300.78	1.24
CS10_1700_3664	3664	375.1	305.53	1.23	281.17	1.33	315.42	1.19	300.78	1.25
CS10_1750_97	97	90.9	87.33	1.04	87.33	1.04	87.33	1.04	87.33	1.04
CS10_1750_387	387	282.6	245.87	1.15	244.51	1.16	250.76	1.13	241.71	1.17
CS10_1750_870	870	339.8	294.24	1.15	273.81	1.24	303.98	1.12	288.24	1.18
CS10_1750_1546	1546	353.4	294.26	1.20	273.81	1.29	303.98	1.16	288.24	1.23
CS10_1750_2416	2416	362.3	294.26	1.23	273.81	1.32	303.98	1.19	288.24	1.26
CS10_1750_3480	3480	363.8	294.26	1.24	273.81	1.33	303.98	1.20	288.24	1.26
CS10_1800_92	92	86.0	82.85	1.04	82.85	1.04	82.85	1.04	82.85	1.04
CS10_1800_368	368	269.1	235.05	1.14	234.27	1.15	240.21	1.12	230.65	1.17
CS10_1800_827	827	326.5	283.61	1.15	266.49	1.23	293.25	1.11	276.47	1.18
CS10_1800_1471	1471	342.3	283.62	1.21	266.54	1.28	293.25	1.17	276.49	1.24
CS10_1800_2298	2298	351.5	283.62	1.24	266.54	1.32	293.25	1.20	276.49	1.27
CS10_1800_3309	3309	353.0	283.62	1.24	266.54	1.32	293.25	1.20	276.49	1.28
			Av.	1.17		1.24		1.14		1.18
			Max	1.24		1.36		1.20		1.28
			Min	1.04		1.04		1.04		1.04
			St. dev	0.063		0.109		0.050		0.070

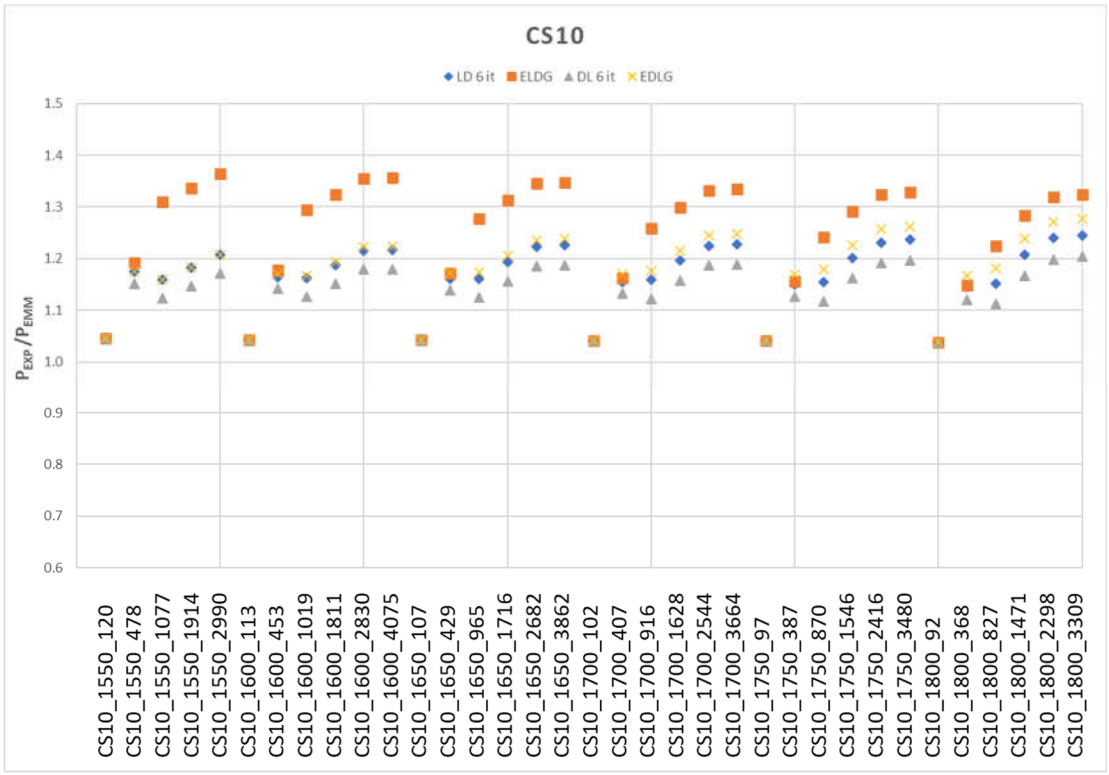

Figure 45 Comparison EMM × numerical results of CS10 specimens

4.1.3 Article from 2014 Rack

To evaluate the interaction between local and distortional buckling modes, in 2014 Dinis et al. [122], conducted a series of experimental tests on cold formed rack sections (Figure 46) shown in Table 20. To ensure a sufficient occurrence of local/ distortional interactions the specimens' proprieties were designed using GBTUL [92].

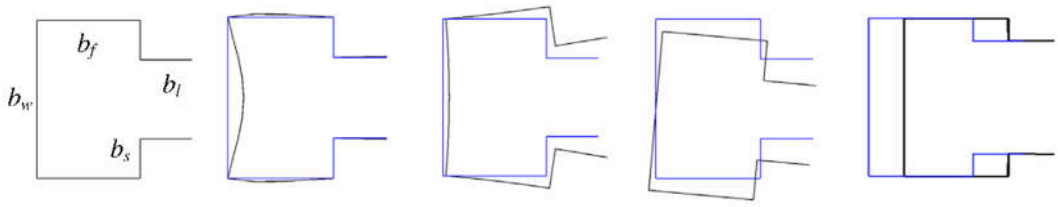

Figure 46 Depictions of Rack-sections and buckling modes.

To test the specimens a servo-controlled hydraulic machine with top and end plates bolted to a rigid flat bearing was used to continuously apply a compression force (see Figure 47). The specimens were fully restrained against warping and minor and major axis torsions.

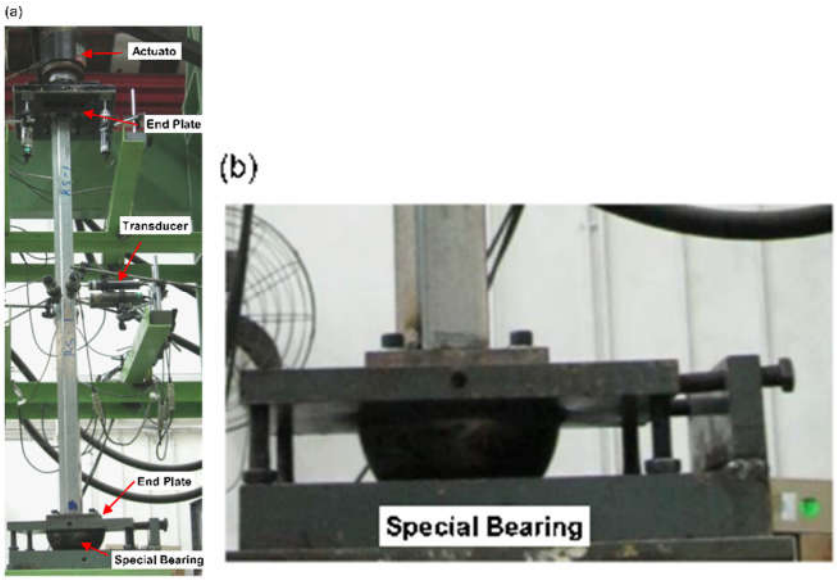

Figure 47 Pictures of set-up during compression tests

The results of the tests, experimental resistances and comparisons with EMM is shown in Table 21 and Figure 48.

Table 20 Rack column specimen's dimensions & critical loads P_{crL}, P_{crD} , P_{crG}.

Specimen	b_w	b_f	b_s	b_l	L	t	A	P_{crL}	P_{crD}	P_{crG}
	mm	mm	mm	mm	mm	mm	mm2	kN	kN	kN
RS-1	73	37.1	17.3	21.3	1300	1.002	224.85	52.4	71.7	110.9
RS-2	78.4	47.4	17.2	21	1800	0.998	249.10	48.9	66.1	98.2
RS-3	83.6	52.3	17.1	20.4	2100	0.982	258.46	43.1	63.1	92.4
RS-4-1	88.6	57.2	17.2	21.3	2499	0.999	279.72	42.8	60.1	87
RS-4-2	88.6	57.2	17.5	21.4	2500	0.981	275.46	40.7	58.9	84
RS-5	83.5	52.5	17.3	21.6	1397	1.193	317.70	77.6	101.7	155.8
RS-6	88.5	57.9	17.7	21	1599	1.186	334.10	71.5	98.9	151.7
RS-7	93.7	67.3	17.4	20.8	1902	1.227	373.87	74.8	98.1	146.2
RS-8-1	98.7	72.2	17	21	2501	1.201	383.24	66.2	87.1	120.8
RS-8-2	98.8	72.2	17.2	20.8	2501	1.175	375.06	62.1	84.5	117.8

As depicted in Table 21 and Figure 48 the EMM method produced, for this section type, slightly unsafe results when compared with the experimental tests, where the most unsafe ratio falling to 0.84. The results for the ELDG approach are relatively acceptable since only 3 ratios out of the 10 fall below 1.0 but not less than 0.96. However a pattern among the different approaches in the EMM is apparent which shows that for almost all of the EMM comparisons, DL with iterations is the approach with the best accuracy followed up by EDLG, LDG 6 with iterations and finally ELDG. It indicates that rather than matching the ELDG approach with this type of section for accurate results, the equations could slightly be adapted when dealing with Rack-sections to improve accuracy. Furthermore, this was the only sample of Rack-sections testes and compared with EMM, which should be taken with a grain of salt and comparison with a lot more specimen samples need to be done in order to properly determine the accuracy of EMM for Rack typed sections.

Table 21 Comparison EMM × experimental results of Rack specimens

Specimen	f_y	f_{EXP}	LDG 6 Iterations		ELDG		DLG6 Iterations		EDLG	
	MPa	MPa	MPa	/ LDG	MPa	/ ELDG	MPa	/ LDG	MPa	/ LDG
RS-1	500	259.0	278.54	0.93	262.98	0.98	281.13	0.92	289.79	0.89
RS-2	500	218.3	238.99	0.91	215.77	1.01	241.73	0.90	250.27	0.87
RS-3	500	210.2	220.56	0.95	192.18	1.09	220.59	0.95	229.81	0.91
RS-4-1	464	183.7	195.28	0.94	166.81	1.10	195.90	0.94	203.08	0.90
RS-4-2	500	185.0	194.62	0.95	161.02	1.15	193.54	0.96	200.07	0.92
RS-5	550	256.8	286.79	0.90	266.13	0.96	291.04	0.88	300.23	0.86
RS-6	550	238.9	269.68	0.89	244.60	0.98	272.26	0.88	282.95	0.84
RS-7	550	213.5	242.17	0.88	211.27	1.01	245.61	0.87	254.13	0.84
RS-8-1	550	196.9	205.04	0.96	169.99	1.16	206.51	0.95	210.58	0.93
RS-8-2	550	198.1	203.55	0.97	167.85	1.18	203.91	0.97	208.49	0.95
			Av.	0.93		1.06		0.92		0.89
			Max	0.97		1.18		0.97		0.95
			Min	0.88		0.96		0.87		0.84
			St. dev	0.031		0.078		0.035		0.037

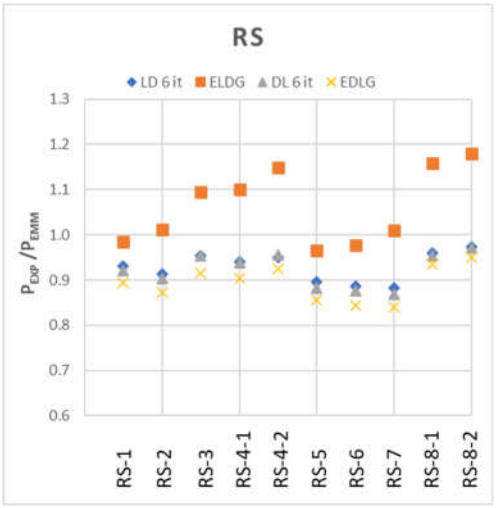

Figure 48 Comparison EMM × experimental results of Rack specimens

4.1.4 Article from 2012 C-profiles Loughlan

In an effort to analyse and compare the failure of thin-walled lipped channel members under compression due to coupled local/distortional interactions, in 2012 Loughlan J et al [123] took the finite element approach to analyse a set of specimens already experimentally tested some 20 years before by other authors. In the article the simulations were made with quadrilateral shell elements of the Patran/ Nastran finite element software.

The critical loads P_{crL}, P_{crD} , P_{crG} were not given in [R_{EFF}] so for the purpose of comparing EMM with the results obtained in this paper the critical loads were first determined using GBTUL [92] with the boundary conditions set as shown in Figure 49.

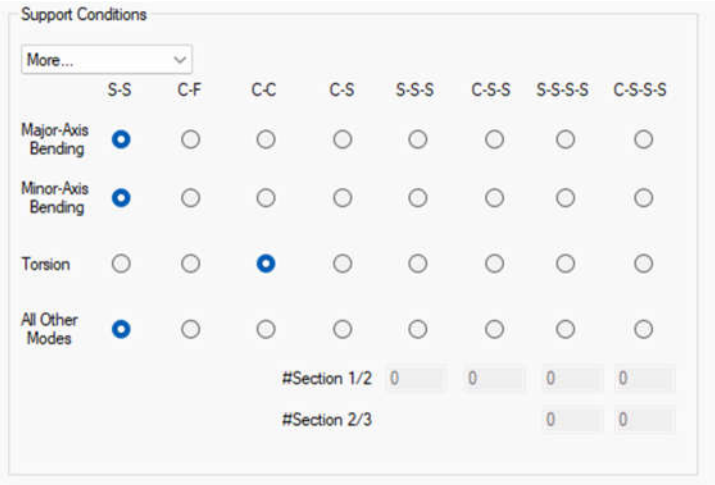

Figure 49 Boundary conditions used to determine the critical loads P_{crL}, P_{crD} , P_{crG} of the specimens.(GBTUL [92])

The specimens proprieties are shown in Table 22 and the comparison of the results with EMM is shown in Table 23 and Figure 50.

Table 22 column specimen's dimensions & critical loads P_{crL}, P_{crD} , P_{crG}.

Specimen	b_w mm	b_f mm	b_s mm	t mm	L mm	A mm^2	P_{crL} kN	P_{crD} kN	P_{crG} kN
1	178.04	62.7	12.22	0.96	1800	314.8	10.68	34.25	336.81
2	178.7	63.1	11.8	0.96	1600	315.4	10.36	33.57	427.62
3	178.54	62.8	12.29	0.96	1400	315.6	10.15	37.94	560.84
4	179.54	63.0	11.77	0.96	1200	316.0	10.07	40.70	762.01
5	178.64	63.0	11.87	0.96	1000	315.3	10.24	43.40	1092.40
6	152.24	56.1	10.52	0.96	1800	274.0	12.91	32.80	224.85
7	151.84	56.9	10.52	0.96	1600	275.2	12.80	34.76	288.58
8	151.54	56.8	11.02	0.96	1400	275.7	12.58	36.99	380.10
9	151.54	56.6	10.92	0.96	1200	275.2	12.21	39.31	513.72
10	151.04	57.0	10.58	0.96	1000	274.8	12.31	44.28	735.76
11	127.34	49.0	9.72	0.96	1800	235.1	16.13	35.64	144.40
12	127.34	49.7	8.52	0.96	1600	233.9	15.79	31.63	178.34
13	127.64	49.6	9.52	0.96	1400	236.1	15.55	36.63	240.61
14	127.04	49.0	9.02	0.96	1200	233.4	15.16	36.31	315.00
15	127.04	49.5	9.02	0.96	1000	234.4	14.71	37.82	458.98
16	101.05	63.0	12.02	0.96	1800	241.1	24.59	43.53	137.58
17	100.64	63.0	12.02	0.96	1600	240.7	24.81	44.84	172.58
18	100.58	63.0	12.02	0.96	1400	240.7	24.50	46.20	224.86
19	100.44	63.0	12.02	0.96	1200	240.5	24.05	50.94	304.92
20	100.54	63.0	12.02	0.96	1000	240.6	23.35	58.40	439.44

Table 23 Comparison EMM × numerical results of C-profile specimens

Specimen	f_y MPa	f_{NUM} MPa	LDG 6 Iterations MPa	/ LDG	ELDG MPa	/ ELDG	DLG6 Iterations MPa	/ DLG	EDLG MPa	/ EDLG
1	209	91.5	122.96	0.74	110.17	0.83	119.56	0.77	135.89	0.67
2	209	99.9	133.53	0.75	122.86	0.81	131.00	0.76	147.95	0.67
3	209	99.4	144.83	0.69	136.57	0.73	143.20	0.69	159.75	0.62
4	209	100.5	156.28	0.64	150.34	0.67	155.57	0.65	170.84	0.59
5	209	101.0	171.17	0.59	168.17	0.60	169.61	0.60	181.85	0.56
6	209	108.8	118.38	0.92	107.19	1.01	115.50	0.94	127.54	0.85
7	209	106.7	130.66	0.82	121.29	0.88	128.68	0.83	141.85	0.75
8	209	108.8	144.90	0.75	138.40	0.79	142.23	0.77	155.22	0.70
9	209	102.1	155.69	0.66	150.68	0.68	154.43	0.66	166.94	0.61
10	209	107.3	168.61	0.64	165.56	0.65	168.02	0.64	178.70	0.60
11	209	124.1	114.71	1.08	107.13	1.16	111.43	1.11	117.98	1.05
12	209	114.3	123.81	0.92	115.83	0.99	122.50	0.93	130.98	0.87
13	209	126.4	138.86	0.91	132.95	0.95	137.02	0.92	146.36	0.86
14	209	128.9	150.42	0.86	145.83	0.88	149.19	0.86	158.69	0.81
15	209	127.1	164.52	0.77	161.57	0.79	163.85	0.78	172.65	0.74
16	209	120.7	146.35	0.82	142.67	0.85	146.95	0.82	152.20	0.79
17	209	134.4	156.61	0.86	153.87	0.87	157.11	0.86	162.37	0.83
18	209	123.8	166.23	0.74	164.25	0.75	166.72	0.74	171.87	0.72
19	209	135.9	175.10	0.78	173.71	0.78	175.86	0.77	180.67	0.75
20	209	123.8	184.66	0.67	183.93	0.67	184.81	0.67	188.75	0.66
			Av.	0.78		0.82		0.79		0.74
			Max	1.08		1.16		1.11		1.05
			Min	0.59		0.60		0.60		0.56
			St. dev	0.118		0.136		0.123		0.119

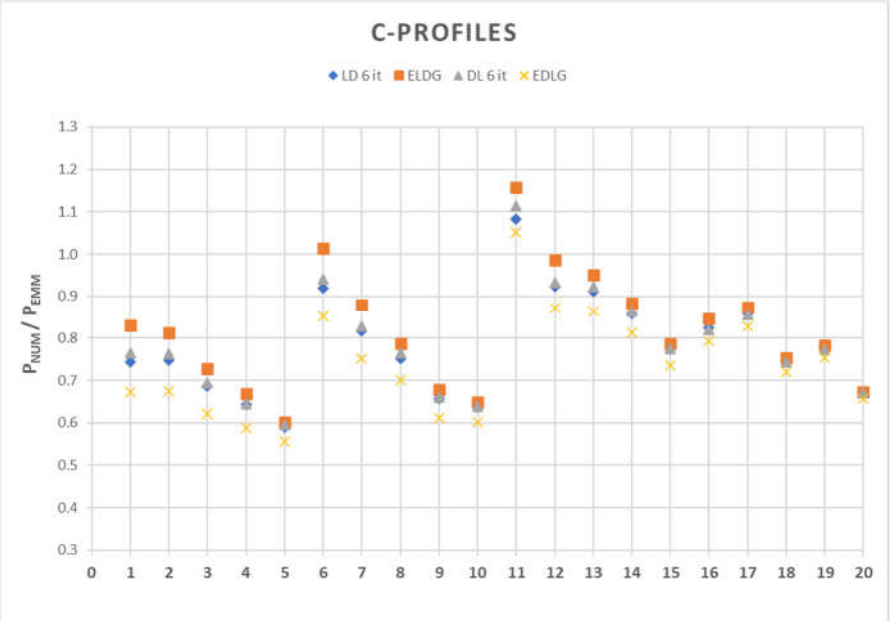

Figure 50 Comparison EMM × numerical results of C-profile specimens

As one can see the EMM × numerical results for this set of specimens is slightly poor. This can be explained by the very high global critical load when compared with the local and distortional critical loads affecting the formulas. In an attempt to see if the EMM × numerical results could be improved the same calculations were made leaving the part of the global safety factor out.

The EMM results in Table 24 and Figure 51 show a drastic improvement but in order to gain confidence in the EMM methodology when the global buckling load is significantly higher than the local and distortional loads a bigger sample of specimens and varying proprieties should be tested.

Table 24 Comparison EMM × numerical results of C-profile specimens (only LD & DL)

Specimen	f_y	f_{EXP}	LD		DL	
	MPa	MPa	MPa	/ LD	MPa	/ DL
1	209	91.5	71.34	1.28	72.97	1.25
2	209	99.9	70.36	1.42	72.02	1.39
3	209	99.4	69.64	1.43	71.44	1.39
4	209	100.5	68.43	1.47	70.64	1.42
5	209	101.0	73.77	1.37	72.60	1.39
6	209	108.8	82.06	1.33	84.81	1.28
7	209	106.7	81.43	1.31	84.19	1.27
8	209	108.8	85.28	1.28	85.06	1.28
9	209	102.1	82.27	1.24	83.52	1.22
10	209	107.3	82.12	1.31	83.47	1.29
11	209	124.1	100.35	1.24	101.93	1.22
12	209	114.3	94.78	1.21	99.34	1.15
13	209	126.4	97.98	1.29	99.73	1.27
14	209	128.9	97.33	1.32	99.09	1.30
15	209	127.1	96.43	1.32	97.99	1.30
16	209	120.7	113.23	1.07	119.77	1.01
17	209	134.4	115.14	1.17	120.73	1.11
18	209	123.8	115.21	1.07	120.23	1.03
19	209	135.9	112.86	1.20	118.63	1.15
20	209	123.8	115.90	1.07	118.64	1.04
			Av.	1.27		1.24
			Max	1.47		1.42
			Min	1.07		1.01
			St. dev	0.112		0.119

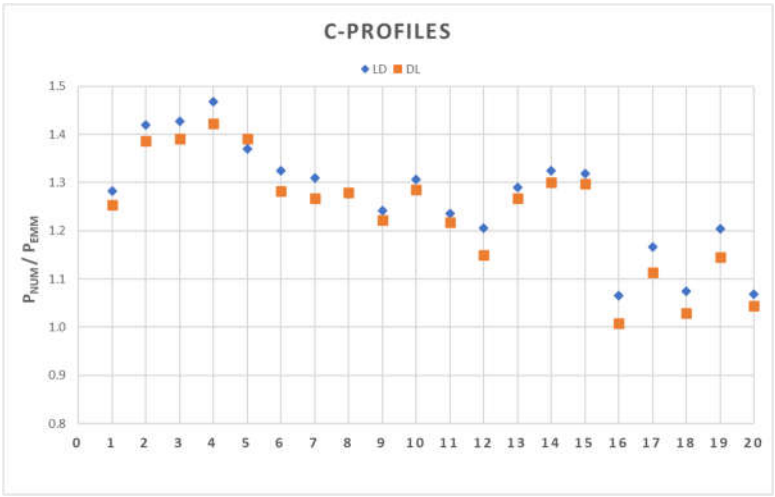

Figure 51 Comparison EMM × numerical results of C-profile specimens (only LD & DL)

4.1.5 Article from 2017 Sigma -Profiles

As a response to designers and contractors needs, the sigma shaped section (Figure 52) has in recent years been used as an alternative section. Sigma sections main advantages is having an intermediate web and more stiffeners. So, to better understand and investigate the behaviour of this sections El Aghoury M.A.et al [124] carried out experimental and theoretical studies. Eight specimens were used for that purpose the specimen's characteristics are depicted in Table 25 and Figure 52.

The numerical tests were made using the finite elements software ANSYS. The specimen models were designed as four node isoparametric thin-shell elements and had six degrees of freedom, 3 translations and 3 rotations and boundary conditions set to satisfy pin end configuration with warping of the cross section constrained.

The experimental tests (see Figure 52) were done in a vertical set-up that applied a controlled compressive load on the centroid of the cross-sections. To ensure the same boundary conditions as the specimens models the two ends of each specimen were connected to thick head bearing plates.

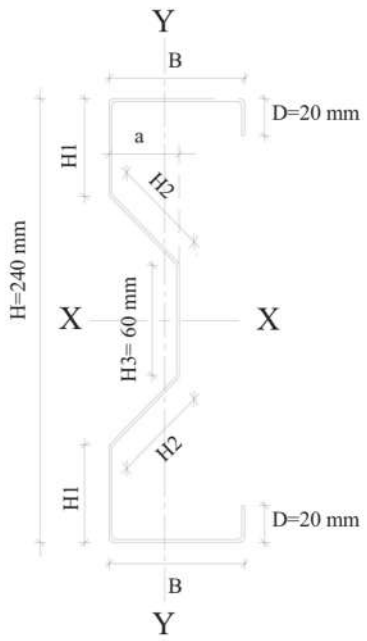

Figure 52 Geometrical proprieties of sigma sections used [124]

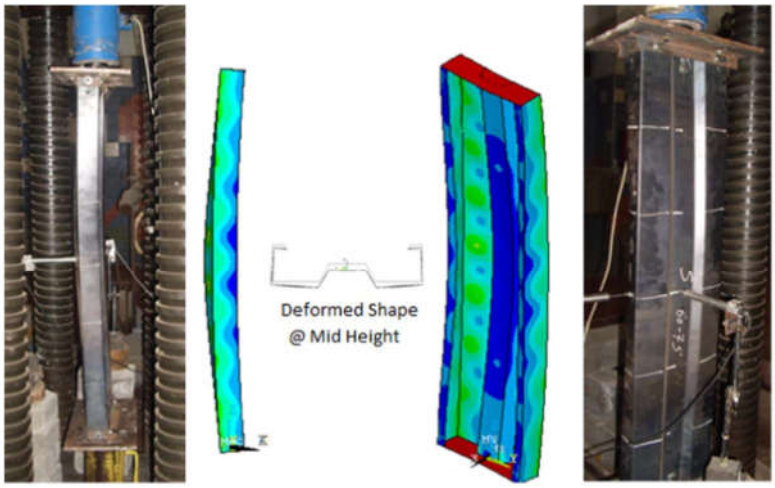

(a) Specimen S-60-75-50

Figure 53 Comparison between of A specimen experimentally and theoretically tested [124]

The critical loads P_{crL} P_{crD} and P_{crG} were not given in the article and were determined using GBTUL [92] with boundary conditions as depicted in Figure 54.

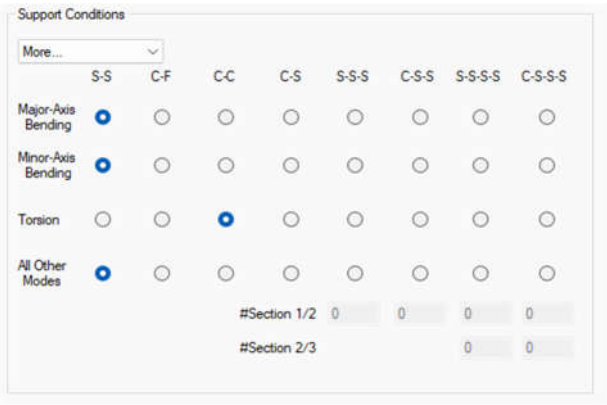

Figure 54 Support conditions used in CBTUL to obtain the critical values of the Sigma specimens.

Table 25 column specimen's dimensions & critical loads P_{crL}, P_{crD} , P_{crG}.

Specimen	**L** mm	**B** mm	**D** mm	**H** mm	**H_1** mm	**H_2** mm	**H_3** mm	**A** mm^2	**P_{crL}** kN	**P_{crD}** kN	**P_{crG}** kN
S60-25-50	1060	60	20	240	75	21.21	60	609.6	279.6	150.9	456.7
S60-75-50	1036	60	20	240	45	63.64	60	646.9	342.8	275.9	520.9
S75-25-50	1318	75	20	240	71.25	26.52	60	659.3	264.0	167.6	496.6
S75-75-50	1279	75	20	240	33.75	79.53	60	705.8	268.4	211.2	541.2
S60-25-100	2060	60	20	240	75	21.21	60	609.6	337.5	152.6	120.9
S60-75-100	2013	60	20	240	45	63.64	60	646.9	419.6	242.8	163.4
S75-25-100	2500	75	20	240	71.25	26.52	60	659.3	316.9	168.5	138.0
S75-75-100	2500	75	20	240	33.75	79.53	60	705.8	344.6	185.0	141.6

4.1.5.1 Experimental Results

Table 26 and Figure 55 display mixed review on the comparison of EMM x experimental results, in fact on the first four specimen observed the results are unsatisfactory but as good as it comes on the last four specimens.

As this set of specimen has both good and bad results, it shows that the EMM equations should be adjusted for this (and possibly other) types of profiles, particularly those with internal bends and stiffeners.

Table 26 Comparison EMM × experimental results of Sigma specimens

Specimen	f_y	f_{EXP}	LDG 6 Iterations		ELDG		DLG6 Iterations		EDLG	
	MPa	MPa	MPa	/ LDG	MPa	/ ELDG	MPa	/ LDG	MPa	/ LDG
S60-25-50	265	153.7	228.53	0.67	228.53	0.67	219.51	0.70	218.86	0.70
S60-75-50	265	201.4	228.36	0.88	228.26	0.88	230.90	0.87	230.90	0.87
S75-25-50	265	148.4	228.71	0.65	228.71	0.65	220.09	0.67	219.49	0.68
S75-75-50	265	188.2	223.85	0.84	223.57	0.84	226.89	0.83	224.70	0.84
S60-25-100	265	169.6	151.50	1.12	151.50	1.12	143.28	1.18	141.87	1.20
S60-75-100	265	180.2	170.80	1.06	170.80	1.06	168.01	1.07	167.77	1.07
S75-25-100	265	161.7	156.01	1.04	156.01	1.04	147.74	1.09	146.38	1.10
S75-75-100	265	180.2	152.48	1.18	152.48	1.18	145.09	1.24	143.90	1.25
			Av.	0.93		0.93		0.96		0.96
			Max	1.18		1.18		1.24		1.25
			Min	0.65		0.65		0.67		0.68
			St. dev	0.188		0.188		0.204		0.207

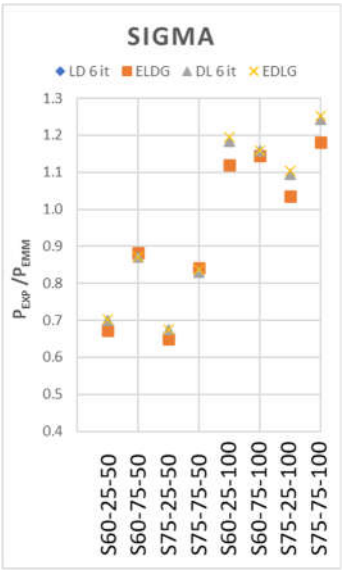

Figure 55 Comparison EMM × experimental results of Sigma specimens

4.1.5.2 Numerical results

The observation can be made for the EMM Numerical results comparison as with the EMM experimental results comparison. Indeed Table 27 and Figure 56 also show a better outcome on the last four specimens compared to the first four.

Table 27 Comparison EMM × numerical results of Sigma specimens

Specimen	f_y	f_{NUMM}	LDG 6 Iterations		ELDG		DLG6 Iterations		EDLG	
	MPa	MPa	MPa	/ LDG	MPa	/ ELDG	MPa	/ LDG	MPa	/ LDG
S60-25-50	265	185.5	228.53	0.81	228.53	0.81	219.51	0.85	218.86	0.85
S60-75-50	265	198.8	228.36	0.88	228.26	0.88	230.90	0.87	230.90	0.87
S75-25-50	265	185.5	228.71	0.65	228.71	0.65	220.09	0.67	219.49	0.68
S75-75-50	265	201.4	223.85	0.84	223.57	0.84	226.89	0.83	224.70	0.84
S60-25-100	265	169.6	151.50	1.12	151.50	1.12	143.28	1.18	141.87	1.20
S60-75-100	265	190.8	170.80	1.06	170.80	1.06	168.01	1.07	167.77	1.07
S75-25-100	265	180.2	156.01	1.04	156.01	1.04	147.74	1.09	146.38	1.10
S75-75-100	265	185.5	152.48	1.18	152.48	1.18	145.09	1.24	143.90	1.25
			Av.	0.95		0.95		0.98		0.98
			Max	1.18		1.18		1.24		1.25
			Min	0.65		0.65		0.67		0.68
			St. dev	0.169		0.168		0.186		0.189

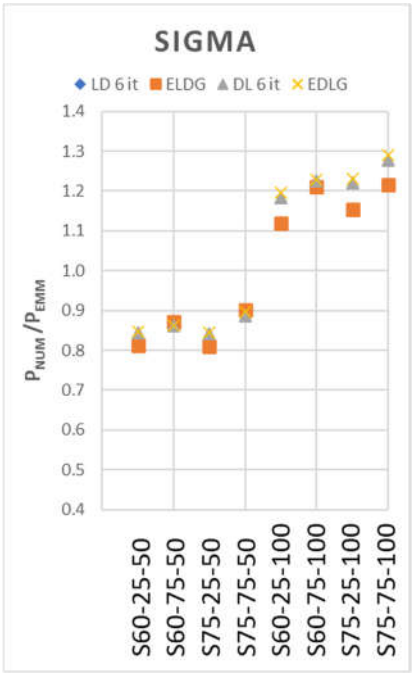

Figure 56 Comparison EMM × numerical results of Sigma specimens

4.2 RESULTS FOR BENDING

Two sets of results available in the literature to sections subjected to bending (beams) were chosen for comparison with the *EMM* results. These experimental results refer to pure (uniform) [114.115] and non-uniform [116] bending.

4.2.1 Uniform Bending

4.2.1.1 Article from 2020

To test simple C-sections (named LC) subjected to uniform and nonuniform bending moments, Chen et. all [113,115] conducted experimental studies using the scheme represented in the Figure 57. When L_{s1} length is equal L_{s2}, the bending moment diagram between two applied loads are uniform [113]. Otherwise, when, L_{s1}= L_{s2}, the bending moment is uniform (pure) [115].

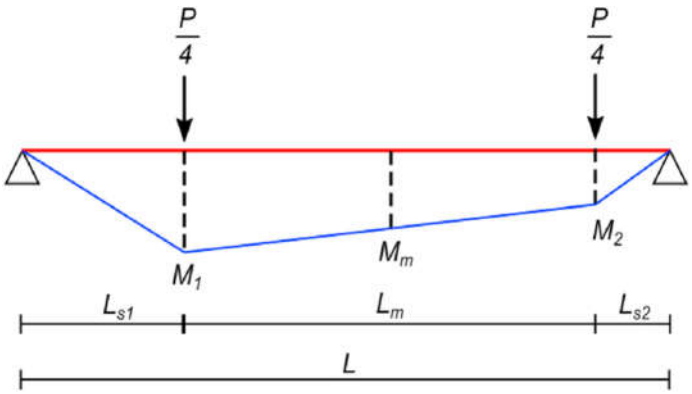

Figure 57 Bending moment diagram acting on the beam specimens tested [114]

Table 28 shows the dimensions of the LC-section, the column specimens' uniform bending moment resistance obtained from the experimental results (M_{exp}) the critical bending moment associated with *LM* (M_{crL}) and *DM* (M_{crD}) (see [113, 116]).and the bending moment obtained by the *EMM*: (i) *LD* ($M_{R\text{-}LD}$) and (ii) *DL* ($M_{R\text{-}DL}$).

Table 28 Beam specimen's dimensions.

Specimen	b_w mm	b_f mm	b_s mm	t mm	L mm	A mm^2
LC1	130	120	12	1.5	1800	591.0
LC2	130	120	12	1.5	2200	591.0
LC3	150	130	12	1.5	2200	651.0
LC4	150	130	12	1.5	2600	651.0
LC5	130	120	12	1.5	2600	591.0
LC6	170	130	12	1.5	2600	681.0
LC7	170	110	12	1.5	2600	621.0
LC8	190	130	12	1.5	2600	711.0
LC8R	190	130	12	1.5	2600	711.0
LC9	190	130	12	1.5	2200	711.0
LC10	170	100	12	1.2	2600	472.8
LC11	210	150	12	1.5	2600	801.0
LC12	210	130	12	1.5	2600	741.0
LC13	230	160	12	1.5	2600	861.0
LC14	230	140	12	1.5	2600	801.0
LC14R	230	140	12	1.5	2600	801.0
LC15	230	120	12	1.5	2600	741.0
LC16	130	110	12	1.5	2600	561.0
LC17	130	110	12	1.2	2600	448.8
LC18	130	100	12	1.2	2600	424.8

The results in Table 28 and in Figure 58 (M_{EXP}/M_{RD}) show that, for uniform bending moment, the values of the *DL* methodology are very close to the experimental ones (mean 0.94 and standard deviation 0.047), however showing non-conservative values. The *LD* methodology presents reliable results although with significantly lower precision (average 1.4 and standard deviation 0.1).

Table 29 Comparison EMM × experimental results

Specimen	M_{exp} kNcm	M_{crL} kNcm	M_{crD} kNcm	M_{R-DL} kNcm	M_{exp}/M_{R-DL}	M_{R-LD} kNcm	M_{exp}/M_{R-LD}
LC1	560	439	568	643.54	0.87	455.34	1.23
LC2	558	435	507	624.04	0.89	420.71	1.33
LC3	687	467	574	711.97	0.96	472.56	1.45
LC4	645	464	515	691.49	0.93	438.02	1.47
LC5	535	433	473	612.53	0.87	400.85	1.33
LC6	746	536	598	782.17	0.95	505.81	1.47
LC7	709	656	683	805.71	0.88	571.50	1.24
LC8	877	611	690	877.94	1.00	579.41	1.51
LC8R	801	611	690	877.94	0.91	579.41	1.38
LC9	838	619	802	914.92	0.92	643.71	1.30
LC10	541	380	462	538.98	1.00	376.50	1.44
LC11	915	585	743	965.33	0.95	612.67	1.49
LC12	954	686	791	976.79	0.98	658.00	1.45
LC13	1065	609	828	1063.08	1.00	672.45	1.58
LC14	1030	699	883	1073.25	0.96	720.71	1.43
LC14R	1044	699	883	1073.25	0.97	720.71	1.45
LC15	1052	817	935	1079.63	0.97	767.49	1.37
LC16	520	482	514	622.02	0.84	431.18	1.21
LC17	395	249	323	407.29	0.97	264.01	1.50
LC18	384	281	355	416.85	0.92	287.84	1.33
				Av.	0.94	**Av.**	1.40
				Max	1.00	**Max**	1.58
				Min	0.84	**Min**	1.21
				St. dev	0.047	**St. dev**	0.101

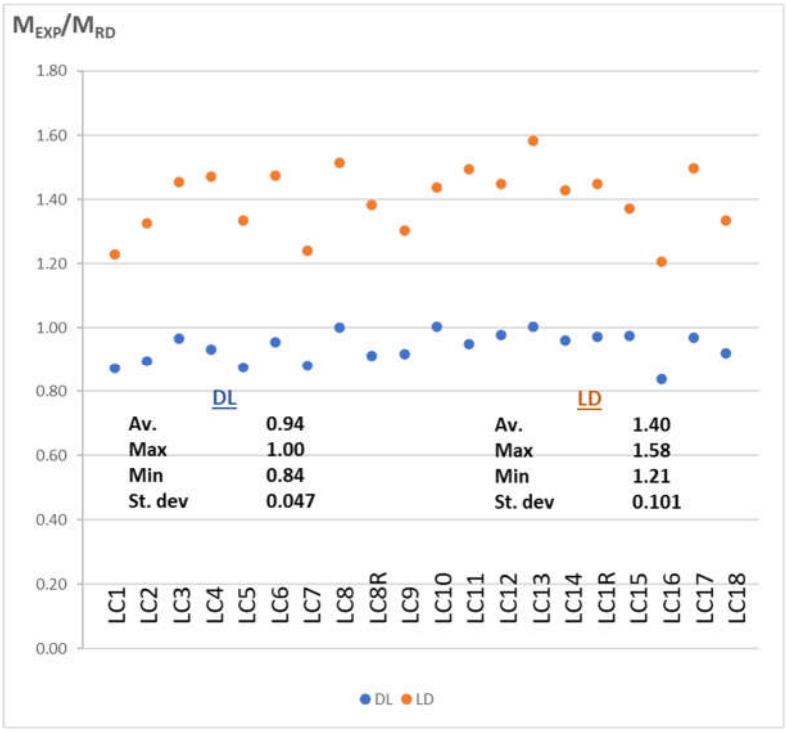

Figure 58 Comparison EMM × experimental results

4.2.1.2 Article from 2012

In 2012 Pham and Hancock [115] conducted experiments on simple C-sections (C) and web stiffened C-sections (SC) subject to uniform bending (Figure 59). The dimensions and the of the C-section and SC-section are shown in Table 30.

Table 30 Column specimen's dimensions [18

Test	Section	t mm	D mm	B mm	L mm	l mm	l_r mm	GS mm	S mm	θ_1 °	θ_2 °
Ms	C15015	1.5	153.46	64.53	15.02	-	-	-	-	-	-
Ms	C15019	1.9	153.54	65.01	16.27	-	-	-	-	-	-
Ms	C15024	2.4	153.43	63.58	20.88	-	-	-	-	-	-
Ms	C20015	1.5	203.74	75.88	16.16	-	-	-	-	-	-
Ms	C20019	1.9	203.53	79.27	17.51	-	-	-	-	-	-
Ms	C20024	2.4	202.3	77.58	21.26	-	-	-	-	-	-
Ms	SC15012	1.2	153.68	42.31	-	5.78	6.35	63.84	40.37	53.5	83.5
Ms	SC15015	1.5	152.61	42.85	-	4.75	5.91	63.53	41.31	55.5	82.5
Ms	SC15024	2.4	153.75	44.57	-	4.84	5.25	60.89	42.32	51.5	82.5
Ms	SC20012	1.2	205.37	54.57	-	6.92	6.29	109.39	42.36	56	83
Ms	SC20015	1.5	203.99	54.36	-	7.01	6.72	109.56	42.17	57	85
Ms	SC20024	2.4	203.21	54.63	-	6.79	8.38	110.34	41.54	55.5	85.5
Mw	C15015	1.5	152.7	64.77	16.51	-	-	-	-	-	-
Mw	C15019	1.9	153.38	64.47	16	-	-	-	-	-	-
Mw	C15024	2.4	152.6	62.7	19.7	-	-	-	-	-	-
Mw	C20015	1.5	203.7	76.08	16.42	-	-	-	-	-	-
Mw	C20019	1.9	202.6	77.92	17.28	-	-	-	-	-	-
Mw	C20024	2.4	203.35	76.61	20.88	-	-	-	-	-	-
Mw	SC15012	1.2	153.78	43.02	-	5.41	6.03	63.39	40.75	55	86
Mw	SC15015	1.5	153.47	42.82	-	4.97	6.93	64.68	41.64	56.5	83.5
Mw	SC15024	2.4	153.88	43.95	-	5.43	5.71	60.53	42.55	53	84
Mw	SC20012	1.2	205.65	54.35	-	6.36	7.09	109.49	42.51	56.5	85
Mw	SC20015	1.5	203.91	54.05	-	7.18	6.95	109.49	42.54	55	85.5
Mw	SC20024	2.4	203.64	54.87	-	6.87	8.41	110.51	41.74	57	86.5

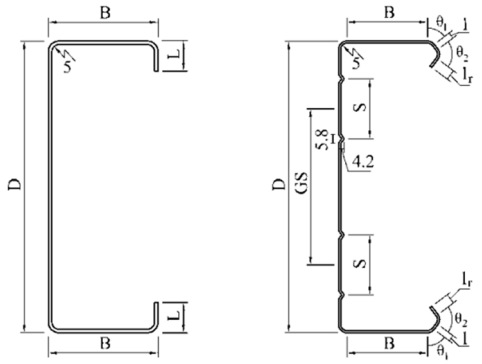

Figure 59 simple C sections "C" & web stiffened C-sections "SC" [117]

With the purpose to force the members to buckle locally rather than distortionaly, in the experiments, Phan and Hancock [115] used the steps showed in Figure 60. Thus, *Ms* is used to name members with straps, and *Mw*, without straps. The bending moment distribution between two support is uniform.

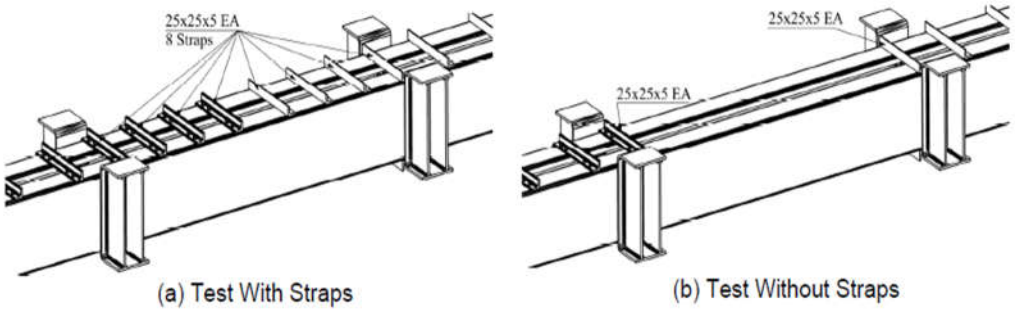

Figure 60 tests with and without straps [116]

Table 31 compares the column specimens' uniform bending moment resistance obtained from the experimental results (M_{exp}) [115] with the bending moment obtained by the two of methodologies of the *EMM*: (i) *LD* ($M_{R\text{-}LD}$) and (ii) *DL* ($M_{R\text{-}DL}$). The minimum value of critical bending moments for local (M_{crL}) and distortional (M_{crD}) modes are considered in calculations, as usual in *DSM*, and the same values considered by Pham and Hancock [18]. Figure 61 presents the relation between the experimental and *EMM* results.

From Table 31 and Figure 61 it can be concluded that the *EMM* results show a good correlation with the experimental ones: (i) for *DL* methodology, with average equal 1.44 and standard deviation equal 0.198, for *Ms SC20015* specimen (all results are on the safe side) and (ii) for *LD* methodology with average equal 1.2 and standard deviation equal 0.105, for *Ms C20019* specimen (only one specimen, *Mw SC15012*, presents unsafe result - about 3%).

Table 31 Comparison EMM × experimental results

Test	Specimen	M_{exp} kNm	M_{crL} kNm	M_{crD} kNm	M_{R-DL} kNm	M_{exp}/M_{R-DL}	M_{R-LD} kNcm	M_{exp}/M_{R-LD}
Ms	C15015	10.43	10.37	7.36	8.03	1.30	6.23	1.67
Ms	C15019	15.86	21	13	12.58	1.26	10.34	1.53
Ms	C15024	19.84	43	27	16.84	1.18	15.81	1.26
Ms	C20015	13.47	10	9	10.00	1.35	7.36	1.83
Ms	C20019	21.76	21	15	16.08	1.35	12.47	1.74
Ms	C20024	31.39	42	29	25.03	1.25	21.59	1.45
Ms	SC15012	8.19	8	7	6.54	1.25	5.36	1.53
Ms	SC15015	11.4	13	10	9.04	1.26	7.83	1.46
Ms	SC15024	21.19	46	27	17.37	1.22	16.18	1.31
Ms	SC20012	10.71	7	8	8.13	1.32	6.15	1.74
Ms	SC20015	16.48	13	13	11.74	1.40	9.77	1.69
Ms	SC20024	33.82	46	36	26.81	1.26	24.26	1.39
Mw	C15015	9.47	10	8	8.21	1.15	6.56	1.44
Mw	C15019	12.94	21	13	12.51	1.03	10.27	1.26
Mw	C15024	17.76	42	26	16.45	1.08	15.34	1.16
Mw	C20015	12.2	10	9	10.05	1.21	7.43	1.64
Mw	C20019	18.85	21	15	15.93	1.18	12.41	1.52
Mw	C20024	27.88	42	29	24.96	1.12	21.53	1.30
Mw	SC15012	6.56	8	7	6.55	1.00	5.34	1.23
Mw	SC15015	10.1	13	11	9.24	1.09	8.13	1.24
Mw	SC15024	18.84	47	28	17.41	1.08	16.46	1.14
Mw	SC20012	9.27	7	8	8.19	1.13	6.27	1.48
Mw	SC20015	13.7	13	13	11.74	1.17	9.77	1.40
Mw	SC20024	29.15	46	36	26.98	1.08	24.47	1.19
					Av.	1.20	**Av.**	1.44
					Max	1.40	**Max**	1.83
					Min	1.00	**Min**	1.14
					St. dev	0.105	**St. dev**	0.198

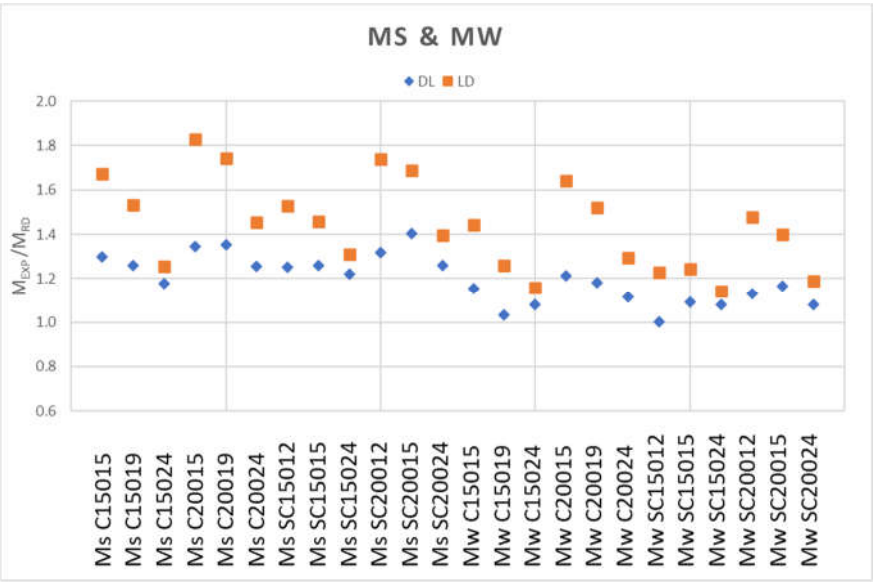

Figure 61 Comparison EMM × experimental results

4.2.2 Non-uniform Bending

To test simple C-sections (named LC) subjected to non-uniform bending moments, Chen et. all [115] conducted experimental studies using the same scheme represented in the Figure 57. When L_{s1} length is different than L_{s2}, when the bending moment diagram between two applied loads are non-uniform.

Table 32 shows the dimensions of the LC-section, the column specimens' bending moment resistance obtained from the experimental results (M_{exp}), the critical bending moment associated with LM (M_{crL}) and DM (M_{crD}) (see [115,116]) and the bending moment obtained by the EMM: (i) LD ($M_{R\text{-}LD}$) and (ii) DL ($M_{R\text{-}DL}$). Figure 62 presents the relation between EMM and experimental results.

Table 32 Beam specimen's dimensions.

Specimen	b_w mm	b_f mm	b_s mm	t mm	L_{S2} mm	L_m mm	A mm^2
LC4-0.5-a	149.2	128	12.9	1.49	234	1716	642.19
LC4-0.5-b	148.9	127.9	12.9	1.48	234	1716	637.14
LC4-0.625-a	148.9	128.1	13	1.49	312	1638	642.34
LC4-0.625-b	149.4	128	13.1	1.49	312	1638	643.08
LC4-0.75-a	149.2	128	12.9	1.49	390	1560	642.19
LC4-0.75-b	149.3	127.9	13.1	1.49	390	1560	642.64
LC4-0.875-a	149.2	127.6	13.2	1.48	520	1430	637.58
LC4-0.875-b	149.2	127.7	13.4	1.49	520	1430	642.79
LC6-0.5-a	168.9	127.6	13.1	1.47	234	1716	661.94
LC6-0.5-b	168.7	128	13	1.49	234	1716	671.54
LC6-0.625-a	168.7	127.8	13.2	1.48	312	1638	667.04
LC6-0.625-b	168.9	127.8	13.1	1.48	312	1638	667.04
LC6-0.75-a	168.8	127.8	13	1.48	390	1560	666.59
LC6-0.75-b	169.3	127.8	13.1	1.48	390	1560	667.63
LC6-0.875-a	169.1	127.8	13.1	1.48	520	1430	667.33
LC6-0.875-b	168.9	127.7	13	1.49	520	1430	670.95
LC8-0.5-a	188.4	128.1	13	1.48	234	1716	696.49
LC8-0.5-b	189	127.6	13.1	1.48	234	1716	696.19
LC8-0.625-a	188.5	128.3	12.7	1.48	312	1638	696.34
LC8-0.625-b	188.6	128	13	1.48	312	1638	696.49
LC8-0.75-a	188.2	128.2	13	1.48	390	1560	696.49
LC8-0.75-b	188.3	128.3	13.1	1.48	390	1560	697.23
LC8-0.875-a	188.5	128	13.2	1.48	520	1430	696.93
LC8-0.875-b	188.4	128.2	13	1.47	520	1430	692.08
LC12-0.5-a	209.6	128.1	12.8	1.5	234	1716	737.10
LC12-0.5-b	209.4	128.3	12.9	1.49	234	1716	732.78

LC12–0.625-a	208.9	128.3	12.6	1.5	312	1638	736.05
LC12–0.625-b	209.2	128.3	12.8	1.48	312	1638	727.27
LC12–0.75-a	209.2	128.1	12.8	1.49	390	1560	731.59
LC12–0.75-b	209.2	128.3	12.8	1.48	390	1560	727.27
LC12–0.875-a	209	128.1	12.8	1.48	520	1430	726.38
LC12–0.875-b	209.3	128	12.8	1.49	520	1430	731.44

The results in Table 33 and Figure 62 show that, for non-uniform bending moment, the values of the *DL* methodology practically coincide with the experimental results, with some unsafe values (average equal 0.98 and standard deviation equal 0.032). The *LD* methodology produces secure estimated values (with average equal 1.34 and standard deviation equal 0.057).

Table 33 Comparison EMM × experimental results

Specimen	M_{exp} kNm	M_{crL} kNm	M_{crD} kNm	$M_{R\text{-}DL}$ kNm	$M_{exp}/M_{R\text{-}DL}$	$M_{R\text{-}LD}$ kNcm	$M_{exp}/M_{R\text{-}LD}$
LC4-0.5-a	745	507	639	715.31	1.04	515.45	1.45
LC4-0.5-b	745	510	646	715.63	1.04	518.46	1.44
LC4-0.625-a	741	525	641	729.13	1.02	516.62	1.43
LC4-0.625-b	741	528	669	740.18	1.00	532.33	1.39
LC4-0.75-a	728	514	628	721.61	1.01	506.01	1.44
LC4-0.75-b	728	516	638	719.90	1.01	516.16	1.41
LC4-0.875-a	680	487	617	695.09	0.98	499.10	1.36
LC4-0.875-b	680	498	636	715.63	0.95	506.32	1.34
LC6-0.5-a	864	603	810	846.42	1.02	638.93	1.35
LC6-0.5-b	864	624	831	875.44	0.99	650.27	1.33
LC6-0.625-a	863	600	807	848.08	1.02	635.65	1.36
LC6-0.625-b	863	600	804	853.09	1.01	630.37	1.37
LC6-0.75-a	826	585	754	831.95	0.99	599.57	1.38
LC6-0.75-b	826	588	762	832.99	0.99	607.57	1.36
LC6-0.875-a	760	563	721	812.25	0.94	576.99	1.32
LC6-0.875-b	760	574	727	814.81	0.93	588.28	1.29
LC8-0.5-a	991	697	992	990.59	1.00	764.33	1.30
LC8-0.5-b	991	703	1003	1005.65	0.99	764.50	1.30
LC8-0.625-a	971	678	912	963.81	1.01	718.18	1.35
LC8-0.625-b	971	682	928	975.23	1.00	722.53	1.34
LC8-0.75-a	907	663	875	943.86	0.96	696.31	1.30
LC8-0.75-b	907	664	880	949.25	0.96	697.36	1.30
LC8-0.875-a	881	639	853	935.05	0.94	670.82	1.31
LC8-0.875-b	881	624	816	912.16	0.97	649.67	1.36
LC12-0.5-a	1106	816	1172	1151.50	0.96	902.94	1.22
LC12-0.5-b	1106	799	1151	1137.81	0.97	883.82	1.25
LC12–0.625-a	1076	792	1079	1127.52	0.95	839.19	1.28
LC12–0.625-b	1076	764	1098	1105.17	0.97	844.18	1.27
LC12–0.75-a	1057	762	1013	1086.78	0.97	800.38	1.32

LC12–0.75-b	1057	746	1048	1083.97	0.98	816.46	1.29
LC12–0.875-a	972	716	958	1046.07	0.93	757.63	1.28
LC12–0.875-b	972	732	977	1061.14	0.92	774.71	1.25
				Av.	0.98	**Av.**	1.34
				Max	1.04	**Max**	1.45
				Min	0.92	**Min**	1.22
				St. dev	0.032	**St. dev**	0.057

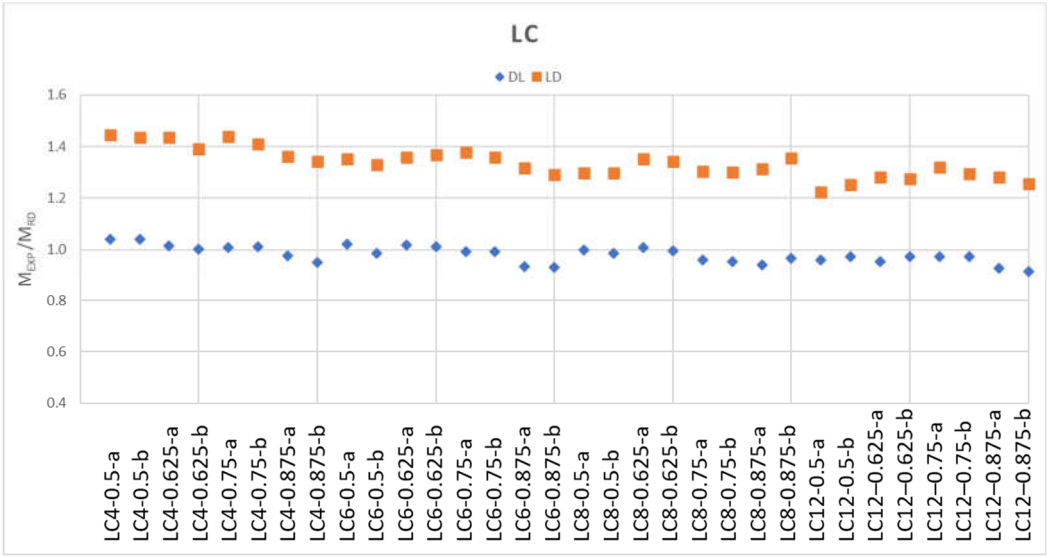

Figure 62 Comparison EMM × experimental results

5. CONCLUSIONS AND FUTURE WORKS

5.1 Conclusions

The dissertation presents the concept of the Effective Modulus Method (EMM) of a plate and suggests a new methodology for evaluating the strength of columns beams affected by local-distortional-distortional interaction. This methodology applies the concept of effective modulus using correction factors like those used in the Direct Strength Method (DSM) to reduce the strength due to post-buckling behaviour.

The EMM assumes that the post-buckling effect of the local and distortional modes interact with each other and with the global mode by the loss of stiffness. This effect is modelled with a reduction in the modulus of elasticity of the material, which manifests itself in a direct relationship with the reduction of the critical stresses and, consequently, the reduction of the compressive strength.

The dissertation begins with a literature review on plate instability. Then a literature review on section instability is conducted to demonstrate the consistency of applying the concept of effective modulus to post-buckling resistance, illustrating examples of effective elasticity modulus distributions in the post-buckling stage of columns and beams.

An algorithm for calculating the resistance of columns and beams based is proposed. Initially, an innovative criterion for post-buckling resistance of plates without imperfections is derived, using a new relationship between stresses and deformations. In this propose the post-buckling resistance of the plate is found when the average stress corresponds to yield deformation, by means an effective elasticity modulus. After, since a consistent parametric study has not yet been conducted to calibrate the equations of effective modulus for local and global instability modes, reduction coefficients of elasticity modulus equivalent to the well-known Direct Strength Method are used.

Results obtained by the new proposal are compared with data available in the literature. It is observed that:

(i) for columns.

An excellent correlation is found with the experimental [119] and numerical [120] results of lipped channel columns. Since the chosen examples have critical stresses with close values for studies of mode interaction, it was not possible to test the limits of the interaction between the instability modes as suggested by Martins et al. [118] because the ratio between the critical distortional and local stresses is greater than 0.8.

It is important to note that to address some issues, a condition and different formulas should be considered for cases where the global critical buckling mode load is much higher then the local and distortional buckling modes. Furthermore, for specimens particularly those that have geometries with internal bends and more stiffeners, the formulas should be adjusted and calibrated.
Lastly, the yield stress of the specimen should also be considered in future equations optimisation in cases where the yield stress falls outside the "normal" range.

(ii) for beams,

From the tests carried out, it was concluded that DL is the methodology that presents the most accurate results, although it makes some estimates (very close to experimental results) that are unsafe. On the other hand, the LD methodology presents always safe results, but with less accuracy.

The unsafe results provided by the DL methodology can be explained by using the reduction coefficients of the DSM elasticity modulus. The effective modulus reduction coefficients are based on the concept that the average stress is limited by the yield deformation, while the DSM uses the stress limitation criterion. This suggests that parametric studies must be carried out to adjust the coefficients of equation (18).

5.2 Future works

To validate, ensure consistency, and broaden the application scope of the method, the following future works are suggested:

(i) the method should be tested for other types of sections, boundary conditions, and loading conditions.

(ii) cases of interaction of local, distortional, and global modes for beams should also be performed by means of the EMM.

(iii) it is planned to carry out parametric studies to validate the better approach LD or DL.

(iv) in addition, there are ongoing studies to find new formulations for reducing the coefficient of elasticity modulus for columns and beams.

(v) another potential use of the EMM, to be tested, is in the determination of member deflection, as it is enough to change the modulus of elasticity of the material.

6. REFERENCES

[1] Rasmussen, K.J.R.; Hasham, A.S. "Flexural and flexural-torsional bifurcation of locally buckled beam-columns", Thin-Walled Structures 29(1-4), pp. 203-233, 1997. DOI: 10.1016/S0263-8231(97)00023-2

[2] Rasmussen, K.J.R. "Bifurcation of Locally Buck-led Members", Thin-Walled Structures 28(2), pp. 117-154, 1997. DOI: 10.1016/S0263-8231(97)00004-9

[3] Rasmussen, K.J.R.; Zhang, X.; Zhang, H. (2016) "Beam-element-based analysis of locally and/or distortional buckled members: theory", Thin-Walled Structures 98, Part B, pp. 285–292. DOI: 10.1016/j.tws.2015.06.020

[4] Camotim, D.; Prola, L.C. (2001) "On the Accounting of Local Post-Buckling Effects in the Global Behaviour of Cold-Formed Steel Columns", Proceedings of 2001 Annual Structural Stability Research Council Tech-nical Session and Meeting, Fort Lauderdale, Florida, USA, pp. 383-402.

[5] Prola, L.C.; Camotim, D. "On the accounting of local post-buckling effects in the global behaviour of cold-formed steel columns)", Proceedings of the Memorias das XXIX Jornadas Sudamericanas de Ingenieria Estructural, Punta del Este, Uruguai, pp. 122, 2000 (In Portuguese).

[6] Estrella Jr., L.F. – "Simulation de L'Interaction entre le Voilament Local et les Modes Globaux d'Instabilité des Profils a Froid par une Combination de la Méthode des Largeurs Effectives et de L'Element Fini Non-Lineaire de Poutre Spatiale", *Thèse de Doctorat*, Faculté des Sciences Appliquées, Université de Liège, Belgique, 1993. (in french)

[7] Prola, L. C "Estabilidade Local e Global de Elementos Estruturais de Aço Enformados a Frio", Tese de Doutoramento, Universidade de Lisboa, Lisboa, 2002. (in Portuguese)

[8] Saint-Venant, B. – *Théorie de L'Elasticité des Corps Solides*, Clebsch, Paris, 1883. (in frence)

[9]Bryan, G.H. – "On the Stability of a Plane Plate Under Thrusts in its own Plane with Applications on the Buckling of the Side of a Ship", *Proceedings of the London Mathematical Society*, Vol. 22, p. 54, 1891.

[10] Timoshenko, S.P. – "Einige Stabilitätsprobleme der Elastizitätstheorie", *Zeitschrift für angewande Mathematik und Physik* (ZAMP), Vol. 58, Nº 4, pp. 337-385, 1910. (in germany)

[11] Reissner, H. – "Uber die Knicksicherheit ebener Bleche", *Zentralblatt der Bauverwaltung*, p. 93, 1909. (in German)

[12] Bulson, P.S. – *The Stability of Flat Plates*, Chatto & Windus, London, 1970.

[13] Becque J. "Inelastic Plate Buckling", ASCE Journal of Engineering Mechanics 2010;136(9):1123–30

[14] Becque J.; Lathourakis, P. , "Experimental verification of an inelastic plate theory based on plastic flow theory", Thin-Walled Structures 49, 2011, 1563–1572.

[15] Zienkiewicz, O.C. e Taylor, R.L. – *The Finite Element Method* (4th Edition – 2 Volumes), McGraw-Hill, London, 1988.

[16] Przemieniecki, J.S. – "Finite Element Structural Analysis of Local Instability", *Journal of the American Institute of Aeronautics and Astronautics* (AIAA), Vol. 11, Nº 1, pp. 33-39, 1973.

[17] Kármán, T.V. "Festigkeitsprobleme im Maschinenbau. Encyklopädie der Matematischen Wissen-schaften", Vol. 4, Part 4, pp. 348-350, 1910 (In German).

[19] Marguerre, T. – "Zur Theorie der Gekrümten Platte Grosser Formänderung", *Proceedings of the Fifth International Congress on Applied Mechanics, Cambridge, Massachussets*, John Wiley & Sons, pp. 93-101, 1939. (in German)

[20] Levy, S. – "Bending of Rectangular Plates with Large D_{eff}lections", *NACA Technical Note Nº 737*, 1942.

[21] Coan, J.M. – "Large Deflection Theory of Plates with Small Initial Curvature Loaded in Edge Compression", *Journal of Applied Mechanics* (ASME), Vol. 18, Nº 2, pp. 143-151, 1951.

[22] Fok, C.D. e Murray, N.W. – "The Efffect of Initial Imperfection on the Elastic Behaviour of Isolated Thin Steel Plates with In-Plane", *Aspects of Analysis of Plate Structures*, Eds. D.J. Dawe, R.W. Horsington, A. G. Kamtekar e G.H. Little, pp. 225-249, 1985.

[23] Yamaki, N. – "Post-Buckling Behaviour of Rectangular Plates with Small Initial Curvature Loaded in Edge Compression", *Journal of Applied Mechanics* (ASME), Vol. 26, pp 407-414, 1959.

[24] Rhodes, J., e Harvey, J.M. – "Plates in Uniaxial Compression with Various Support Conditions at the Unloaded Boundaries", *International Journal of Mechanical Sciences*, Vol. 13, pp. 787-802, 1971.

[25] Rhodes, J., e Harvey, J.M. – "Effects of Eccentricity of Load or Compression on the Buckling and Post-Buckling Behaviour of Flat Plates", *International Journal of Mechanical Sciences*, Vol. 13, pp. 867-879, 1971

[26] Rhodes, J., Harvey, J.M. e Fox, W.C. – "The Load-Carrying Capacity of Initially Imperfect Eccentrically Loaded Plates", *International Journal of Mechanical Sciences*, Vol. 17, pp. 161-175, 1975.

[27] Rhodes, J. e Harvey, J.M. – "Examination of Plate Post-Buckling Behaviour", *Journal of the Engineering Mechanics Division* (ASCE), Vol. 103, Nº 3, pp. 461-478, 1977.

[28] Usami, T. – "Post-Buckling of Plates in Compression and Bending", *Journal of the Structural Division* (ASCE), Vol. 108, Nº 3, pp. 591-609, 1982.

[29] Galambos, T.V. (Ed.) – *Guide to Stability Design Criteria for Metal Structures* (5th Edition), John Wiley & Sons, New York, 1998.

[30] Galambos, T.V. (Ed.) – *Guide to Stability Design Criteria for Metal Structures* (5th Edition), John Wiley & Sons, New York, 1998.

[31] Sherbourne, A.N. e Bedair, O.K. – "Plate-Stiffener Assemblies in Uniform Compression – Part II: Postbuckling", *Journal of Engineering Mechanics* (ASCE), Vol. 119, Nº 10, pp. 1956-1972, 1993.

[32] Turner, M.J., Dill, E.H., Martin, H.C. e Melosh, R.J. – "Large D_{eff}lections of Structures Subjected to Heating and External Loads", *Journal for Aerospace Science*, Vol. 27, Nº 2, pp. 97-106, 1960.

[33] Brebbia, C. e Connor, J. – "Geometrically Nonlinear Finite Element Analysis", *Journal of the Engineering Mechanics Division* (ASCE), Vol. 95, Nº 2, pp. 463-483, 1969.

[34] Murray, D.W. e Wilson, E.L. – "Finite Element Postbuckling Analysis of Thin Elastic Plates", *American Institute of Aeronautics and Astronautics (AIAA) Journal*, Vol. 7, Nº 10, pp. 1915-1920, 1969.

[35] Yang, T.Y. – "A Finite Element Procedure for Large D_{eff}lections Analysis of Plates with Initial D_{eff}lections", *American Institute of Aeronautics and Astronautics (AIAA) Journal*, Vol. 9, Nº 8, pp. 1468-1473, 1971.

[36] Rerkshanandana, N., Usami, T. e Karasudhi, P. – "Ultimate Strength of Eccentrically Loaded Steel Plates and Box Sections", *Computers and Structures*, Vol. 13, pp. 467-481, 1981.

[37] Ueda, Y., Matsuichi, M., Yamauchi, Y. e Topaka, M. – "Nonlinear Analysis of Plates Using the Finite Strip Method", *Journal of the Kansai Society of Naval Architects*, Nº 154, pp. 83-92, 1974.

[38] Becque J. "Linking the von Karmán equations to de design of steel plates", Proceedings of the 8th conference on Coupled Instabilities in Metal Structures, Lodz University of Technology, Poland, July 12-14, 2021.

[39] Simulia Inc, Abaqus standard.

[40] Ueda, Y., Matsuichi, M., Yamauchi, Y. e Topaka, M. – "Nonlinear Analysis of Plates Using the Finite Strip Method", *Journal of the Kansai Society of Naval Architects*, Nº 154, pp. 83-92, 1974.

[41] Graves Smith, T.R. e Sridharan, S. – "A Finite Strip Method for the Post-Locally-Buckled Analysis of Plate Structures", *International Journal of Mechanical Sciences*, Vol. 20, pp. 833-842, 1978.

[42] Gierlinski, J.T. e Graves Smith, T.R. – "The Geometrical Nonlinear Analysis of Thin-Walled Structures by Finite Strips", *International Journal of Mechanical Sciences*, Vol. 20, pp. 833-842, 1978.

[43] Hancock, G.J. – "Interaction Buckling of *I*-Section Columns", *Journal of the Structural Division* (ASCE), Vol. 107, Nº 1, pp. 165-179, 1981.

[44] Hancock, G.J. – "Non-Linear Analysis of Thin-Walled *I*-Sections in Bending", *Aspects of the Analysis of Plate Structures*, Eds. D.J. Dawe, R.W. Horsington, A.G. Kamketar e G.H. Little, Oxford University Press, pp. 251-268, 1985.

[45] Cheung, M.S. e Li, W. – "A Modified Finite Strip Method for Geometrically Nonlinear Analysis of Plates", *Computers and Structures*, Vol. 33, Nº 4, pp. 1031-1035, 1989

[46] Bradford, M.A. e Hancock, G.J. – "Interaction of Local and Lateral Buckling in Beams", *Thin-Walled Structures*, Vol. 2, Nº 1, pp. 1-25, 1984.

[47] Kwon, Y.B. e Hancock, G.J. – "A Nonlinear Elastic Spline Finite Strip Analysis for Thin-Walled Sections", *Thin-Walled Structures*, Vol. 12, pp. 295-319, 1991.

[48] Von Kárman, T., Sechler, E.E. e Donnell, L.H., – "The Strength of Thin Plates in Compression", *Transactions of the American Society of Mechanical Enginneers* (ASME), Vol. 54, pp. 53-57, 1932.

[49] Reis, A.; Camotim, D. *Estabilidade Estrutural*, McGraw-Hill, 2001 (In Portuguese).

[50] Winter, G. – "Strength of Thin Steel Compression Flanges", *Transactions of the American Society of Civil Engineers* (ASCE), Vol. 112, pp. 527-555, 1947.

[51] Lundquist, E.E., Stowel, E.Z. e Schuette, E.H. – "Principles of Moment Distribution Applied to Stability of Structures Composed of Bars or Plates", *NACA Wartime Report L326*, 1943.

[52] Chilver, A.H. – "Behaviour of Thin-Walled Structural Members in Compresssion", *Engineering*, Vol. 172, pp. 281-282, 1951.

[53] Bleich, F. – *Buckling Strength of Metal Structures*, McGraw-Hill, New York, 1952.

[54] Chilver, A.H. – "A Generalised Approach to the Local Instability of Certain Thin-Walled Struts", *The Aeronautical Quarterly*, Vol. 4, pp. 245-260, 1953.

[55] Bulson, P.S. – "Local Instability and Strength of Structural Sections", *Thin-Walled Structures*, Ed. A.H. Chilver, Chatto & Windus, pp. 153-207, 1967.

[56] Walker, A.C. – "Local Instability in Plates and Channel Struts", *Journal of the Structural Division* (ASCE), Vol. 92, Nº 3, pp. 39-55, 1966.

[57] Rhodes, J. e Harvey, J.M. – "Plain Channel Section Struts in Compression and Bending Beyond the Local Buckling Load", *International Journal of Mechanical Sciences*, Vol. 18, pp. 511-519, 1976.

[58] Rhodes, J., e Harvey, J.M. – "Plates in Uniaxial Compression with Various Support Conditions at the Unloaded Boundaries", *International Journal of Mechanical Sciences*, Vol. 13, pp. 787-802, 1971.

[59] Rhodes, J., e Harvey, J.M. – "Effects of Eccentricity of Load or Compression on the Buckling and Post-Buckling Behaviour of Flat Plates", *International Journal of Mechanical Sciences*, Vol. 13, pp. 867-879, 1971.

[60] Gallagher, R.H. e Padlog, J. – "Discrete Element Approach to Structural Instability Analysis", *Journal of the American Institute of Aeronautics and Astronautics* (AIAA), Vol. 1, Nº 6, pp. 1437-1439, 1963.

[61] Kapur, K.K e Hartz, B.J. – "Stability of Plates Using the Finite Element Method*", Journal of the Engineering Mechanics Division* (ASCE), Vol. 92, Nº 4, pp. 1555-1571, 1966.

[62] Wittrick, G. – "General Sinusoidal Stiffness Matrices for Buckling and Vibration of Thin-Walled Structures", *International Journal of Mechanical Sciences*, Vol. 10, pp. 949-966, 1968.

[63] Przemieniecki, J.S. – "Discrete Element Method for Stability Analysis of Complex Structures", *The Aeronautical Journal*, Vol. 72, pp. 1077-1086, 1968.

[64] Przemieniecki, J.S. – "Matrix Analysis of Local Instability in Plates, Stiffened Panels and Columns", *International Journal for Numerical Methods in Engineering*, Vol. 5, pp. 209-216, 1972.

[65] Chin, C.-K., Al-Bermani, F.G. e Kitipornchai, S. – "Finite Element for Buckling Analysis of Plate Structures", *Journal of Structural Engineering* (ASCE), Vol. 119, Nº 4, pp. 1048-1068, 1993.

[66] Graves Smith,T.R. e Sridharan, S. – "A Finite Strip Method for the Buckling of Plate Structures Under Arbitrary Loading", *International Journal of Mechanical Sciences*, Vol. 20, pp. 685-693, 1978.

[67] Hancock, G.J. – "Local, Distortional and Lateral Buckling of *I*-Beams", *Journal of the Structural Division* (ASCE), Vol. 104, Nº 11, pp. 1787-1798, 1978.

[68] Batista, E.M. – "Etude de la Stabilité des Profils à Parois Minces et Section Ouverte de Types *U* et *C*", *Thèse de Doctorat*, Faculté des Sciences Appliquées, Université de Liège, Belgique, 1989.

[69] Lau, S.C. e Hancock, G.J. – "Buckling of Thin Flat-Walled Structures by a Spline Finite Strip Method", *Thin-Walled Structures*, Vol. 4, Nº 4, pp. 269-294, 1986.

[70] Bradford, M.A. e Azhari, M. – "Buckling of Plates with Different End Conditions Using the Finite Strip Method", *Computers and Structures*, Vol. 56, Nº 1, pp.75-83, 1995.

[71] Azhari, M. e Bradford, M.A. – "Local Buckling by Complex Finite Strip Method Using Bubble Functions", *Journal of Engineering Mechanics* (ASCE), Vol. 120, Nº 1, pp. 43-57, 1994.

[72] Sharp, T.P., Peköz, T. and Winter, G. – "Longitudinal Stiffeners for Compression Members", *Journal of Structural Engineering* (ASCE), Vol. 107, Nº 2, pp. 329-353, 1981.

[73] Sharp, T.P., Peköz, T. and Winter, G. – "Longitudinal Stiffeners for Compression Members", *Journal of Structural Engineering* (ASCE), Vol. 107, Nº 2, pp. 329-353, 1981

[74] Desmond, T.P., Peköz, T. and Winter, G. – "Edge Stiffeners for Thin-Walled Members", *Journal of Structural Engineering* (ASCE), Vol. 107, Nº 2, pp. 329-353, 1981.

[75] Desmond, T.P., Peköz, T. and Winter, G. – "Intermediate Stiffeners for Thin-Walled Members", *Journal of Structural Engineering* (ASCE), Vol. 107, Nº 4, pp. 627-648, 1981.

[76] Sridharan, S. – "A Semi-Analytical Method for the Post-Local-Torsional Buckling Analysis of Prismatic Plate Structures", *International Journal for Numerical Methods in Engineering*, Vol. 18, Nº 2, pp. 1685-1697, 1982.

[77] Hancock, G.J. – "Distortional Buckling of Steel Storage Rack Columns", *Journal of Structural Engineering* (ASCE), Vol. 111, Nº 12, pp. 2270-2283, 1985.

[78] Hancock, G.J., Davids, A.J., Key, P.W., Lau, S.C. e Rasmussen, K.J. – "Recent Developments in the Buckling and Nonlinear Analysis of Thin-Walled Structural Members", *Thin-Walled Structures*, Vol. 9, pp. 309-338, 1990.

[79] Hancock, G.J. – "Finite Strip Buckling and Nonlinear Analyses and Distortional Buckling Analysis of Thin-Walled Structural Members", *Coupled Instabilities in Metal Structures: Theoretical and Design Aspects*, Ed. J. Rondal, CISM Course Nº379, pp. 225-289 (part V), Springer-Verlag, Wien, 1998.

[80] Rasmussen, K.J. – "Experimental Techniques in the Testing of Thin-Walled Structural Members", *Coupled Instabilities in Metal Structures* (CIMS'2000), Eds. D. Camotim, D. Dubina e J. Rondal, Imperial College Press, pp. 225-239, 2000.

[81] Hancock, G.J. – *Design of Cold-Formed Steel Structures* (3rd Edition), Australian Institute of Steel Construction, 1998.

[82] Plank, R.J. e Wittrick, W.H. – "Buckling under Combined Loading of Thin, Flat-Walled Structures by a Complex Finite Strip Method", *International Journal for Numerical Methods in Engineering*, Vol. 8, Nº 2, pp. 323-339, 1974.

[83] Lau, S.W. – "Distortional Buckling of Thin-Walled Columns", *Ph.D. Thesis*, School of Civil and Mining Engineering, University of Sydney, Australia, 1988.

[84] Lau, S.C. e Hancock, G.J. – "Distortional Buckling Formulas for Channel Columns", *Journal of Structural Engineering* (ASCE), Vol. 113, Nº 5, pp. 1063-1078, 1987.

[85] Hancock, G.J. – "Design for Distortional Buckling of Flexural Members", *Thin-Walled Structures*, Vol. 27, Nº 1, pp. 3-12, 1997.

[86] Bambach, M.R., Merrick, J.T. e Hancock, G.J. – "Design for Distortional Buckling Formulae for Thin-Walled Channel and *Z*-Sections with Return Lips", *Proceedings of 14th International Specialty Conference on Recent Research and Developments in Cold-Formed Steel Design and Construction*, University of Missouri-Rolla, St. Louis, USA, pp. 21-37, 1998.

[87] Hancock, G.J., Kwon, Y.B. e Bernard, E.S. – "Strength Design Curves for Thin-Walled Sections Undergoing Distortional Buckling", *Journal of Constructional Steel Research*, Vol. 31, Nº 2-3, pp. 169-186, 1994.

[88] Kwon, Y.B. e Hancock, G.J. – "Design of Channels Against Distortional Buckling", *Proceedings of 11th International Specialty Conference on Recent Research and Developments in Cold-Formed Steel Design and Construction*, University of Missouri-Rolla, St. Louis, USA, pp. 323-352, 1992.

[89] Kwon, Y.B. e Hancock, G.J. – "Strength Tests of Cold-Formed Channel Sections Undergoing Local and Distortional Buckling", *Journal of Structural Engineering* (ASCE), Vol. 117, Nº 2, pp. 1786-1803, 1992.

[90] SCHAFER, B. W. "*CUFSM 5.04 - Cross-Section Elastic Buckling Analysis*: constrained and unconstrained finite strip method", 2020. Available at: https://www.ce.jhu.edu/cufsm/downloads/

[91] NGUYEN, V. V.; HANCOCK, G. J.; PHAM, C. H. "Development of the Thin-Wall-2 Program for buckling analysis of thin-walled sections under generalised loading". *In*: INTERNATIONAL CONFERENCE ON ADVANCES IN STEEL STRUCTURES, 8., 2015, Lisboa, Portugal. *Proceedings* . Lisboa: ICASS, 2015. Available at: https://structuresgroup-eng.sydney.edu.au/thin-wall-2/

[92] Bebiano R., Camotim D., Gonçalves R., "GBTUL 2.0 − A second-generation code for the GBT-based buckling and vibration analysis of thin-walled members", Thin-Walled Structures, 124, pp. 235 - 257, 2018.. Available at: GBTUL | gbt (unl.pt)

[93] Chicaiza, A , Prola, L , Martinez, L, Graça, P. "FSplines: um aplicativo para análise linear de estabilidade", XII Congresso de Construção Metálica e Mista, 21 a 22 de novembro de 2019, Coimbra. Available at: Grupo de Construções Metálicas | Departamento de Engenharia Civil (ipleiria.pt)

[94] Benthem, J.P. – "The Reduction in Stiffness of Combinations of Rectangular Plates in Compression after Exceeding the Buckling Load", *National Aeronatical Research Institute Report NLL-TRS.539*, Amsterdam, 1959.

[95] Graves Smith, T.R. – "The Postbuckled Behaviour of Thin-Walled Columns", *Proceedings of the Eighth Congress of the International Association for Bridge and Structural Engineering* (IABSE), New York, pp. 311-320, 1968.

[96] Graves Smith, T.R. – "The Ultimate Strength of Locally Buckled Columns of Arbitrary Length", *Thin-Walled Steel Structures*, Eds. K.C. Rockey e R.V. Hill, Crosby-Lockwood and Son, London, pp. 35-60, 1969.

[97] Graves Smith, T.R. – "The Postbuckled Behaviour of Thin-Walled Box Beams in Pure Bending", *International Journal of Mechanical Sciences*, Vol. 14, pp. 711-722, 1972.

[98] Rhodes, J. e Harvey, J.M. – "Plain Channel Section Struts in Compression and Bending Beyond the Local Buckling Load", *International Journal of Mechanical Sciences*, Vol. 18, pp. 511-519, 1976.

[99] Rhodes, J. e Harvey, J.M. – "The Local and Post-Local Buckling of Thin-Walled Beams", *Aeronautical Quarterly*, Vol. 22, pp. 363-388, 1971.

[100] Rhodes, J. e Harvey, J.M. – "The Local Instability of Thin-Walled Sections Under Combined Compression and Bending", *Proceedings of 3rd International Specialty Conference on Recent Research and Developments in Cold-Formed Steel Design and Construction*, University of Missouri-Rolla, St. Louis, USA, pp. 51-87, 1975.

[100] Lee, H.P. e Harris, P.J. – "Post-Buckling Strength of Thin-Walled Members", *Computers and Structures*, Vol. 10, pp. 689-702 1979.

[101] Graves Smith, T.R. e Sridharan, S. – "A Finite Strip Method for the Post-Locally-Buckled Analysis of Plate Structures", *International Journal of Mechanical Sciences*, Vol. 20, pp. 833-842, 1978.

[102] Sridharan, S. – "A Finite Strip Analysis of Locally Buckled Plate Structures Subject to Nonuniform Compression", *Engineering Structures,* Vol 4, October, pp. 249-255, 1982.

[103] Hancock, G.J. – "Non-Linear Analysis of Thin Sections in Compression", *Research Report R355*, School of Civil and Mining Engineering, University of Sydney, Australia, 1979.

[104] Loughlan, J. e Rhodes, J. – "Interaction Buckling of Lipped Channel Columns", *Stability Problems in Engineering Structures and Components*, Eds. T.H. Richards e P. Stanley, Applied Science Publishers, London, pp. 179-198, 1979.

[105] DeWolf, J.T., Pekoz, T. e Winter, G. – "Local and Overall Buckling of Cold-Formed Members", *Journal of the Structural Division* (ASCE), Vol. 100, Nº 10, pp. 2017-2036, 1974.

[106] Prola, L.; Gala, P.; Ruben, R.B.; Monteiro, C.; Simões, A. "Effective Modulus Method (EMM) concept applied to thin-walled steel columns", *Proceedings of the 10th Eurosteel Conference*, Amsterdam, The Netherlands, 2023.

[107] Koiter, W.T. "Over der Stabiliteit van het Elastische Evenwicht (English translation: On the Stability of Elastic Equilibrium)", *Doctoral Thesis*, Delft University of Technology, The Netherlands, 1945 (In Dutch).

[108] Hutchinson, J.W.; Koiter, W.T. "Postbuckling Theory", Applied Mechanics Reviews, 23, 1353-1366, 1970.

[109] American Iron and Steel Institute (AISI) North American Specification for the design of Cold-formed steel structural members – AISI S100-16. Washington (DC), USA, 2016.

[110] Winter, G. "Cold-Formed Light-Gauge Steel Construction", Journal of the Structural Division of the American Society of Civil Engineers (ASCE), 85(9), 151-171, 1959.

[111] Schafer, B.W.; Peköz, T. "Direct strength prediction of cold-formed steel members using numerical elastic buckling solutions*". Proceedings of 14th International Specialty Conference on Cold-Formed Steel Structures*, St. Loius, Missouri, USA, 1998. https://scholarsmine.mst.edu/isccss/14iccfsss/14iccfsss-session2/4.

[112] Schafer, B.W. "Review: the direct strength method of cold-formed steel member design", *Journal of Constructional Steel Research*, 64(7–8), 766–778, 2008. DOI: 10.1016/j.jcsr.2008.01.022.

[113] Martins, A.D.; Camotim, D.; Dinis, P.B. "Local-distortional interaction in cold-formed steel beams: behaviour, strength and DSM design", *Thin-Walled Structures,* 118, 879–901, 2017.

[114] Chen, M-T.; Young, B.; Martins, A.D.; Camotim, D.; Dinis, P.B. "*Uniformly bent CFS lipped channel beams experiencing local-distortional interaction: Experimental investigation", Journal of Constructional Steel Research*, 170, 106098, 2020.

[115] Pham, C. H.; Hancock, G. J. "Experimental investigation and direct strength complex C-section in pure bending", *Research Report R925*, ISSN1833-2781, School of Civil Engineering, The University of Sidney, Sidney, Australia, 2012.

[116] Chen, M-T.; Young, B.; Martins, A.D.; Camotim, D.; Dinis, P.B. "Experimental investigation on cold-formed steel lipped channel beams affected by local-distortional interaction under non-uniform bending", *Thin-Walled Structures*, 161, 107494, 2021.

[117] Carvalho, C.; Prola, L. "Moment resistance analysis of thin-walled stiffened sections by the alternative method of EN1993: Part:1-3", *The International Colloquium on Stability and Ductility of Steel Structures (SDSS)*, University of Aveiro, Aveiro, Portugal, 2022.

[118] Martins, A.D.; Camotim, D.; Dinis, P.B.; Chen, M-T.; Young, B. (2022) *Design approach against column local–distortional interactive failures based on the Direct Strength Method*. Thin-Walled Structures 181. DOI: 10.1016/j.tws.2022.110081

[119] Young, B; Dinis, P.B.; Camotim, D. (2018) *CFS lipped channel columns affected by L-D-G interaction. Part I: Experimental investigation*. Computers and Structures 207, pp. 219-232. DOI: 10.1016/j.compstruc.2017.03.016

[120] Dinis, P.B.; Camotim, D.; Young, B.; Batista, E.M. (2018) *CFS lipped channel columns affected by L-D-G interaction. Part II: Numerical simulations and design considération*s. Computers and Structures 207, pp. 200-218. DOI: 10.1016/j.compstruc.2017.03.017

[121] Cava, D.; Camotim, D.; Dinis, P.B.; Madeo, A. (2016) Numerical investigation and direct strength design of cold-formed steel lipped channel columns experiencing local-distortional-global interaction. Thin-Walled Structures 105, pp. 231–247. DOI: 10.1016/j.tws.2016.03.025

[122] Pedro B. Dinis, Ben Young b, Dinar Camotim; (2014) *Local–distortional interaction in cold-formed steel rack-section columns Local–distortional interaction in cold-formed steel rack-section columns.* Thin-Walled Structures 81 pp 185-194. DOI: 10.1016/j.tws.2013.09.010

[123] J. Loughlan, N. Yidris, K. Jones; *The failure of thin-walled lipped channel compression members due to coupled local-distortional interactions and material yielding.* Thin-Walled Structures 61, pp. 14-21. DOI: 10.1016/j.tws.2012.03.025

[124] M.A. El Aghoury, M.T. Hanna, E.A. Amoush; *Experimental and theoretical investigation of cold-formed single lipped sigma columns.* Thin-Walled Structures 61, pp. 14-21. DOI: 10.1016/j.tws.2016.10.025